

Copyright
by
Ethan Stewart Rapp
2021

The Dissertation Committee for Ethan Stewart Rapp
certifies that this is the approved version of the following dissertation:

**Enhanced Implantable Device Evaluation Using A
Hardware-in-the-Loop Circulatory Simulator**

Committee:

Raul G. Longoria, Supervisor

Dongmei Chen

Junmin Wang

Manuel Rausch

**Enhanced Implantable Device Evaluation Using A
Hardware-in-the-Loop Circulatory Simulator**

by

Ethan Stewart Rapp

DISSERTATION

Presented to the Faculty of the Graduate School of

The University of Texas at Austin

in Partial Fulfillment

of the Requirements

for the Degree of

DOCTOR OF PHILOSOPHY

THE UNIVERSITY OF TEXAS AT AUSTIN

August 2021

Enhanced Implantable Device Evaluation Using A Hardware-in-the-Loop Circulatory Simulator

Ethan Stewart Rapp, Ph.D.
The University of Texas at Austin, 2021

Supervisor: Raul G. Longoria

As the number of patients experiencing severe heart failure increases, so too does the need and use of implantable mechanical circulatory support devices, such as ventricular assist devices (VADs) and total artificial hearts (TAHs), for patient treatment. These devices assist the failing heart by taking over the blood pumping process either partially or completely and must be properly vetted and verified for human use by undergoing many years of testing, both using in vitro benchtop and in vivo animal testing. To expedite the laboratory testing process, hardware-in-the-loop (HIL) systems called mock circulation loops (MCLs) have been developed that can test assist devices within a mechanical realization of the human cardiovascular environment. This research focuses on the evaluation of nominal and enhanced VAD function using a hybrid mock circulation loop (hMCL) as a HIL test platform. The research can be split into three major aims: (1) hMCL construction and performance characterization for nominal VAD testing, (2) hMCL based evaluation of enhanced VAD onboard estimation algorithms, (3) Method for HIL

implementation of arrhythmic and VAD induced cardiac events in hMCL. Regarding Aim 1, test results of the current hMCL design show that root-mean-square error between simulated and realized physiological pressures across a range of VAD flowrates can be maintained within 1.5-3.5 [mmHg]. The hMCL is able to simulate different levels of patient cardiovascular health and basic sensitivity tests indicate responsiveness to changes in the simulated model parameters; a necessary requirement to accomplish Aim 2. Completed work towards Aim 2 involves evaluating the onboard sensing algorithms being developed on VADs using sensor-based estimation of systemic vascular resistance (SVR) as an example. Preliminary experiments using the hMCL showed that SVR value estimates were accurate within 1.3% and 0.7% compared to the set numerical model values for tests run on continuous and pulsatile flow VADs, respectively. Lastly, methods for incorporating arrhythmic cardiac events and valvular stenosis have been presented towards Aim 3. Preliminary results show less than 2% and 4% mean percent error between aortic and left ventricular pressure tracking, respectively, as well as good agreement between referenced and measured frequency content.

Table of Contents

| | |
|--|-----------|
| Abstract | iv |
| List of Tables | ix |
| List of Figures | x |
| Chapter 1. Introduction | 1 |
| 1.1 Mock Circulation Loops | 1 |
| 1.1.1 Ventricular Assist Devices | 2 |
| 1.1.2 MCL Validation of VADs | 4 |
| 1.2 Estimation using the hMCL | 5 |
| 1.3 Cardiac Event Generation | 7 |
| 1.4 Introduction Summary | 8 |
| 1.5 Research Aims | 9 |
| Chapter 2. Hybrid Mock Circulation Loop Review | 13 |
| 2.1 History of MCLs | 13 |
| 2.1.1 Conventional MCLs | 16 |
| 2.1.2 Hybrid MCLs | 21 |
| 2.2 Common hMCL Design Components | 25 |
| 2.3 Verification and Validation of VADs | 26 |
| Chapter 3. Modeling and Construction of Electro-Mechanical hMCL | 28 |
| 3.1 Design Criteria | 28 |
| 3.1.1 hMCL Design | 30 |
| 3.2 hMCL Materials | 32 |
| 3.2.1 Hardware | 32 |
| 3.2.2 Software | 36 |
| 3.3 Cardiovascular Model Simulation | 38 |
| 3.4 Electromechanical hMCL system model | 40 |
| 3.5 Control | 42 |
| 3.5.1 Model analysis and control structure | 42 |
| 3.5.2 Controller tuning and stability | 46 |
| Chapter 4. Evaluation of hMCL in VAD Test Applications | 48 |
| 4.1 Test Overview | 48 |
| 4.2 Experimental Results with Continuous Flow VAD Analog | 50 |

| | | |
|-------------------|---|------------|
| 4.2.1 | Chamber Pressure Tracking | 50 |
| 4.2.2 | P-V Loop Generation | 52 |
| 4.2.3 | CVS Model Parameter Sensitivity | 54 |
| 4.3 | Test Discussion | 55 |
| Chapter 5. | Estimation of SVR in hMCL | 60 |
| 5.1 | Objective | 60 |
| 5.2 | State of the Art | 61 |
| 5.2.1 | Measurement of SVR | 62 |
| 5.2.2 | Model-based estimation of SVR | 63 |
| 5.3 | Reduced Order SVR Model for Estimation | 63 |
| 5.3.1 | Model Overview | 64 |
| 5.3.2 | Model Equations | 67 |
| 5.3.3 | Model Simulation vs hMCL CVS Model | 69 |
| 5.4 | SVR Estimation Using EKF | 69 |
| 5.4.1 | Estimability and Convergence | 69 |
| 5.4.2 | LVAD Flowrate and Differential Pressure | 72 |
| 5.5 | SVR Estimation Simulation Results | 74 |
| 5.6 | SVR Estimation Results using hMCL Data | 74 |
| 5.6.1 | Test procedure | 77 |
| 5.6.2 | SVR estimation in CF pump testing | 78 |
| 5.6.3 | SVR estimation in PF LVAD testing | 80 |
| 5.7 | Discussion | 81 |
| Chapter 6. | hMCL Cardiac Event Generation | 86 |
| 6.1 | Cardiac Event Definition | 86 |
| 6.2 | Objective | 86 |
| 6.3 | State of the Art | 87 |
| 6.3.1 | MCLs with Atypical Heart Function Realization | 87 |
| 6.3.2 | Physiological Control and Patient Monitoring Algorithms | 89 |
| 6.4 | Methods of Cardiac Event Generation | 90 |
| 6.4.1 | Method 1 - CVS Model Parameter Modification | 91 |
| 6.4.2 | Method 2 - Clinical Data Tracking | 91 |
| 6.4.3 | Method 3 - CVS Model with Processed ECG Input | 95 |
| 6.5 | Cardiac Event List | 101 |
| 6.5.1 | Aortic Valve Stenosis (AoSten) | 103 |
| 6.5.2 | Sinus Bradycardia (S.Brady) and Tachycardia (S.Tach) | 103 |
| 6.5.3 | Atrial Fibrillation (AFib) | 103 |
| 6.5.4 | Ventricular Fibrillation (VFib) | 105 |
| Chapter 7. | Cardiac Event Generation Results | 106 |
| 7.1 | Preliminary hMCL Realization Results | 106 |
| 7.1.1 | Performance Criteria for Evaluation | 106 |
| 7.1.2 | Method 1 - CVS Model Parameter Modification | 107 |
| 7.1.3 | Method 2 - Clinical Data Tracking | 108 |

| | | |
|---------------------|--|------------|
| 7.1.4 | Method 3 - CVS Model with Processed ECG Input . . . | 109 |
| 7.2 | Discussion | 110 |
| 7.2.1 | Method 1 - CVS Model Parameter Modification | 112 |
| 7.2.2 | Method 2 - Clinical Data Tracking | 113 |
| 7.2.3 | Method 3 - CVS Model with Processed ECG Input . . . | 114 |
| Chapter 8. | Conclusion and Future Work | 117 |
| 8.1 | Conclusion | 117 |
| 8.2 | Future Work | 120 |
| Appendices | | 125 |
| Appendix A. | List of Publications | 126 |
| A.1 | Publications | 126 |
| A.2 | Conference Poster Presentations | 126 |
| A.3 | Master's Thesis | 127 |
| A.4 | Papers Submitted | 127 |
| Appendix B. | Electromechanical hMCL System Dynamic Equations | 128 |
| Appendix C. | Physiological Effects of VAD Support | 132 |
| Bibliography | | 133 |

List of Tables

| | | |
|-----|--|-----|
| 3.1 | hMCL ISO Standards | 29 |
| 3.2 | hMCL Controller Gains | 46 |
| 5.1 | Continuous - Discrete Extended Kalman Filter equations | 71 |
| 5.2 | Systemic circulation CVS parameters | 76 |
| 5.3 | Results of the two SVR estimation experiments | 78 |
| 7.1 | Results from all 3 methods of cardiac event generation. | 110 |
| B.1 | hMCL simulation open-loop eigenvalues | 130 |
| B.2 | hMCL Simulation Parameter Values | 131 |

List of Figures

| | | |
|-----|---|-----|
| 1.1 | Human-implanted LVAD and support equipment | 3 |
| 2.1 | Kolff conventional mock circulatory system | 14 |
| 2.2 | Ochsner et al. hybrid mock circulation loop | 15 |
| 3.1 | hMCL schematic | 31 |
| 3.2 | hMCL setup - numbered items are discussed in text | 32 |
| 3.3 | Reference cardiovascular system model on hMCL | 37 |
| 3.4 | Example CVS Model Simulation Results | 39 |
| 3.5 | Bond graph of the hMCL | 42 |
| 3.6 | RGA analysis of hMCL | 44 |
| 3.7 | hMCL control block diagram | 45 |
| 4.1 | Example hMCL pressure tracking results | 51 |
| 4.2 | RMS pressure tracking results per VAD flow rate | 52 |
| 4.3 | hMCL P-V loop generation | 53 |
| 4.4 | hMCL P-V loop generation per VAD flow rate | 54 |
| 4.5 | Pressure tracking response to step SVR changes | 56 |
| 5.1 | hMCL signal flow diagram | 61 |
| 5.2 | Circuit analog of systemic circulation for SVR estimation | 64 |
| 5.3 | Reduced order CVS model versus full CVS model | 70 |
| 5.4 | TORVAD TM pumps | 73 |
| 5.5 | Simulated SVR estimation results | 75 |
| 5.6 | CF VAD EKF Performance | 79 |
| 5.7 | PF VAD EKF Performance | 82 |
| 5.8 | EKF SVR estimate convergence over time | 84 |
| 6.1 | CVS model simulation of aortic stenosis | 92 |
| 6.2 | Circuit analog of systemic circulation for P_{AO} calculation | 93 |
| 6.3 | Method 3 Flowchart | 96 |
| 6.4 | Phase space method of ECG processing | 99 |
| 6.5 | ECG processing method results for AFib case | 102 |
| 6.6 | Measured LV pressure during AFib from Dodge 1957 | 104 |
| 7.1 | hMCL pressure tracking for aortic stenosis | 108 |
| 7.2 | hMCL AFib pressure tracking using Method 2 | 109 |
| 7.3 | hMCL tachycardia pressure tracking and frequency analysis | 111 |
| 7.4 | CVS model matching and hMCL tracking results for VFib | 115 |

| | | |
|-----|---|-----|
| 8.1 | Prototype cardiac event generator (CEG) picture | 122 |
| 8.2 | CEG Preliminary Experiment Data | 124 |
| C.1 | CVS model aortic valve and VAD flows | 132 |

Chapter 1

Introduction

This chapter provides a brief background on mock circulation loops, introduces a new mock loop with an electromechanical means of pressure generation, and discusses some of the various uses of the apparatus. Research aims are outlined at the end of the chapter.

1.1 Mock Circulation Loops

The prevalence of heart disease is growing in the US with current records showing over 121.5 million American adults having some form of cardiovascular disease (CVD) between 2013 and 2016. In 2016, heart failure (HF) specifically was the underlying cause of death for 9.3% of all patients diagnosed with cardiovascular disease. The rate of HF is projected to increase by 2030 with an estimated heart failure population of over 8 million people at a medical cost of \$69.8 billion [1]. Treatment options for patients exhibiting heart failure range from pharmacological management for low risk patients to heart transplants for patients in the end-stages of the disease. The number of patients experiencing severe heart failure (around 250k), however, greatly exceeds the number of donor hearts per year (≈ 3000) [2, 3]. The increasing number of end-stage

heart failure (HF) patients coupled with the limited supply of donor hearts has caused increased waiting times for patients requiring heart transplantation. Of the 3273 heart transplant cases recorded in 2017, the percentage of patients waiting over a year increased to 21.7% [3]; a worrisome metric considering patient mortality rate within the first year of onset HF remains high at a value of 29.6% [1]. To combat this, the use of mechanical circulatory support, specifically ventricular assist devices (VADs), has become more prevalent as a method of patient therapy for prolonging patient cardiovascular health and stability.

1.1.1 Ventricular Assist Devices

Ventricular assist devices (VADs) are implantable pumps used to lighten the load on a failing heart by mechanically regulating blood flow. In the case of left ventricular assist devices (LVADs), the pump pulls blood from the left ventricle and output flow is directed back into the aorta, thus bypassing the aortic valve. A typical LVAD implantation configuration is shown in Figure 1.1, where the left ventricle (LV) and aorta are cannulated to the inlet and outlet ports of the LVAD, respectively.

Originally designed as a means to keep patient health stable until a donor heart became available, referred to as bridge-to-transplantation, improvements in VAD technology has opened more avenues for use in recent years. The rise of compact, reliable VADs which operate using continuous flow (CF) rotary mechanisms (i.e., axial or centrifugal impellers) has not only reduced

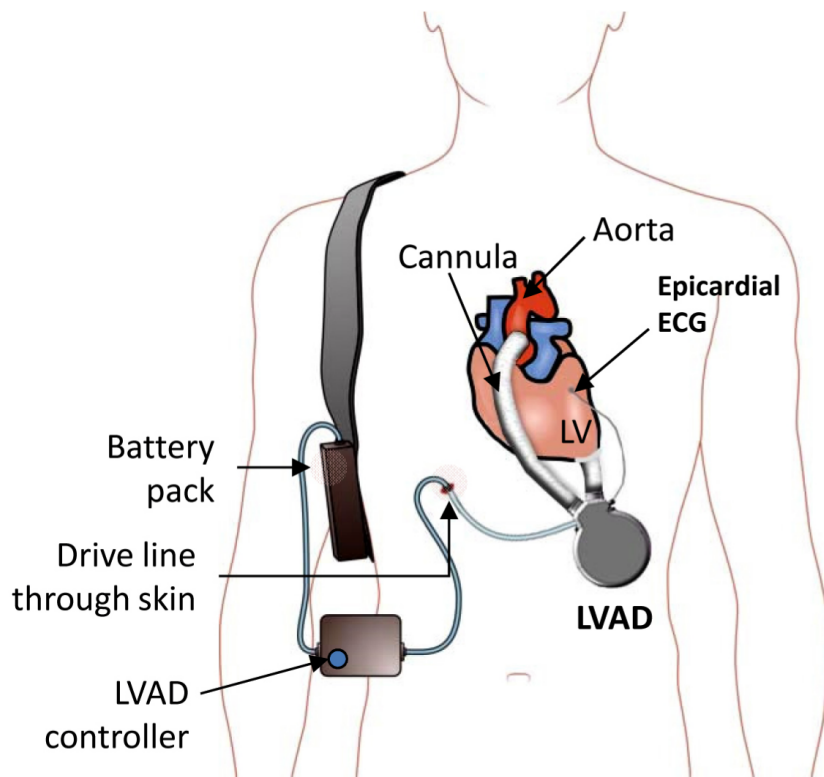


Figure 1.1: Human-implemented LVAD and support equipment

the overall mortality associated with LVAD implantation [4–6], but has also provided physicians with a more effective and reliable means of treating HF patients [7–9]. In addition to bridge-to-transplantation, VADs can be used as a means to help patients reach physiological stability requirements before a heart transplant can be performed (called bridge-to-candidacy), aid in the recovery of a weak heart (called bridge-to-recovery), or lastly as a means to improve quality of life for patients ineligible for heart transplant (called destination therapy) due to age or disease [2, 10–12].

Despite the gains made in recent years, critical unresolved complications and difficulties persist in the use of LVADs. Levels of hemorrhagic stroke, gastrointestinal bleeding, right heart failure, and sepsis, for example, continue to impact about a third of all patients [13,14]. Device specific complications, such as controller or pump failure, are also causes for concern [15]. While research continues to be done to better understand the root causes, it is evident that improvements are needed in how LVADs interact with the human cardiovascular system (CVS). For example, there is a continuing need to minimize shear stress during operation, a challenge for all types of blood pumps and especially those meant for long term implantation. This challenge and related issues are the subject of ongoing studies in academia and by manufacturers [16–18].

1.1.2 MCL Validation of VADs

As VAD technology continuously improves, the need for enhanced validation measures increases. It is necessary to fully evaluate and verify the performance of these devices many times over, via lab and animal testing, by subjecting them to both expected and unexpected operating conditions. Validation of these devices is most commonly done in vitro using mock circulation loops (MCLs) which mechanically recreate the human circulatory system in a repeatable and controllable environment. When connected to an MCL, the VAD under test (VUT) runs as if it were implanted in a heart failure patient. As such, the operation of the VAD, both hardware and software, can be evaluated at various levels of patient heart health, mechanical circulatory support

requirements, and desired lengths of time. An extended discussion regarding the use and state of art in mock circulation loops is provided in Chapter 2 of this dissertation.

1.2 Estimation using the hMCL

One such example of improved VAD technology is the addition of estimation techniques to ensure or enhance VAD performance using onboard sensor data. With the desire to reduce the need for invasive measurements for patient health monitoring, studies have begun emerging regarding the integration of estimation techniques into the field of implantable devices. This process utilizes the onboard sensors of VADs to collect data which is then analyzed using various estimation algorithms. Currently, studies have shown positive preliminary results in developing non-invasive methods to both predict and confirm desired VAD operation [19–23]. Further preliminary studies have shown promise in the ability to estimate VAD patient physiological states or parameters with the intent to use this information to influence the functional control of the VAD itself [24–27].

One such physiological parameter of importance is systemic vascular resistance, or SVR. SVR is an important diagnostic metric that indicates a heart failure patient’s level of activity under normal conditions and commonly requires pharmacological management. Increases in patient SVR may occur in circumstances such as during an adrenaline surge, after ingestion of vasocon-

strictors such as decongestants, or if the patient forgets to take their vasodilator medication. This can cause the systemic blood pressure to increase rapidly, resulting in increased risk for worsening congestive heart failure (CHF) or, worse yet, intracranial hemorrhage. As stated previously, hemorrhagic stroke is one of the major, and potentially preventable, complications of continuous flow (CF) LVADs. Flowrate settings are usually changed only during visits to the clinic, so these types of events can be difficult to avoid. Further, SVR can be indicative of clinical issues including sepsis or autonomic dysfunction, both of which are common outcomes after CF LVAD implantation [28, 29]. Variation in SVR is also common following implantation in pediatric patients, another patient population where careful monitoring can be critical.

This dissertation describes multiple methods of estimating SVR, firstly in simulation using a batch of generated CVS measurement data to confirm algorithm validity, then evaluated again using a batch of hMCL experimental data. Once the estimation algorithm validity has been established for batches of data, SVR estimation is done continuously in real-time using both hMCL measurements as well as measurements only available from an implanted LVAD system. The goal is to demonstrate how an hMCL can be used to evaluate a method of VAD sensor based estimation that could be used to guide therapy by automatically adjusting LVAD operation and/or by communicating with physicians and caregivers.

1.3 Cardiac Event Generation

As VAD research continues in the aim to reduce the documented complications as stated in [13, 14], further studies have reported incidence of VAD implantation causing or aggravating cardiac arrhythmias. Nearly 50% of VAD patients experience some form of atrial arrhythmia after implantation [30]. In particular, patient development of atrial fibrillation ranges from 20-30%, ventricular arrhythmias ranges from 22-59%, and ventricular tachycardia is around 18% [30, 31]. Though incidence rates are high, methods for managing and treating VAD patients experiencing these events are limited with strategies based mainly on non-VAD population procedures [32].

With such a large patient population experiencing these arrhythmic cardiac events, it is vital that VAD operation is properly assessed to be able to not only withstand these events and keep patients hemodynamically stable (as motivated in [33]), but also prevent operation that exacerbates the issue. Currently, VADs achieve FDA approval through rigorous in vitro and in vivo animal testing. In some cases, arrhythmic events are induced via pharmacological means in vivo (though, according to current ISO Standards, arrhythmic event validation is not a requirement). A limitation with in vivo testing is that tests are often difficult or impossible to reproduce due to the variability of animal health and disparities between animals. Further, simulating various levels of heart failure is also difficult to achieve pharmacologically. These limitations motivate the need for in vitro generation of arrhythmic events for the enhanced validation of VADs.

As an extension to the MCL validation efforts towards VAD estimation algorithms as stated in Section 1.2, further updates to MCL technology can be made regarding the generation of atypical patient health states (e.g., arrhythmias or changes in systemic vascular resistance) and VAD induced (e.g., valvular stenosis or suction events) cardiac events¹ experienced by patients after VAD implantation. It is vital for the implanted device to endure these events without resulting in control or pump failure. The addition of these cardiac events in a repeatable mock circulation loop environment would provide an increased level of validation and overall confidence in the robustness of VAD hardware and software. Further, it provides a method to analyze the performance of physiological monitoring and patient-specific control that is currently being developed in next generation VAD technology.

1.4 Introduction Summary

As the number of end-stage heart failure patients in the US continue to rise, the need for reliable mechanical circulatory support, such as ventricular assist devices, also increases. Since their conception, the technology in VADs has improved greatly regarding their ability regulate cardiac output, minimize energy consumption, as well as log, send/receive, and evaluate data as it is collected from the device for patient monitoring. Furthermore, improved computational speed of onboard processors provides the ability to monitor and update device

¹Cardiac events refer to moments of abnormal heart function in which the heart or cardiovascular system can be adversely affected.

operation, as well as make patient specific predictions. These many improvements in VAD technology drives a need for enhanced verification and validation of hardware and software performance before implantation. Thus, to meet the increasing needs for robust evaluation of all VAD subsystems, mock circulation loop capabilities must also increase.

1.5 Research Aims

The proposed research will attempt to answer the following questions:

- What baseline metrics can be used to qualify mock circulation loop performance in VAD test applications, and what are some necessary tests required to adequately judge this performance?
- How can a hybrid mock circulation loop be used to evaluate enhanced VAD onboard sensing algorithm performance?
- How can hybrid mock circulation loop control be modified such that further atypical cardiovascular events can be modeled and realized in the loop, and what are the limitations to realizing these events?

To address these questions, three research aims are proposed:

Aim 1 - Design, prototype, and validate an electro-mechanically actuated hybrid mock circulation loop

Using a simulation driven design process, a hybrid mock circulation loop running a real-time lumped parameter model of the cardiovascular system has

been designed and constructed. This hMCL interfaces with the VAD under test using two (2) pressure chambers to recreate the physiological pressures of the left ventricle (LV) and aorta (AO) via electromagnetic voice coil actuators. A backflow pump connects the two pressure chambers and regulates the height of the fluid in each tank during VAD operation. Performance of the hMCL has been assessed using a newly developed set of metrics for use in general VAD testing, VAD parameter estimation, and advanced cardiac event generation applications.

Aim 1 is developed in Chapters 3-4 of this dissertation. Chapter 2 (Hybrid Mock Circulation Loop Review) provides a literature survey and summary of conventional and hybrid mock circulation loops along with discussion of their use in evaluating performance of mechanical circulatory support (MCS) devices, such as VADs. Chapter 3 (Modeling and Construction of Electro-Mechanical hMCL) details the electro-mechanical hMCL prototype design process, including the hardware and software components. Pressure and chamber volume control methodology and analysis are also provided using an hMCL simulation model as a reference. Chapter 4 (Evaluation of hMCL in VAD Test Applications) explores various metrics which can be used to assess performance of the hMCL in VAD test applications based on modes of VAD operation and cardiovascular system model parameters (which determine the relative ‘health’ of the numerically simulated patient).

Aim 2 - Simulate and test methods for systemic vascular resistance (SVR) parameter estimation using available VAD measurements of hMCL data

As ventricular assist devices become more advanced, so too must the means to evaluate them. To test these devices, mock circulation loops are required to assess the accuracy and robustness of the developing data processing methods. The MCL must realize desired cardiovascular hemodynamics and have the ability to update parameter values or operating conditions in real-time in a controlled, stable manner to adequately evaluate the newly implemented software (discussed in Aim 1 of this dissertation). One such method of validating onboard VAD sensing algorithm performance takes the form of Systemic Vascular Resistance estimation, where onboard VAD sensor measurements are used in conjunction with nonlinear estimation techniques to determine and monitor the magnitude of patient SVR. The methods and preliminary results of this estimation application using both a continuous and pulsatile flow VAD are presented here.

Aim 2 is developed in Chapter 5 (Estimation of SVR in hMCL) of this dissertation. Following the work of Yu et al. [34], a reduced order model of the systemic circulation is provided for use in estimating SVR using VAD sensor data. The nonlinear model is explained in detail, along with the Extended Kalman Filter [35] algorithm used to estimate SVR and the other model states.

Aim 3 - Analyze potential for recreating typical cardiac events experienced during VAD operation for enhanced VAD performance testing

The next step in evaluating onboard measurement and patient monitoring capabilities of next-generation VADs and other mechanical circulatory support (MCS) devices is to recreate common cardiac events experienced by patients after implantation such as cardiac arrhythmias and valvular stenosis. Several methods to include these events into the mock circulation loop are presented in this work utilizing clinically documented and diagnosed measurement data and/or cardiovascular system model based updates for event generation. In all presented methods the left ventricular and aortic pressure chambers track the provided reference pressures just as is done in normal operation (as discussed in Aim 1). The methods and preliminary results of generating arrhythmic and VAD induced cardiac events in the MCL have been assessed along with the proposed future work that could be done in this area.

Aim 3 is developed in Chapters 6 - 7 of this dissertation. Chapter 6 (hMCL Cardiac Event Generation) provides a literature review current hMCL efforts in event generation, details the various cardiac events typically experienced by VADs during operation, and describes the methods used for hMCL implementation. Chapter 7 (Cardiac Event Generation Results) provides preliminary experimental data along with a discussion into future methods for adaptable, model-based cardiac arrhythmia and VAD induced event realization.

Chapter 2

Hybrid Mock Circulation Loop Review

This chapter provides an in depth review of mock circulation loop (MCL) technology as well as how MCLs can be used for mechanical circulatory support device verification and validation.

2.1 History of MCLs

The first mechanical device used to emulate full cardiovascular function was developed in 1959 by Willem J. Kolff [36]. This device was referred to as a mock circulation due to its ability to hydraulically recreate systemic and pulmonary pressures and flows of a human circulatory system. In the article, Kolff details the necessity for this in vitro testing device as a means to improve and test the designs of the various artificial heart devices being developed at the time as well as a means to reduce animal experimentation. An image of the Kolff mock circulatory system is provided in Figure 2.1.

Mock circulation loops can be divided into two main categories: conventional and hybrid. In conventional mock loops, the lumped physiological components of the circulation (compliances, resistances, inertances) are realized physically

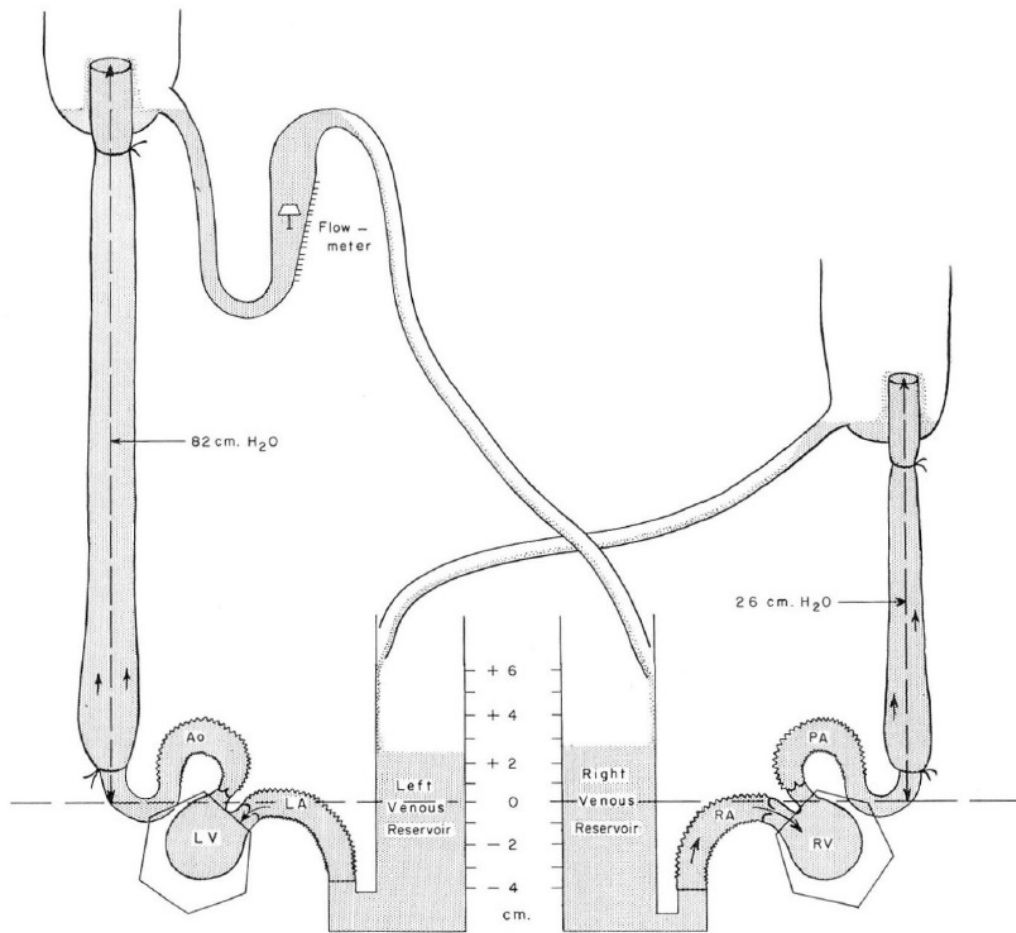


Figure 2.1: Kolff conventional mock circulation as shown in [36]

in hardware. For example, in the Kolff MCL compliances are manifested using columns of fluid whose heights could be adjusted. Further, resistances are mechanically represented and adjusted using screw clamps or partially occluding the tubing connections. Hybrid MCLs, however, use numerical models to simulate these lumped physiological components in real-time and then realize corresponding pressures and flows in the loop at mechanical interfaces

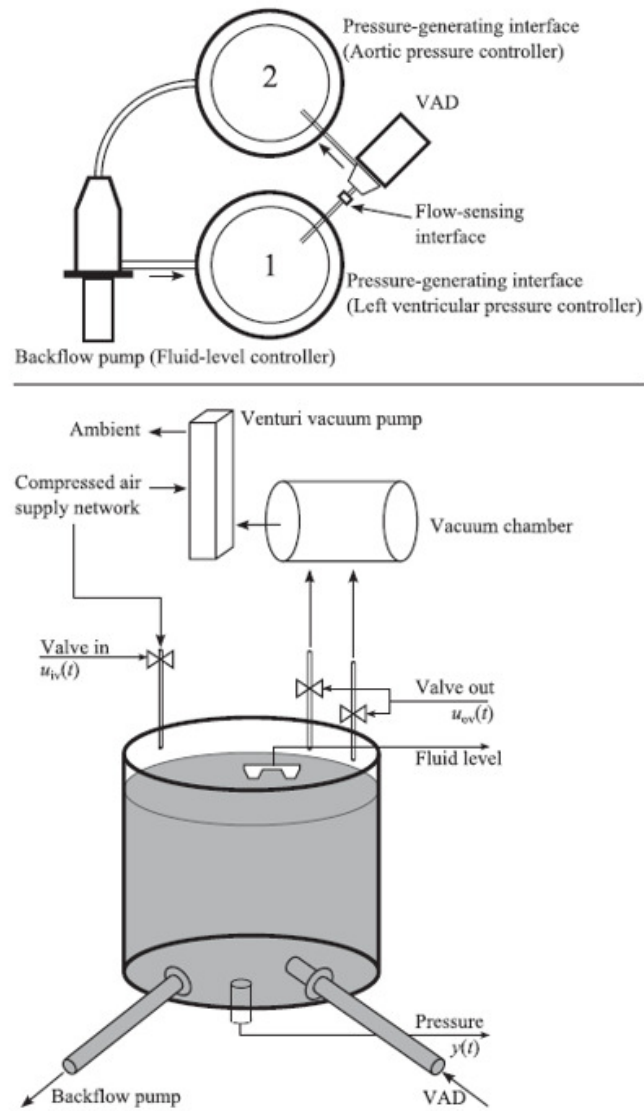


Figure 2.2: Ochsner et al. hybrid mock circulation loop as shown in [37]

which connect the hMCL to a device under test. Consider the example of VAD validation testing using an hMCL presented by Ochsner et al. in [37]. In this example, a hybrid mock circulation loop (hMCL) was presented that

could test the performance of a continuous flow VAD. The hMCL used a numerical model of the cardiovascular system running in real-time to propagate appropriate left ventricular and aortic pressures incorporating flow measurement updates from VAD output. The distinction here between conventional and hybrid MCLs can be seen in the fact that CVS parameters/components were set in the numerical model, not physically manifested in MCL hardware. Yet, with high fidelity models and the ability to realize necessary pressures and flows at the mechanical interfaces, the VAD under test still experiences appropriate human circulatory hemodynamics.

Mock circulation loop nomenclature for conventional and hybrid designs varies in the literature (e.g., mock circulation, mock circulatory system (MCS), and hybrid mock circulation (HMC)). For the remainder of this dissertation, the terms mock circulation loop (MCL) and hybrid mock circulation loop (hMCL) will be used to denote conventional and hybrid MCLs, respectively.

2.1.1 Conventional MCLs

As stated previously, conventional mock loops use physical hydraulic components, configured in analogical form, to simulate the dynamic cardiovascular system (CVS) interacting with an implantable device under test. Following Kolff's work in 1959, independent researchers and implantable device manufacturers began developing MCLs of their own. The 1970s, particularly, saw an increase in not only the quantity of functional MCLs [38–44], but in research specifically investigating hydraulic methods of artificially recreating cardiovas-

cular subsystems, such as arterial trees or ventricles [45–47].

Notable improvements to the initial Kolff MCL were made by F. M. Donovan in 1975 [48] and Rosenberg et al. between 1971 and 1981 [49]. Each MCL design incorporated methods of setting and adjusting the mechanical components to better emulate desired cardiovascular hemodynamics. These adjustments were made possible in the Donovan MCL by using hermetically sealed tanks with a desired volume ratio of working fluid to air for capacitances, as well as an inflatable bellows and lever mechanism to adjust hydraulic resistances. Similarly, the Rosenberg MCL provided the ability to set desired cardiovascular parameter magnitudes by adjusting tank volume for capacitances, tube length for inertances, and pressurizing tube connections for resistances. Further, these improvements in MCL adjustability allowed Rosenberg et al. to provide the first instance of simulated cardiovascular disease conditions, such as shock, hypertension, and hypovolemia [49].

Between the years of 1987 and 1994, Ferrari et al. developed an open-loop MCL using lumped parameter models to reduce the size and quantity of physical components necessary for MCL function [50, 51]. The mechanical component magnitudes (capacitances and resistances) were set based on impedance analysis of the expected ventricular load determined using numerical CVS models. The MCL also included a mock left ventricle to evaluate the impact of assist devices on the circulatory network when run in parallel. The mock ventricle was controlled to follow the self-regulatory mechanisms as defined by Starling’s law (by updating contractility and timing), thus providing an interconnection

between total assist device support and left ventricular output (i.e., increased assist device output reduces total ventricular output).

Also in 1994, Williams et al. expanded the idea of utilizing an MCL with a mock ventricle built-in to begin the development of LVAD control algorithms as well as provide a means to test prosthetic valves [52]. Similarly to Ferrari et al., the mock ventricle was controlled using a time-varying elastance model based on the Starling mechanism. In this work, the LV was comprised of a voice-coil actuated piston and polyurethane trileaflet inlet/outlet valves which were designed to be replaced by prosthetic valves in future experiments.

Furthering the idea of control algorithm evaluation, Baloa et al. (2001) implemented elastance-based control (based again on the Starling mechanism) of a left ventricle housed in an MCL [53]. In this work, however, the elastance-based control updated the desired reference pressure based on real-time displacement measurements of the ventricle as well as changes in preload and afterload. It was theorized that this ability to update based on cardiovascular environment changes could provide improved pathological testing conditions for the evaluation of cardiac devices. Later in 2004, Loh et al. proposed a full-state feedback control methodology as another means of realizing this desired elastance-based control of the left ventricle [54]. Loh utilized a similar model of the Baloa MCL with the addition of a right atrial compliance to limit the coupling between the left (systemic) and right (pulmonary) side of the circulation.

Improvements in elastance-based control, active component hardware, and

the ability to better characterize hemodynamic parameters for cardiovascular modeling, mock circulation loops in this time period of the late 1990s to early 2000s began emulating cardiovascular function at a very high level and brought conventional MCLs closer to the realm of hybrid MCLs. The work by Ferrari et al. in 1998 [55] and Pantalos et al. in 2004 [56] both detail the use of an MCL that could reproduce various levels of patient heart health (normal, failure, and recovery) for the improved evaluation of implantable ventricular assist devices (VADs). Using a four element Windkessel model and empirically characterized impedance of the vascular input (representative of afterload), the Pantalos MCL was able to provide the appropriate hydraulic load to the ventricle to preserve native ventricular function (defined by the Starling mechanism) for all patient heart health test cases. Characterized impedance values were found to be comparable to native heart values found in patients, with the only exception being the heart failure test case. Further, the authors motivate the analysis of this impedance data for potential use in clinical assessment of patient health as well as the use of the overall MCL for training purposes regarding VAD operation and maintenance.

In 2005, work by Liu et al. and Timms et al. added further to the characterization of hemodynamic parameters in MCLs for various physiological cardiovascular conditions. Though the Liu et al. MCL had difficulty replicating the Starling mechanism during actuation, cardiovascular parameter values were provided based on various expected situations in which a patient with an implanted assist device would encounter [57, 58]. Timms et al. created an MCL

which included both the systemic and pulmonary circulations with a series of pneumatic independently controlled compliances and ventricles. Right and Left heart physiological pressures were generated while preserving the Starling mechanism (qualitatively observed) for resting and left heart failure test cases. The novelty in the Timms MCL comes in the form of the ability to evaluate both singular and bi-VADs in a full circulation with the added ability to independently influence hemodynamic parameters during operation. The use of pneumatically actuated MCL components, though not a new concept, was enhanced as a cost effective method for updating physiological conditions within the loop [59, 60]. Additionally, in 2011, Gregory and Timms et al. introduced autoregulation to both ventricles within the MCL to recreate the nonlinear end systolic pressure volume relationship (ESPVR) found in humans [61].

Using an updated Pantalos MCL (referred to as the Louisville Mock Circulation System) from [56], Sharp and Pantalos et al. studied the effects of MCL input impedance on prosthetic valve acceleration [62]. It was determined that matching a target input impedance in the MCL does not necessarily emulate desired physiological response during MCL based testing of implantable devices or prostheses, though it is necessary for providing the appropriate load to the ventricle or assist device. The paper details the need for further research into the dynamic response of assist devices during operation and the effective load they may place on the cardiovascular system.

2.1.2 Hybrid MCLs

Hybrid mock circulation loops represent the intersection of numerical modeling and software to the conventional mock circulation hardware. Beginning in the early 1990s, the improvements in computers and embedded processors made it possible and affordable to begin incorporating this real-time technology into experimental test setups, denoted as hardware-in-the-loop (HIL) simulations or experiments. With the rise of computational ability, numerical modeling of cardiovascular system function for use in these HIL experiments grew as an area of research. Notably, Ferrari et al. introduced a numerical model of the left ventricle in 2001 which was then tested in 2002 in a numerically driven HIL experiment to realize LV function [63, 64].

The idea of minimizing MCL size by reducing the number of components made it necessary for impedance based analysis in conventional mock loops. Rather than physically manifesting each component of the cardiovascular system, they could be lumped together while still recreating accurate cardiovascular hemodynamics. Logic follows that, as MCL size decreased further, the remaining lumped components would require active, cardiovascular model based control to provide the same required load; a thought introduced by Pillon et al. in 1992 [65]. This requirement, in conjunction with the increased computational abilities described previously, led to the use of numerical modeling and real-time realization of physiological components in MCLs.

The work by Ferrari et al. between the late 1980s and 2000s paved the way for

modern hMCLs. In 2002, Ferrari et al. built the first mock circulation loop to incorporate a simulated variable elastance numerical model of the left ventricle cylinder-piston system to reproduce ventricular function in a mock circulation loop. The simulated model required atrial and arterial pressure inputs in order to compute the necessary ventricular output flow. Measurement samples and the Euler integrated numerical model were iterated at a time step of 5ms (200 Hz), which provided enough model fidelity to prove the merit of the hMCL concept [63, 64].

The following year, Kozarski and Ferrari et al. implemented an electro-hydraulic (E-H) impedance simulator to open the hMCL loop while maintaining the appropriate afterload to the hybrid ventricle [66]. The actively controlled E-H impedance again used a numerical model of the CVS to determine the necessary load to place following the hardware based arterial system. Similar to the impedance matching based updates discussed in conventional MCLs, this method of numerically simulating multiple vasculature components and recreating them as a hydraulic load allowed for the reduction in overall hMCL size, reduction in hardware costs, and most importantly the ability to update hMCL hemodynamics in real-time.

Work by Hanson et al. in the years following provided another major improvement to the numerical model driven hMCL: the interaction between the numerical simulation of the CVS and assist device operation. In the cases defined by Hanson et al., a method of cardiac assistance using dynamic cardiac compression via elastic bands that squeezed the heart from the outside was

tested in a hybrid MCL [67, 68]. Based on the level of force being measured during assist device actuation, the numerical model would update the CVS simulation and subsequent ventricular load accordingly and output reference diameter information back to the assist device for the next iteration.

Later in 2010, Timms et al. introduced numerical models to their conventional MCL as provided in [59]. The updated Timms hMCL in [69] was made into a compact cube shape (only 600 mm in all dimensions), made possible due to the use of computer driven simulation for active MCL component control. The experimental results of this study showed the ability to replicate healthy and failure heart hemodynamic conditions in real-time, enforce the Starling mechanism in both ventricles, as well as recreate physiological effects based on common genetic defects (septal defects and valvular disease). These results further demonstrated the capabilities of hybrid MCLs and provided a unique platform for cost-effective evaluation of assist devices.

Arguably the most influential update to hMCL technology was presented in 2013 by Ochsner et al. detailing a hybrid MCL comprised of only two pressure chambers, a backflow pump, and an interface for VAD or other mechanical circulatory support (MCS) device attachments [37]. In this hMCL, a numerical model of the cardiovascular system runs in real-time using pressure and VAD flow measurements to generate control pressures and regulate fluid volume in each tank using pneumatics and the backflow pump, respectively. The novelty in this method of cardiovascular system emulation is the use of a cardiovascular model to simulate the entire circulation and realize dynamic pressures only at

the interface points around the VAD itself (i.e., left ventricular pressure generated at the inlet of the VAD and aortic pressure at the outlet). This method of MCS device testing reduced the necessary components of the hMCL down to its conceivable limit while keeping cardiovascular hemodynamic fidelity at the VAD interface. In the following years, the hMCL design structure was commonly used to emulate both human [70] and animal [71] physiology.

Due to increasing computational power of embedded systems, hMCL improvements began to take the form of robust and optimal control of active systems [72]. The ability to actively control and update hMCL performance in real-time provides methods of subjecting VADs and other MCS devices to varying levels of simulated patient heart health instantaneously while maintaining a stable hemodynamic environment during device operation. Criteria to assess hMCL performance and sensitivity to operational mode changes has also been developed as a reference for future hMCL design purposes [73].

The most recent forms of hMCL innovation have been made towards the validation of onboard VAD algorithms used to detect VAD status, provide active patient monitoring, and perform VAD control adjustments during operation. For the validation of said algorithms, hMCL technology has advanced to incorporate VAD induced suction events [74], control fluid viscosity during operation [75], monitor simulated aortic valve status [76], as well as simulate an electro-cardiogram (ECG) to reproduce appropriate cardiac electrophysiology signals for ECG-triggered assist devices [77]. Further, the use of hMCLs to emulate patient specific hemodynamics for the evaluation of device intervention

scenarios is a field of increasing relevance [78].

2.2 Common hMCL Design Components

Existing hybrid mock circulation loops commonly use pneumatics for active pressure generation, which is accomplished through a series of regulating valves connecting high and low pressure tanks to the pressure chamber. Inherent nonlinearities in these systems can provide difficulties in both modeling and control applications. A remedy for these nonlinearities include using electro-mechanical actuators, such as linear voice coils, which simplify dynamic models and provide increased control bandwidth. However, allowable pressure range is often limited compared to pneumatic counterparts. Passive components for hMCLs include hydraulic chambers or accumulators, which act as passive compliances, and tubing, which acts as an inductance.

In closed loop hMCLs, such as in [37, 73], a recirculation or back-flow pump is required to regulate fluid height in the chambers surrounding the VAD cannula connections. Open loop hMCLs, such as in [72], use an accumulator from which fluid is pumped and rely on inlet and outlet positive displacement pumps for fluid and pre-/after-load regulation. Typical sensors for hMCLs include pressure sensors at each pressure chamber connected to the device under test, fluid height sensors, as well as a flow sensor to measure VAD flow output.

2.3 Verification and Validation of VADs

Implantable VADs require a range of rigorous benchtop tests, from assessing bio-compatibility to testing sensors, actuators, and controllers. Only after such testing is a VAD found suitable for in vivo testing on animals, which is essential for evaluating thrombogenicity, and ultimately proven suitable for clinical testing on humans. Modern VADs are increasingly incorporating more sophisticated sensing and control technology, including algorithms for online device and patient diagnostics. This trend is driving a demand for advanced methods for benchtop testing, motivating the development and use of HIL methods for mock loops, or hybrid mock circulatory loops (hMCL), over the past decade [37, 65, 66].

Unlike its application in aerospace, automotive, and electrical power systems applications, for example, the use of HIL for mock loops is relatively new. Researchers have experimented with various configurations to manage the interface between a LVAD under test and a real-time simulation of the CVS [37, 66, 68, 79, 80]. Nevertheless, guidelines for design have yet to be established. These guidelines should arise from requirements based on the range and types of physiological conditions that need to be simulated. For these reasons, hMCL systems have been suggested for evaluating LVAD systems under a wider range of conditions than possible with conventional mock loops. A fully hybrid mock circulatory loop has the capacity to generate pressure and flow conditions at the two port connections of a VAD under test that make it appear the system is implanted in a human CVS. This would make it possi-

ble to test different patient conditions (sleep, exercise), arrhythmias, disease states, as well as different patient sizes (from infant to large adults).

Building a HIL system requires designing an appropriate interface that matches the device under test to the computational environment. This interface, or interface algorithm [81], is comprised of sensors, actuators, and feedback control. For a hMCL, for example, the interface should have a bandwidth that enables operating over the expected frequency content required. It is also important to use a suitable real-time simulation model of the CVS, and for the design of the system not to degrade the accuracy or overall stability. Indeed, since mock circulatory loops play a key role in the LVAD regulatory process, reliable operation and achievable levels of accuracy are essential. These methods should be factored into development of a hMCL, adopting metrics on performance that form part of a process of certifying these test environments for VAD benchtop testing. Recent studies in related areas of physiological benchtop testing have reported on similar work toward use of HIL in testing suitable for regulatory processes [82–84].

Chapter 3

Modeling and Construction of Electro-Mechanical hMCL

This chapter presents the methodology used to design and construct an electro-mechanical hybrid mock circulation loop. Hardware, software, and dynamic modeling of the hMCL system are presented along with real-time control discussion.

3.1 Design Criteria

Improvements in VAD and other assist device technologies has led to the increasing use of mock circulation loops for in vitro performance assessment and validation. Methods to qualify the performance of MCLs themselves have widely been based off independent researcher goals with little consensus on design objectives or performance qualification. In recent years, however, design objectives have been added to ISO Standard documentation, for example the Annex BB section of ISO/DIS 14708-5 includes recommended physiological operation ranges for MCLs [85]. Table 3.1 lists these recommended operational ranges, which includes both hydraulic system design and biological human blood considerations.

Table 3.1: ISO Standard recommended physiological operation ranges for mock circulation/circulatory loops.

| Parameter | Range |
|---------------------------------------|----------------------|
| Systolic to Diastolic Ratio: | 2:3 (at 72 BPM) |
| Body temperature: | 35 °C to 40 °C |
| Salt concentration: | 0,9 % NaCl |
| Blood pH: | 7,15 to 7,5 |
| Haematocrit (%) | 20 to 50 % |
| Blood fluid viscosity ^{a)} : | 2,3 to 3,4 mPa*s |
| Flow-rate range: | 2,5 L/min to 8 L/min |
| Mean Arterial Pressure (mmHg) | 55 to 110 |
| PULSE PRESSURE (mmHg) | 2,5 to 55 |
| Heart Rate (BPM) | 55 to 125 |

For the purposes of designing an hMCL for in vitro applications, the criteria of most relevance are the hydraulic considerations of pressure, flow, and heart rate (which relates to the allowable frequency or bandwidth of pressure generation). In general, accurate biological parameters (such as blood pH or haematocrit %) are of importance when validating an assist device's thrombogenicity or blood shearing levels. These biological test considerations, however, are not typically utilized during nominal device hardware and software test conditions because of their inherent safety concerns (the use of biological agents require special health, safety, and maintenance procedures). Further, methods to recreate blood-like conditions, such as the use of water/glycerin solution to emulate accurate blood viscosity, can be done such that biological agents are not required.

In this work, the design criteria of importance used to develop the hMCL were the pressures, flow-rate, and heart rate. All recommended operational ranges

for these parameters have been met in the hMCL developed here.

3.1.1 hMCL Design

A schematic of the hMCL setup is shown in Figure 3.1. A real-time model of the cardiovascular system (CVS) is used to simulate hemodynamics for any patient condition (see Figure 3.3) and is used to define the reference pressures for the loading pressures on the VAD, from the left ventricle inflow and the arterial outflow. The pressures dictated by the model are passed as reference signals to be tracked by the interface actuators using tracking feedback controllers. Finally, the realized pressures in each pressure chamber couple directly to the VAD (hardware under test), thereby allowing testing under different physiological conditions. Such an approach allows variations in CVS parameters (such as Systemic Vascular Resistance (SVR)), and facilitates not only functional testing of the VAD device, but also testing of advanced onboard sensing and estimation algorithms on the VAD.

A prototype hybrid mock loop is pictured in Figure 3.2. This system is made up of the following components: an aortic (1) and left ventricular (2) pressure-generating interface (PGI) each housing a respective electromagnetic voice coil actuator (3 & 4), a positive displacement gear pump for fluid recirculation (5), a continuous flow VAD equivalent (6), a data acquisition and MCL controller (not pictured), and a computer running Windows operating system (not pictured). The mock loop also has an air release system for when the MCL is filled. The air release system is comprised of $\varnothing_{ID} = 0.75$ inch tygon tubing

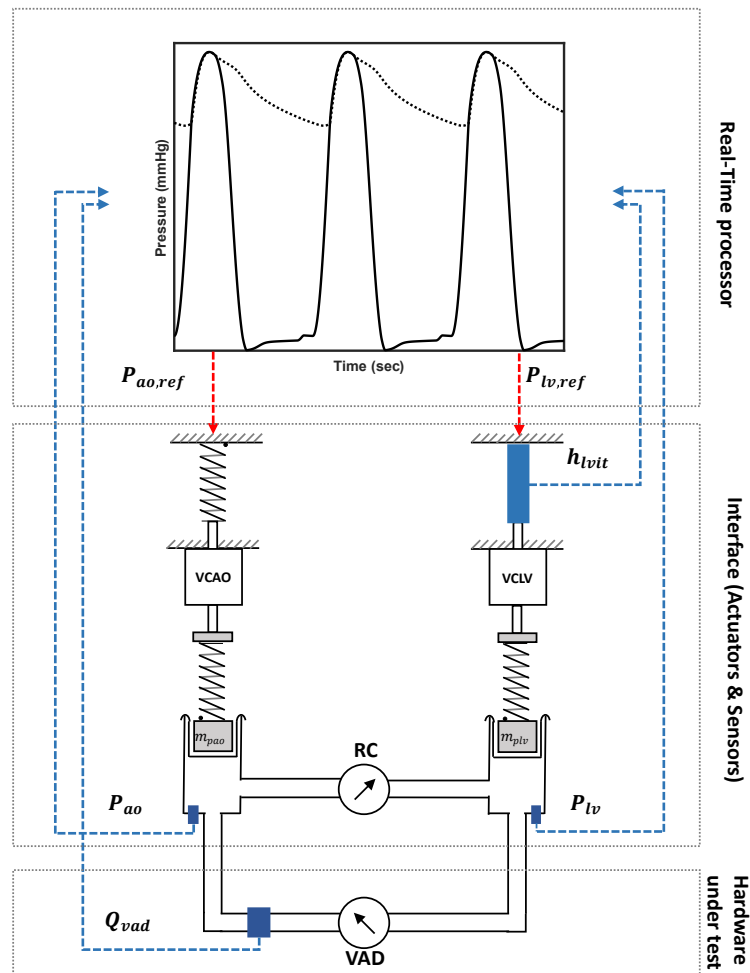


Figure 3.1: Schematic of the hMCL setup. Red arrows show reference pressures generated by a simulated model of CVS, while blue boxes and arrows represent sensors that provide the feedback signals returned to the real-time processor.

and a pressure release valve at the top which has a buoyant latch that closes when the remaining air in the loop has been forced out as the loop is filled to capacity.

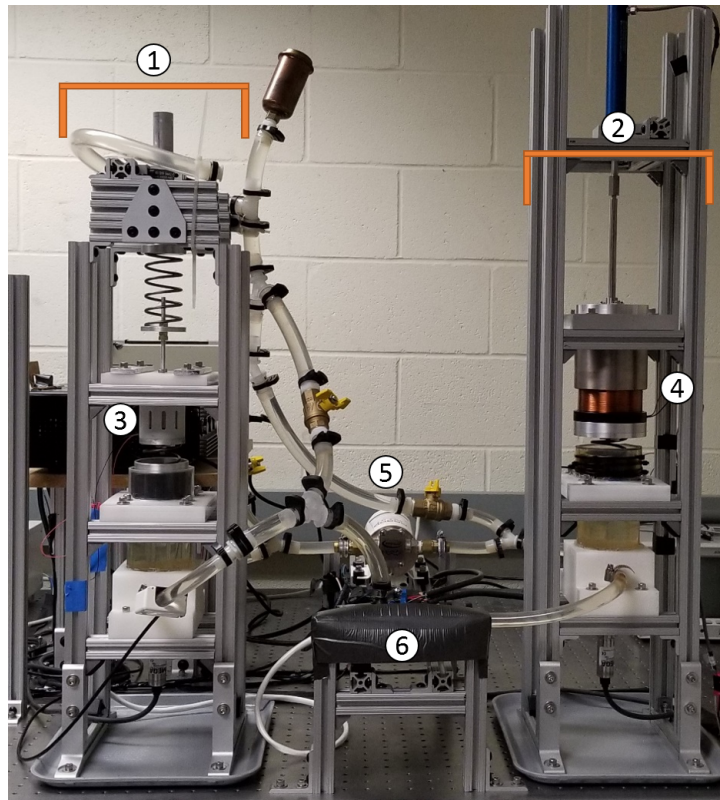


Figure 3.2: hMCL setup - numbered items are discussed in text

3.2 hMCL Materials

3.2.1 Hardware

The hardware associated with building the hMCL is discussed in this section.

Pressure-generating interfaces

An hMCL requires an actively controlled means for managing the pressure and flow at the LVAD fluid ports. Several investigators have demonstrated the utility of pneumatically-driven pressure chambers, however, the desire to

eliminate the need for an air supply and work toward a smaller test setup footprint suggested use of electromagnetic voice coil actuators (MotiCont HVCM-Series, MotiCont, Van Nuys, CA). These actuators can provide sufficient force to generate physiological pressures and can be controlled at high frequencies. In addition, voice coil actuators can also be readily modeled using linear relationships. These factors are desirable so the dynamics of the actuator can be accurately accounted for in simulations and experimental control applications.

Each pressure generating interface (PGI) is formed using an amplifier (Pololu High-Power Motor Driver 36v9, Pololu Corporation, Las Vegas, NV) that conditions a low power 20 kHz duty cycle output (digital output, cRIO controller, National Instruments, Austin, TX) into a higher power signal to drive the voice coil. The voice coil actuator is aligned above a sealed pressure chamber (height = 4 in, \varnothing = 3 in) made of polymethyl methacrylate (PMMA). Between the base of the actuator and the water within the pressure chamber is a tempered steel compression spring housed in an aluminum piston. The piston uses a rolling diaphragm (Bellofram Diaphragms, Class 4, Bellofram Corporation, Newell, WV) with 2.37 inches of allowable travel distance to keep the piston/spring/actuator combination in constant contact with the surface of the water within the pressure chamber. In this hMCL realization, different size voice coil actuators were used for the AO and LV PGIs, having maximum continuous force output of 29.4 N and 72.4 N, respectively. These limits correspond to peak pressures of 48 mmHg and 119 mmHg, respectively, based on the effective area of the diaphragm/piston combination.

The AO PGI incorporates an identical spring above the voice coil actuator, as can be seen in Figure 3.1. In this design, the initial deflection in the top spring can be manually set by lowering the support structure in which it is housed before actuation. By compressing the top spring, the subsequent pressure in the entire hMCL is increased and acts as a DC pressure offset. Also, utilizing position control of the LV voice coil piston, the amount of static pressure in the system can be increased or decreased by setting the desired height lower or higher, respectively. As the voice coil height decreases, the displaced water in the hMCL is sent to the AO chamber, subsequently compressing both the bottom and top springs. This not only adds pressure to the AO PGI, but adjusts the equilibrium pressure offset of the AO chamber. Thus, before beginning the pressure tracking control process in the hMCL, the height of the LV voice coil piston is set such that the AO pressure offset is centered between the maximum and minimum AO pressure reference signals. Utilizing this method of actuation allows for the minimization in the required size of the actuator needed in the AO PGI, hence the 48 mmHg pressure generation capacity. However, it requires the height of the LV voice coil piston to be precisely controlled during actuation.

For future hMCL designs, it would be desirable to have guided voice coil actuators with linear bearings. This preliminary design, however, utilized hollow core voice coils which required external linear bearings to keep the actuator coil and permanent magnet housing concentric. The aortic PGI has a Delrin[®] acetal resin slotted sleeve that is epoxied to the actuator coil to maintain con-

centricity with the permanent magnet housing. The left ventricular PGI uses a hardened steel shaft with linear flange bearings to maintain concentricity.

In order to track piston position and subsequent fluid height level, an LVIT sensor (LDI-127 Series, Omega Engineering, Inc., Norwalk, CT) was connected to the hardened steel shaft on the LV PGI. It is relevant to note from the schematic in Figure 3.1 that the LV PGI does not employ an additional spring as used for the AO PGI. It was decided to deploy two different designs in order to assess any advantage in using the top spring to adjust the mean pressure, or DC pressure offset, in the system. This enabled us to evaluate the impact on performance by these two designs, particularly with respect to controlled pressure tracking.

VAD under test

A centrifugal, continuous flow pump (Iwaki NRD-12-TX24, Iwaki America Inc., Holliston, MA) is used to represent a continuous flow VAD under test. This pump is connected to the PGIs with $\varnothing_{ID} = 0.5$ inch tygon tubing. The mock loop design allows for the centrifugal pump to be disconnected and replaced with any cannulated VAD or VAD equivalent by clamping the input and output lines.

Recirculation pump

A positive-displacement gear pump (Marco UP9-P, Marco s.p.a., Brescia, Italy) is used to regulate fluid height of the LV PGI based on LVIT sensor

measurements. The fluid is drawn from the AO chamber and recirculated back to the LV chamber. The recirculation pump is powered using 20 kHz PWM output from the hMCL controller. The PWM signal is also amplified using a Pololu 36v9 motor driver.

3.2.2 Software

The MCL is run on a computer with a Windows 10 operating system using real-time NI LabVIEW 2018 software and a NI CompactRIO (cRIO) data acquisition device (CompactRIO-9034, National Instruments Corporation, Austin, TX). The NI cRIO is responsible for simulating the numerical circulation model, acquiring sensor input, filtering measurements, and controlling the output of the mock loop all in real-time at the FPGA level.

Cardiovascular model

A lumped-parameter model of the cardiovascular system (CVS) is used to simulate patient hemodynamics. Many CVS models have been reported in the literature, and for the purposes of the testing on this hMCL the lumped parameter model documented in Gohean et al. [86] was used. A circuit analog depiction of the CVS model is provided in Figure 3.3. This model has been used to evaluate different patient conditions and disease states, and verified against experimental data. An advantageous feature of using a lumped parameter CVS model is that it is possible to adjust each parameter value for various levels of patient heart health to be simulated. Further, these parameter values

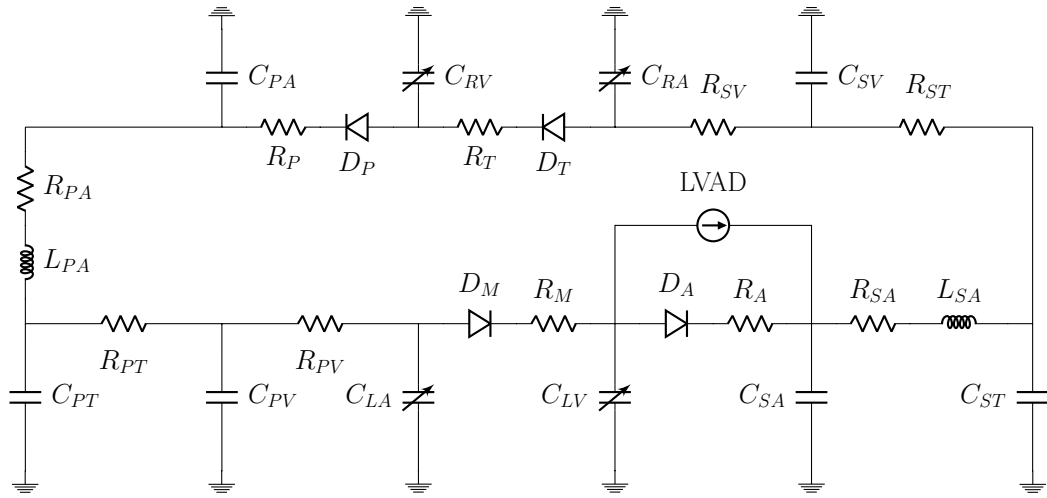


Figure 3.3: Circuit analog of reference model used to simulate the CVS in real-time on the hybrid mock circulatory loop

can be adjusted instantaneously or over time during hMCL operation to emulate deteriorating or recovering patient health conditions. Lastly, the use of passive, linear elements in both the systemic and pulmonary circulations helps reduce the order of the model and simplify the dynamics of the system. It is for these reasons that this CVS model was chosen for use in both simulation and for implementation in the hMCL.

The CVS model is numerically-integrated using a forward-Euler method at a frequency of 5 kHz. Measurements of aortic pressure, left ventricular pressure, VAD flow rate, and left ventricular piston height from the hMCL are taken at a rate of 5kHz as well. The VAD flow, as detected by a ME-11PXL Transonic flow sensor, is treated as a measured disturbance in the CVS model and is used as an input for every iteration of dynamic model propagation (as shown in Figure 3.1). The PGI and recirculation control loop rate is 2 kHz. The

controller was designed at a slower rate than that of the model in order for low- and high-pass filters (with cutoff frequencies set to 30 Hz) to be implemented. By running the controller at 2kHz, the lag incurred from the filters is minimized allowing for higher fidelity in reference output and for the mock loop to run in real-time.

3.3 Cardiovascular Model Simulation

The dynamic equations for the CVS model (provided in detail in [86]) were simulated in MATLAB 2018a software using the ordinary differential equation solver ‘ode23’ for various levels of mean VAD flow rate. As detailed in the reference, sample cardiovascular parameter values have been provided to simulate both ‘healthy’ and ‘heart failure’ cases in the simulated patient. Results from the CVS model using both healthy and heart failure (HF) patient parameters can be seen in Figure 3.4 for 0 LPM and 3.5 LPM of mean VAD flow support cases.

One consideration for hMCL CVS model simulation improvements is the addition of VAD specific dynamics. Since VAD flow is modeled as a measured disturbance, it is set manually for the simulation. This could be further extended for any documented VAD pressure-flow (P-Q or H-Q) curves such that simulated VAD output varies based on the differential pressure across the pump. Note: when implemented in the hMCL, the measurements from the Transonic flow probe are used in each iteration of dynamic model propagation,

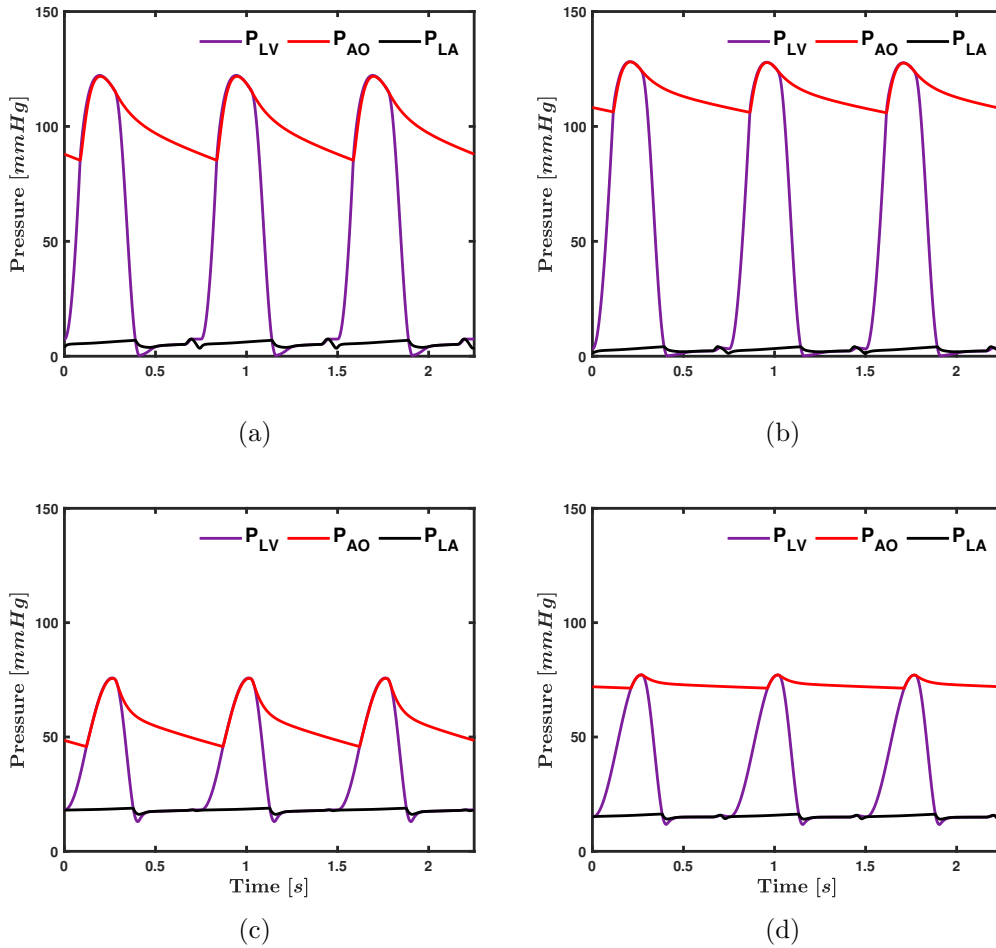


Figure 3.4: Simulated CVS model results using healthy patient parameters for (a) 0 LPM and (b) 3.5 LPM of VAD flow support. Simulated CVS model results using heart failure (HF) patient parameters with (c) 0 LPM and (d) 3.5 LPM of VAD flow support.

thus accounting for the actual VAD pressure-flow relationship during in vitro evaluation.

A second consideration for hMCL CVS model improvements is to incorporate

autoregulatory mechanisms in the systemic and pulmonary circulations. Due to the use of passive, linearly modeled elements in the systemic and pulmonary circulations, it is not possible to recreate autoregulatory responses that occur in the human circulation (such as a systemic vascular resistance increase due to VAD over-pumping). While this update would provide a more accurate hemodynamic realization around the VAD, the increased computational demand on the real-time controller is a consideration that must be accounted for as CVS model complexity increases.

3.4 Electromechanical hMCL system model

The linear state space representation of the hMCL system is summarized in the following set of equations.

$$\text{States: } \mathbf{x}(1 : 4) = [i_{ao} \quad x_{1,ao} \quad v_{ao} \quad x_{2,ao}]^T$$

$$\mathbf{x}(5 : 8) = [v_{pao} \quad x_{dao} \quad V_{ao} \quad V_{lv}]^T$$

$$\mathbf{x}(9 : 13) = [x_{dlv} \quad v_{plv} \quad x_{1,lv} \quad v_{lvt} \quad i_{lv}]^T$$

$$\text{Inputs: } \mathbf{u} = [u_{ao} \quad u_{lv} \quad Q_{rc}]^T$$

$$\text{Disturbances: } \mathbf{\Gamma} = [Q_{vad} \quad g]^T$$

$$\text{Dynamics: } \dot{\mathbf{x}} = A\mathbf{x} + B\mathbf{u} + E\mathbf{\Gamma}$$

$$\text{Measurements: } \mathbf{y} = [P_{ao} \quad P_{lv} \quad h_{LVIT}]^T = C\mathbf{x} + D\mathbf{u} + F\mathbf{\Gamma}$$

In the above equations, i_{ao} and i_{lv} are the currents induced in the aortic and

left ventricle voice coil actuators. The extension in the top spring (refer Figure 3.1) and compression in the bottom spring on the aortic side is represented by $x_{1,ao}$ and $x_{2,ao}$, respectively. The compression in the spring on the left ventricle side is represented by $x_{1,lv}$. x_{dao} and x_{dlv} represent the amount of deformation due to compression in the rolling diaphragms on the aortic and left ventricle chambers, respectively. V_{ao} and V_{lv} are the aortic and left ventricle chamber volumes. The velocity of the voice coil actuator for the aortic and left ventricular side is represented by v_{ao} and v_{lv} , respectively. The inputs to the system are the voice coil voltages, represented here by u_{ao} and u_{lv} for the aortic and left ventricle voice coil, respectively. Q_{rc} is the flow that can be delivered by the recirculation pump. Acceleration due to gravity, g , and the VAD flow rate, Q_{vad} , are treated as disturbances for the system.

All parameters related to commercial off the shelf components in the system (such as pumps, actuators) were taken from the provided data sheets. The spring compliances and losses (assumed linear) were characterized using steady state tests. Along with the state space representation, the system can be represented using a bond graph that captures the flow of power between all the elements. The bond graph representation of the hMCL system model is provided in Figure 3.5. This bond graph is not fully annotated, meaning that not all bond variables are indicated. However, causality is assigned, identifying the key state variables summarized in this section. Dynamic equations for this 13 independent element system were derived using principles of bond graph modeling [87] and can be found in Appendix B.

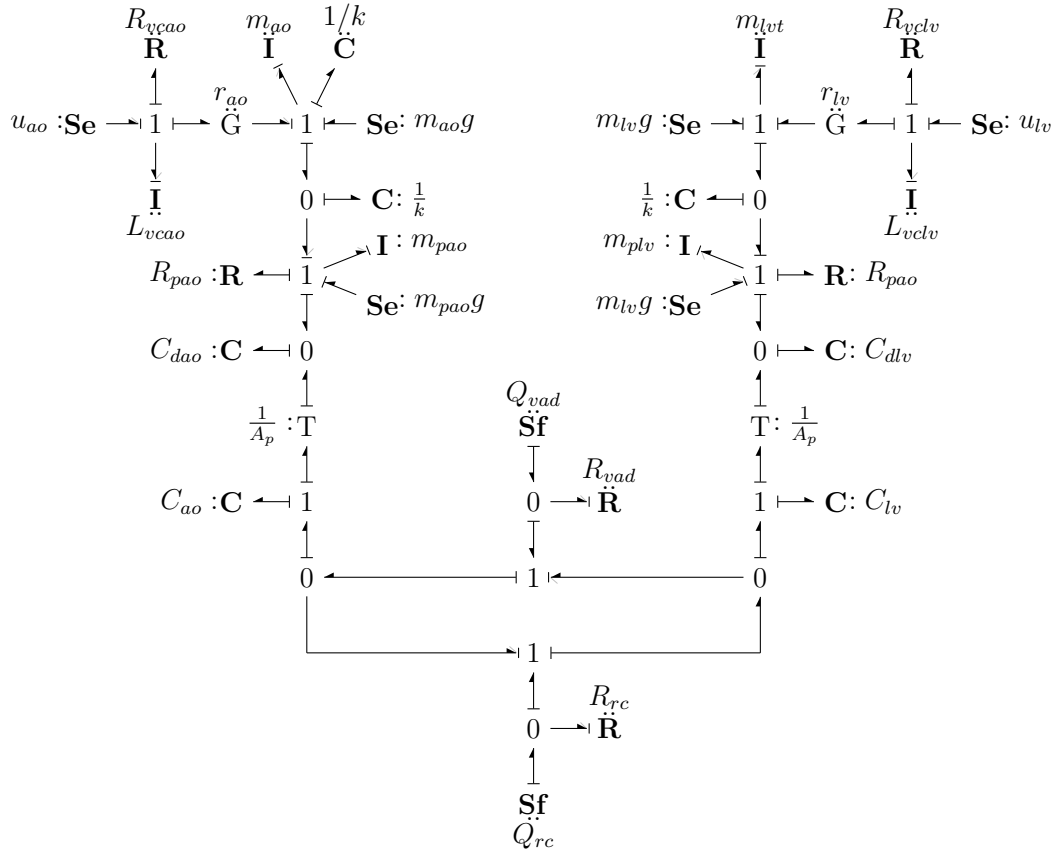


Figure 3.5: Bond graph of the hMCL

3.5 Control

3.5.1 Model analysis and control structure

The linear 13 state model of the system was analyzed using the Control System Toolbox on MATLAB R2018a (The MathWorks, Inc., Natick, Massachusetts). The MIMO model has 3 inputs and 3 outputs. The structure of the system suggests that the recirculation (RC) pump could be used to maintain the LV PGI around a desired operating range of height. This would ensure that

there is always sufficient range of motion for the voice coil actuators, which could then be used to generate reference pressures. The elimination of the RC pump's contribution to controlling the pressures leaves us with 2 inputs and 2 outputs. To verify if independent SISO controllers can be applied to a MIMO system, we must ensure that the control loops, namely the feedback loop controlling P_{ao} and the feedback loop controlling P_{lv} , are decoupled (i.e, do not interact with each other in the frequency range of interest). The Relative Gain Array (RGA) can be used to study such a level of interaction over a frequency range [88]. The RGA matrix, which is evaluated at a particular frequency, gives us a measure of the interaction between feedback loops in our system. The magnitude of each element of this matrix, represented by $|\lambda_{ij}|$ represents the level of interaction between the i^{th} output and the j^{th} input. A magnitude close to 1 would represent strong interaction, while a magnitude close to 0 would imply weak interaction. The magnitude of the RGA elements for the 2x2 MIMO subsystem (with the removal of RC pump as discussed above), are plotted against frequency in Figure 3.6. For both the actuators, the relative gain magnitude of each pressure (P_{ao} and P_{lv}) is shown in dB. As stated in [37], maximum actuator bandwidth required to generate physiological pressures is up to 15 Hz for the aortic pressure and up to 30 Hz for ventricular pressure. In that operating range (94.25 rad/s to 188.5 rad/s), it is clear from Figure 3.6 that the relative magnitudes are at least 50 dB apart. This result allows us to conclude that in the frequency range of interest, the two feedback loops are sufficiently decoupled.

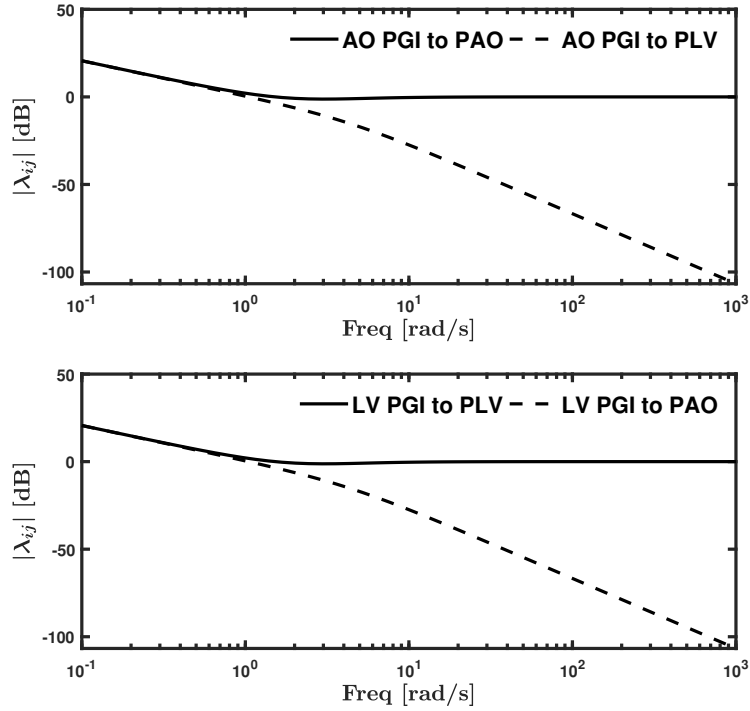


Figure 3.6: Magnitude of RGA elements [dB] for (a) AO PGI to LV Pressure (b) LV PGI to AO pressure

With the insights provided by this analysis, the controller was structured to comprise of two independent PID controllers. Each of the AO and LV PGI voice coils use the low-pass filtered pressure measurement from its respective pressure chamber to calculate error and actively control pressure. A third PID controller is incorporated to allow the RC pump to regulate the LV voice coil height around a desired mean value. Due to delays inherent in the use of low-pass filtering measurement data the realized pressures usually lag behind the reference pressure in phase. A part of this phase lag can be overcome by incorporating an input-delay to the reference signals sent to the PID pressure

controllers. After visual inspection and experimental validation, it was deemed that an input-delay of 20ms significantly minimized the error due to phase lag. For the aortic pressure controller, proportional gain scheduling was used to keep the closed-loop system eigenvalues in the open left hand complex plane as VAD flow increased. Lastly, each independent controller incorporates integrator anti-windup to prevent the integrator build-up during moments of output saturation. The complete control structure is shown in Figure 3.7 in block diagram form and controller gains are detailed in Table 3.2.

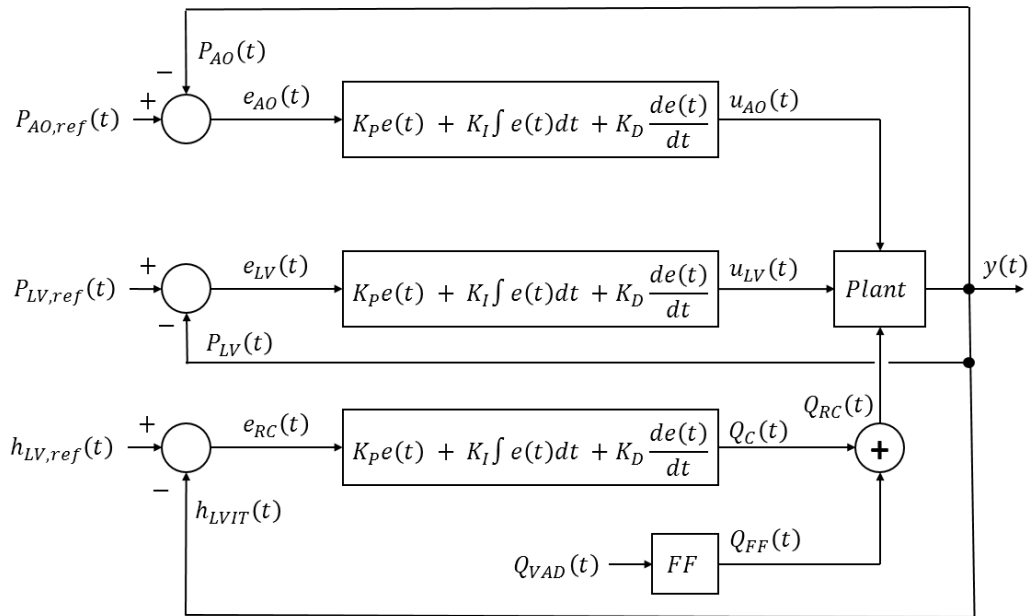


Figure 3.7: Block diagram structure of PID control with available recirculation pump feed forward. (Top) Aortic pressure controller, (Middle) Left ventricular pressure controller, (Bottom) Fluid level controller. Reference signals are generated in the numerical CVS model running in real-time with measured VAD flow.

Table 3.2: Summary of control scheme and gains for each process variable

| Process Input | Control Output | Control Scheme | Gains | Units |
|---------------|----------------|-------------------------------------|------------------|-----------------------|
| P_{ao} | u_{ao} | PID with K_P gain scheduling | $K_P^* = 3.7e-2$ | $[Duty/mmHg]$ |
| | | | $K_I = 5.1e-4$ | $[Duty/mmHg \cdot s]$ |
| | | | $K_D = 9.1e-4$ | $[Duty \cdot s/mmHg]$ |
| P_{lv} | u_{lv} | PID | $K_P = 6.50e-2$ | $[Duty/mmHg]$ |
| | | | $K_I = 1.35e-4$ | $[Duty/mmHg \cdot s]$ |
| | | | $K_D = 1.55e-2$ | $[Duty \cdot s/mmHg]$ |
| h_{lvit} | Q_{rc} | PID with feedforward from Q_{vad} | $K_P = 3.1e-1$ | $[Duty/mmHg]$ |
| | | | $K_I = 8.5e-4$ | $[Duty/mmHg \cdot s]$ |
| | | | $K_D = 3.0e-4$ | $[Duty \cdot s/mmHg]$ |
| | | | $FF_{vad} = 0.5$ | $[LPM/LPM]$ |

* $K_P = 5e-3$ at startup; $1.9e-2$ for $Q_{vad} < 2LPM$; $3.7e-2$ for $Q_{vad} > 2LPM$

3.5.2 Controller tuning and stability

The main objective of the hMCL is to generate the reference aortic and left ventricular pressures as defined by the cardiovascular model as closely as possible, while rejecting the disturbance due to Q_{vad} . Using the Control System Toolbox in MATLAB 2018a, preliminary gains were determined to minimize overshoot and settling time for voice coil pressure tracking. These gains were then heuristically tuned until deemed adequate according to error and overshoot calculations. The chosen control scheme was further applied to the simulated model and stability of the system was verified by confirming that the closed loop eigenvalues were in the open left half complex plane. The final gains obtained using the model based approach are summarized in Table 3.2.

Note that Q_{rc} is modeled as a flow source, but is controlled via duty cycle

similar to each voice coil actuator. Simulated control flow output in liters per minute (*LPM*) is calculated based on a linear calibration relationship to commanded duty cycle (Duty $\in [0,1]$).

Chapter 4

Evaluation of hMCL in VAD Test Applications

In the previous chapter, the prototype hMCL has been modeled, constructed, and controlled for the purpose of realizing various levels of cardiovascular function in real-time. The objective of this chapter is to apply the metrics presented here as a suggested baseline for evaluating general hMCL functionality. Additionally, the use and requirements of hMCLs to evaluate the capabilities of next generation implantable devices is discussed.

4.1 Test Overview

Multiple tests were conducted on the hMCL to examine pressure tracking performance under various VAD flow rate conditions and CVS model states.

The following list provides the experiments conducted:

1. Pressure reference tracking for mean VAD flow rates ranging from 1 - 5 LPM
2. Pressure reference tracking for healthy and heart failure CVS model set points
3. Pressure reference tracking as CVS numerical model parameter values

are adjusted in real-time

These experiments provide methods to assess the desired capabilities of the hMCL to not only track reference pressures, but also to emulate various physiological patient conditions for enhanced VAD test applications. Test #1 is a baseline metric for all hybrid mock loops used for VAD testing. It is necessary for the hMCL to track CVS reference pressures for various mean VAD flow rates in order for the device to be tested in different actuation modes. Further, evaluating hMCL performance at various VAD flow rates provides a method to assess overall disturbance rejection capabilities. The metric for performance for this test is the calculation of root-mean-square (RMS) error between the reference and actual pressures. In this dissertation, the mean and standard deviation of RMS error has been calculated per cardiac cycle for the various flow rates tested. Test #2 determines the ability of the hMCL to operate at various levels of heart health (established in the computational CVS model). The results of this test are depicted on a Pressure-Volume (P-V) plot to illustrate the physiological range of operation, as well as to again show tracking performance versus idealized P-V loops. Lastly, Test #3 determines the ability of the hMCL to update in real-time based on CVS parameter value changes. This test is geared towards evaluating VADs in changing physiological environments, as well as providing a means by which to test enhanced sensing capabilities of VADs with onboard physiological monitoring (e.g., [73, 89]).

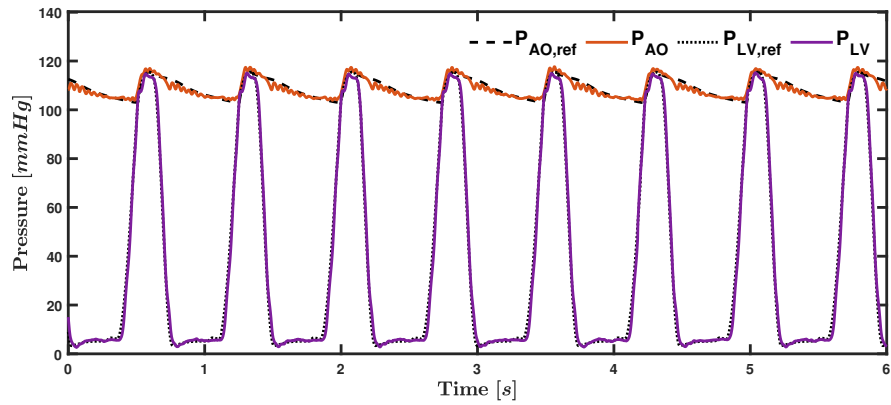
4.2 Experimental Results with Continuous Flow VAD Analog

4.2.1 Chamber Pressure Tracking

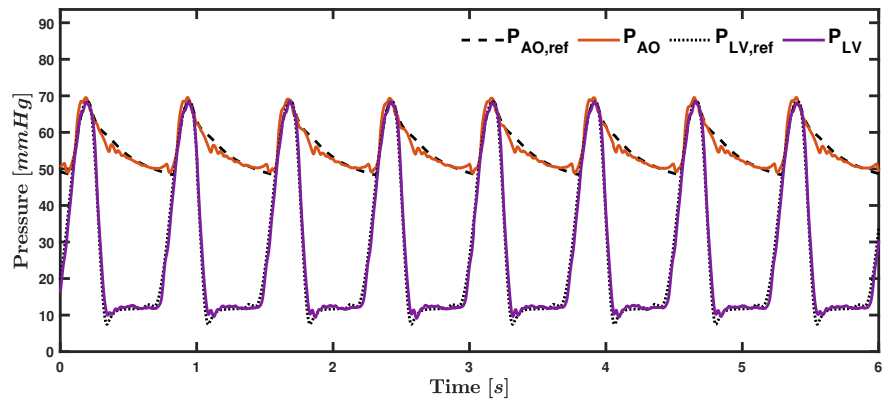
Figure 4.1 shows pressure tracking results from a typical experiment where the VAD flow rate was manually set to a mean value of 4 liters per minute (LPM) for both healthy and heart failure patient parameter set points. This experiment established the ability of the hMCL to generate and track desired physiological pressures with a known VAD flow disturbance.

As discussed in Section 3.2.2, VAD flow is modeled as a measured disturbance in the hMCL, thus the controller must be able to track physiological pressures dictated by the CVS model in the presence of this disturbance. To judge the disturbance rejection, the VAD flow rate was manually adjusted to various values ranging from 1-5 LPM. For a set VAD flow rate, the root-mean-square error (RMSE) between reference and tracked pressures was calculated for each cardiac cycle. Figure 4.2(a) shows the mean and standard deviation for these RMS errors under different VAD flow rates. At VAD flow rates above 1.52 LPM, both AO and LV pressures are tracked with mean RMS error of approximately 3 and 5 mmHg, respectively. These results reveal that at lower VAD flow rates, the RMS tracking errors for the AO PGI are marginally higher.

To improve these results, control of the hMCL was updated from the Real-Time level (i.e., high level) to the FPGA level (i.e., low level) of the cRIO. This update facilitated faster measurement logging, filtering, and subsequent con-



(a)



(b)

Figure 4.1: hMCL pressure tracking results for 4 LPM of VAD flow support using (a) Healthy and (b) Heart Failure (HF) CVS model parameter set points.

trol frequency (2kHz vs 500 Hz). The results of moving the control hierarchy from the Real-Time (RT) level to the much faster, programmable FPGA level can be seen in Figure 4.2(b) where mean RMS pressure tracking errors have been reduced to 1.42 and 3.13 mmHg for the AO and LV, respectively. Additionally, overall standard deviation between cardiac cycles has been greatly

reduced at all VAD flow rates tested. These improvements allowed for stable pressure tracking below the previous minimum of 1.52 LPM mean VAD flow as seen in 4.2(a).

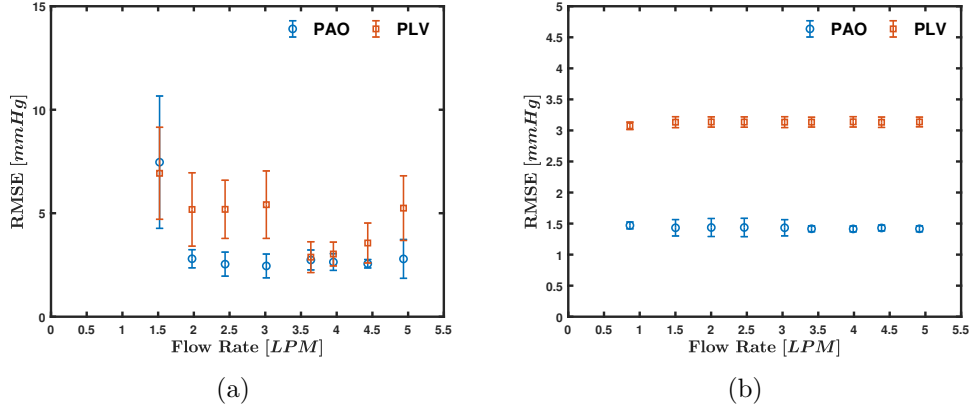


Figure 4.2: Mean and standard deviation of RMS pressure tracking errors per cardiac cycle versus various VAD flow rates for simulated HF patient. Previous RT level controller results are shown in (a) for comparison with updated FPGA level controller results shown in (b).

4.2.2 P-V Loop Generation

For potential VAD validation applications, it is necessary for the hMCL to be able to simulate various levels of heart health. The hMCL was tested using healthy and heart failure conditions as described in [86]. The results of the experiment have been presented as Pressure-Volume (P-V) loops in Figure 4.3 to show the model output versus the realized pressure in the loop. In this figure, the healthy and HF pressure signals are directly measured from the LV pressure transducer, while the volume is computational determined each

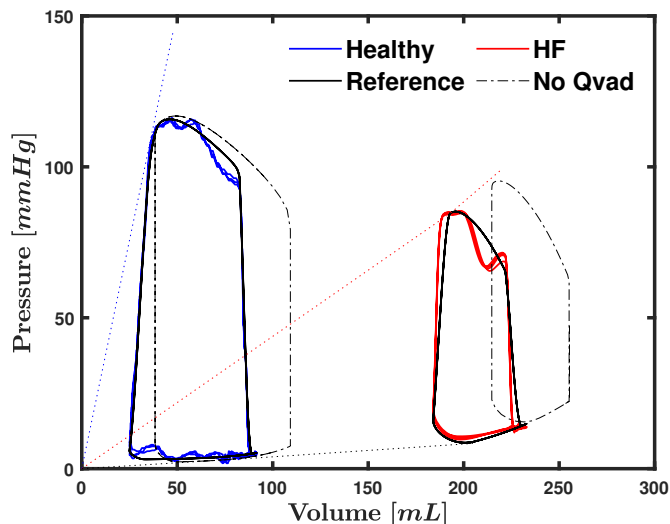


Figure 4.3: P-V loop generation for healthy and failure (HF) heart conditions at a VAD flowrate of 4 LPM. Healthy and HF signals are plotted using measured LV pressures and CVS model propagated LV volumes. Reference signals are plotted using CVS model propagated LV reference pressures and volumes. Respective baseline P-V loops are also shown for 0 LPM VAD flow cases.

step of the numerical solver. The reference signal utilizes the LV pressure references being sent from the hMCL controller to the voice coil actuators. It can be seen from the figure that the hMCL can recreate both healthy and heart failure conditions within the loop with notable error occurring only around the beginning of the ejection phase. Furthermore, by updating the lumped parameter values within the numerical CVS model, it is possible to slowly transition to any set point between the two.

To further explore the hMCL performance capabilities for tracking simulated patient heart failure (HF), P-V loops were generated for various VAD flow rates. As VAD flow rate changes, the measured flow rate is propagated forward

in the CVS model, thus adjusting the idealized P-V relationship. Figure 4.4 shows LV tracking performance for a wide range of VAD flow rates while operating using HF patient cardiovascular parameters at a heart rate of 80 BPM.

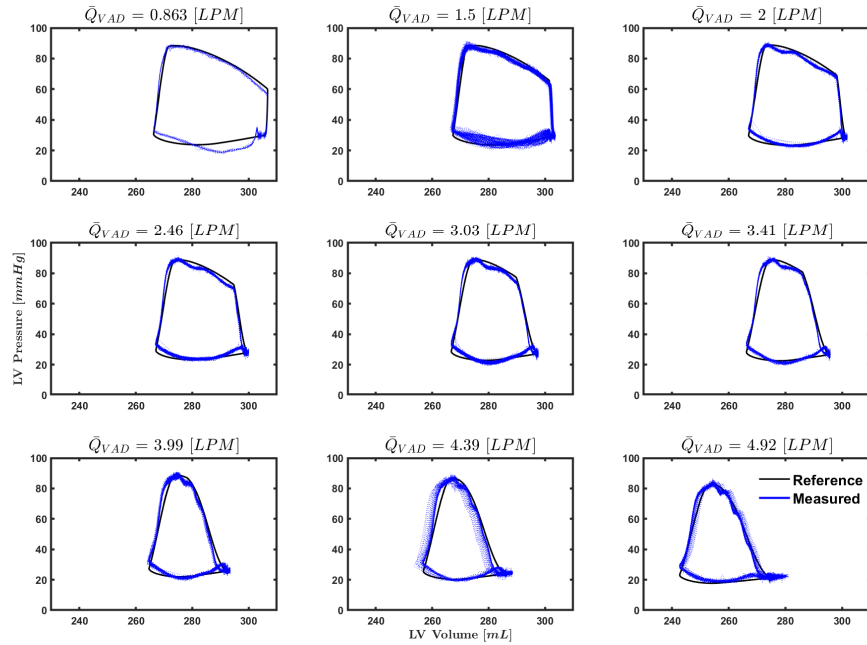


Figure 4.4: Left Ventricle P-V loop generation for failure heart conditions at various VAD flow rates. Experimental signals are plotted using measured LV pressures and CVS model propagated LV volumes. Reference signals are plotted using CVS model propagated LV reference pressures and volumes.

4.2.3 CVS Model Parameter Sensitivity

For the use of onboard estimation algorithms in next generation VADs, it is necessary for the hMCL to be sensitive to CVS parameter changes during op-

eration. Changes made to the numerically simulated CVS result in changes in load on the VAD under test, allowing for the hemodynamic changes to be measured and evaluated. In this test, the CVS parameter value of systemic vascular resistance (SVR) was increased between multiple physiologically feasible magnitudes during hMCL operation. Figure 4.5 depicts the result of this test with the value of SVR at the top, followed by the CVS model propagated reference pressure in the middle, and the hMCL realized pressures at the bottom.

4.3 Test Discussion

Using a model-based approach, a hybrid mock circulation loop was designed and developed for VAD benchtop testing. Starting with the dynamic model of the HIL system, the dynamics and cross-coupling between the pressure chambers were analyzed to determine a suitable method for control of the hMCL, with emphasis on tracking CVS pressures in the PGIs. The RGA analysis results show that, at nominal CVS pressure frequencies, independent controllers can be used for pressure tracking control. The independent PID controllers were first evaluated using a simplified hMCL dynamic model and, once pressure tracking was achieved, to the full hMCL dynamic model. Results from simulation studies showed closed loop stability and provided close agreement with regard to pressure tracking, justifying use of independent PID controllers on the physical hMCL setup. Since a main requirement of the hMCL is to generate physiological pressures and flows when interfacing with the test VAD,

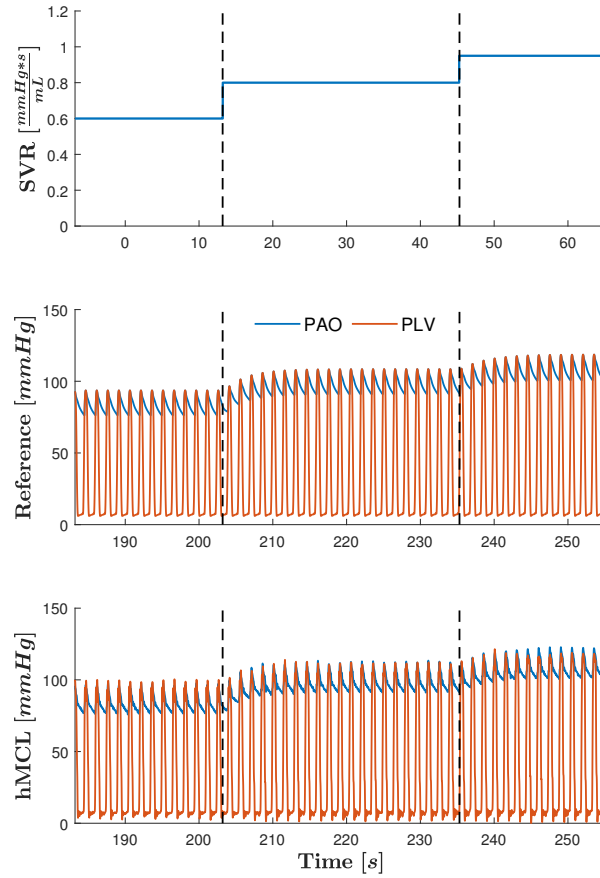


Figure 4.5: Pressure tracking response to sudden changes in systemic vascular resistance (SVR). Top: SVR parameter value, Middle: CVS model reference pressures, Bottom: hMCL realized pressures

disturbance rejection and performance under various physiological parameters are key metrics to evaluate the design and control approach. After a control scheme using independent PID controllers was implemented and heuristically tuned, experiments on pressure tracking were conducted and results analyzed

as follows, to evaluate key performance metrics:

- Reference and measured pressure signals were shown over time (Figure 4.1). Results show close agreement of the signals and demonstrate satisfactory performance of the controller.
- The RMS errors per cardiac cycle for pressure tracking were shown with their mean and standard deviation over a range of VAD flow rates (Figure 4.2). This provides insight into the disturbance rejection capability of the hMCL and operating points where hMCL accuracy could be improved.
- Reference P-V loops vs actual P-V loops were compared for both healthy heart and one in failure (Figure 4.3). The agreement between these loops can be used as another view at the capability of the hMCL to generate physiological pressures.
- A test was conducted in which the value of SVR of the CVS was stepped over three different physiologically feasible values. The subsequent pressures generated by the CVS model and those tracked by the hMCL PGIs were plotted over time in Figure 4.5. The results demonstrate sufficient fidelity of the real-time processor running the CVS simulated model to update reference pressures, and the capability of the hMCL to remain stable through these changes as it tracks both AO and LV pressures (using independent PID controllers). Preliminary investigation has shown that LVADs with on-board sensing are capable of estimating physiological parameters of the CVS [73,89]. The capability of a hMCL to simulate

changes in these physiological parameters is especially attractive when testing these modern LVAD systems.

Limitations in the current hMCL setup include the inability to generate large pressures (> 120 mmHg) using the current AO and LV voice coils. The ability to generate an increased range in pressure would be useful for example in emulating patients exhibiting hypertension. Future updates to the hMCL design include methods to improve this pressure maximum (such as using larger voice coil actuators or reducing the effective area of the PGI pressure chambers). Other such limitations can be seen in Figure 4.2(a) where mean RMS errors and standard deviations begin to increase at low and high mean VAD flow rates. Using the methods discussed here for hMCL performance qualification, updated control methods were implemented in the form of FPGA level control and the use of gain scheduling for the AO PID controller. The results of these updates were lower mean and standard deviation RMS errors, as well as an increased lower range of allowable VAD flow during pressure tracking as can be seen in 4.2(b).

As mock circulatory loops improve in design and ability, so too must the standardization of their design and performance qualification criteria. The key metrics summarized above suggest a possible framework of qualification of the performance of the hMCL. The different structures of the two PGIs in this hMCL allow us to now approach the results from an investigative lens, and infer potential advantages or disadvantages in performance of the two PGI structures. In particular, Figure 4.2 shows overall lower mean RMS errors

over a wide range of VAD flow rates for the AO PGI. Additionally, the figure suggests that the two design approaches provide similar performance regarding minimal RMS error standard deviation and keeping mean RMS error consistent regardless of VAD flow disturbance. These results can help guide future experiments as well as provide insight into where overall design improvements can be made to the hMCL, such as using a larger AO voice coil for enhanced pressure generating capability. Results can also be used to assess control method adjustments, such as the transition from real-time to the FPGA level controller, as well as the potential future utilization of MIMO methods to more optimally control the hMCL between healthy and heart failure set points. Furthermore, control methods can be analyzed (firstly in simulation) to predict if the hMCL can generate various patient conditions, including arrhythmias and disease states, for enhanced VAD operation and sensing evaluation.

Chapter 5

Estimation of SVR in hMCL

Ventricular assist devices and other forms of mechanical circulatory support have evolved to perform an increasing number of processes. These processes include the ability to log, send/receive, and evaluate data as it is collected from the device. In addition, improved computational speed provides the ability to monitor and update device operation, as well as make predictions. This chapter evaluates one such case of VAD prediction: the real-time estimation of systemic vascular resistance.

5.1 Objective

Noninvasive methods of monitoring patient health is an ongoing area of research. The sensors onboard implantable devices provide the potential to monitor and characterize patient health. In this chapter, the estimation of the cardiovascular systemic resistance (SVR) is examined using VAD based measurements while operating in a hybrid MCL. The objective of this chapter is to examine methods to accomplish this estimation using hMCLs as an initial test platform. The signal flow diagram in Figure 5.1 depicts the signal interaction between the hMCL and the estimation algorithm, as well as potential future

uses for the estimation results (dotted lines).

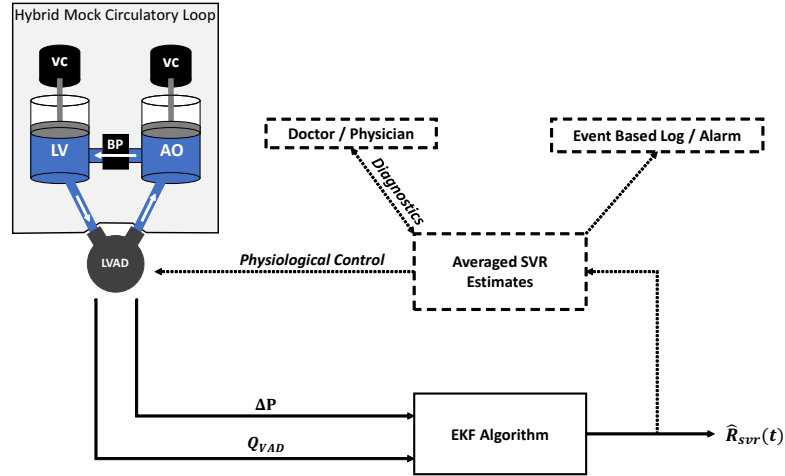


Figure 5.1: Signal flow diagram showing an LVAD in a mock circulation loop. The pump provides measurements of flowrate and pump differential pressure can be calculated from the mock loop, or sensed by the LVAD. Dotted arrows and boxes represent control, diagnostics and monitoring that could be informed by estimated SVR values.

5.2 State of the Art

With the desire to reduce the need for invasive measurements for patient health monitoring, studies have begun emerging regarding the integration of estimation techniques into the field of implantable devices. This process utilizes the onboard sensors of VADs to collect data which is then analyzed using various estimation algorithms. Currently, studies have shown positive preliminary results in developing noninvasive methods to both predict and confirm desired VAD operation [19–23]. Further preliminary studies have shown promise in the ability to estimate VAD patient physiological states or parameters with

the intent to use this information to influence the functional control of the VAD itself [24-27].

5.2.1 Measurement of SVR

Typically, SVR is found from the relation, $SVR = (MAP - CVP)/CO$, using measurements of mean arterial pressure, MAP , central venous pressure, CVP , and cardiac output, CO . Mean arterial pressure is most commonly measured using a sphygmomanometer, central venous pressure (which can be very low, normally around 4 mmHg) is measured invasively at the right atrium by a catheter, and cardiac output is measured by thermodilution techniques [90]. SVR is thus reported in units of pressure over flowrate, such as mmHg·s/mL, dynes·s/cm⁵, or Woods units (mmHg·min/L), and normal adult values range from 0.6 to 0.9 mmHg·s/mL. Techniques for less invasive approaches to estimating SVR have been reported on since the early 1970s [91, 92].

A more recent study by Lee et al. [93] used finger photoplethysmogram (PPG) along with heart rate and mean arterial pressure to estimate SVR. Wang et al. [94] also employed PPG but added a compliant PVDF sensor for externally monitoring peripheral artery size in deriving estimates of SVR. There were limitations due to motion artifact and poor signal quality in PPG. Additionally, there is a need to fine tune parameters for every patient. Nevertheless, these approaches showed promise in employing noninvasive methods for SVR estimation.

5.2.2 Model-based estimation of SVR

A patient's SVR can be estimated using built-in pump measurements combined with a model-based estimation method. In this way, no additional sensors are required. A relatively early example of model-based estimation using an LVAD was reported by Tasch et al. [95]. In this work, the sensed motor voltage and pusher plate motion in an extracorporeal pulsatile LVAD was used to estimate aortic pressure with a linear observer. The observer design required a dynamic model of the interconnected LVAD and circulatory system. A later study by Yu et al. [96] used an Extended Kalman Filter (EKF) [35] to generate optimal estimates of model states and parameters, using a systemic circulation model similar to that shown in Figure 5.2. The LVAD is represented in this model by a current (flowrate) source element. The EKF algorithm in [96] used measurements of pump volume along with arterial pressure measurement. While this implementation required an additional sensor for pressure, Yu et al. showed that the states and parameters of interest, particularly systemic resistance, R_{SVR} , could be estimated using a relatively simple CVS model with just two measurements.

5.3 Reduced Order SVR Model for Estimation

Figure 3.3 shows the reference model used for real-time simulation of the CVS in the hybrid mock circulatory loop (hMCL). This model has been effectively used to in computational studies to assess the hemodynamics subject to LVAD

support in Gohean et al. [86]. It is common when evaluating estimation algorithms using simulation to use a model with more complexity than the one used in the algorithm to generate test data. This approach allows testing the effectiveness of an EKF algorithm that uses a reduced-order model, such as the model shown in Figure 5.2, given the same inputs and measurements that would be used in practice.

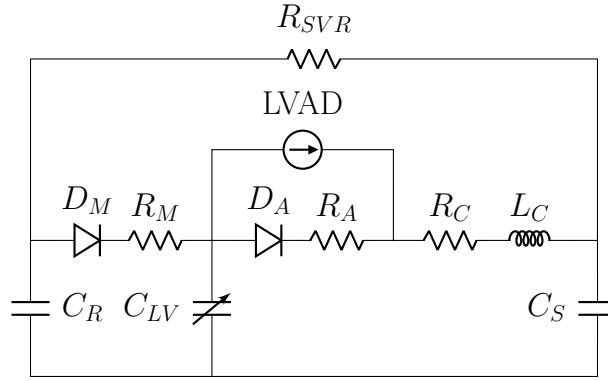


Figure 5.2: Circuit analog representation of the reduced order systemic model of the cardiovascular system: $LVAD$ flow source, R_{SVR} systemic vascular resistance, R_C aortic characteristic resistance, L_C aortic characteristic inertance, C_S systemic compliance, C_R venous return characteristic compliance, D_M mitral valve (diode), R_M mitral valve resistance, D_A aortic valve (diode), R_A aortic valve resistance, C_{LV} left ventricular time-varying compliance

5.3.1 Model Overview

Selection of the estimator model for an EKF plays a key role in ensuring the parameters and states of interest are estimable. For SVR estimation, the input to the EKF algorithm is taken here as the LVAD flowrate, Q_{LVAD} , while the measurement used to update the state and parameter estimates is

the differential pressure across the LVAD, ΔP , between the left ventricle and the aorta (reference Figure 5.2). While higher order models of the human cardiovascular system are available, they are not necessarily observable or estimable using these inputs and measurements.

Another factor in estimator model selection is the overall size and complexity of the model when intended to be deployed onto a device. The complexity of the model affects the memory capacity and processing speed at which a device can operate. For these reasons, the estimator model chosen for use in this study is adapted from the work of Yu et al. [96]. This model both allows for SVR estimation with feasible measurements and inputs from an LVAD, as well as minimizing cardiovascular model complexity.

Updating the estimator model for parameter estimation of SVR (R_{SVR}) augments the system to form, $\underline{x}_{aug} = [P_S \ P_R \ V_{LV} \ Q_{AO} \ R_{SVR}]^T$. Within the dynamic model equations, the unknown parameter, R_{SVR} , is modeled as an unknown constant plus a random walk model of bias, i.e., $\dot{R}_{SVR} = w_{SVR}(t)$, where $w_{SVR}(t) \sim N(0, Q_{SVR}(t))$. In other words, the SVR parameter dynamics are modeled as zero-mean Gaussian white noise, $w_{SVR}(t)$, with variance, $Q_{SVR}(t)$. The addition of a noise term, rather than equating the dynamics to zero, is a common way to force the EKF algorithm to continuously estimate R_{SVR} , preventing convergence in the initial transient period of the filter [97]. The EKF algorithm does require that magnitudes of the model process noise, $Q_{aug}(t)$, and discrete measurement noise covariance, R_k , be tuned appropriately. However, this can be done through simulations and sensor resolution

testing, respectively, prior to deployment on a mobile platform.

It is also important to note that the estimator model selected for this study changes according to key stages of a cardiac cycle: ‘ejection’, ‘filling’ and ‘isovolumic’ expansion/contraction. In these stages, or modes, the unaugmented system states, inputs, dynamic models, and measurements are, respectively,

$$\begin{aligned}
 \text{States :} & \quad \underline{x} = [P_S \quad P_R \quad V_{LV} \quad Q_{AO}]^T \\
 \text{Inputs :} & \quad \underline{u}(t) = Q_{LVAD}(t) \\
 \text{Dynamics :} & \quad \dot{\underline{x}}(t) = \underline{f}(\underline{x}(t), t, \underline{u}(t), \dot{\underline{u}}(t)) \\
 \text{Measurements :} & \quad \Delta P(t) = \underline{h}(\underline{x}(t), \underline{u}(t), \dot{\underline{u}}(t))
 \end{aligned}$$

where the vector functions \underline{f} and \underline{h} , as referenced in Table 5.1, depend on the stage of the cardiac cycle and are defined in 5.3.2. In these relations, P_S represents the pressure of the systemic circulation corresponding to the pressure at the systemic compliance, C_S . P_R is the pressure at compliance C_R , which represents the lumped parameter characterization of the venous return to the left ventricle. V_{LV} is the volume of the left ventricle at time-varying compliance, C_{LV} . And Q_{AO} is the aortic flow through the aortic characteristic inertance, L_C . Finally, ΔP is the difference between the left ventricular pressure and the aortic pressure at the outlet connection of the LVAD. Other forms of the estimator model can be adopted and investigated, and these would require a change in the EKF algorithm design.

5.3.2 Model Equations

The functions \underline{f} and \underline{h} for each stage of the cardiac cycle of the estimator model are summarized here. The switching criteria is based on the status of the aortic and mitral valves, which are represented by the diodes D_A and D_M , respectively, in Figure 5.2. A diode value of 1 suggests an open valve, whereas a diode value of 0 suggests a closed valve.

Ejection ($D_A = 1$, $D_M = 0$)

State equations :

$$\dot{P}_S = \frac{Q_{AO}}{C_S} - \frac{P_S - P_R}{C_S R_{SVR}} \quad (5.1)$$

$$\dot{P}_R = \frac{P_S - P_R}{C_R R_{SVR}} \quad (5.2)$$

$$\dot{V}_{LV} = -Q_{AO} \quad (5.3)$$

$$\dot{Q}_{AO} = \frac{1}{L_C} (P_{LV} - R_A(Q_{AO} - Q_{LVAD}) - R_C Q_{AO} - P_S) \quad (5.4)$$

Measurement equation :

$$\Delta P = R_A(Q_{AO} - Q_{LVAD}) \quad (5.5)$$

Filling ($D_A = 0$, $D_M = 1$)

State equations :

$$\dot{P}_S = \frac{Q_{LVAD}}{C_S} - \frac{P_S - P_R}{C_S R_{SVR}} \quad (5.6)$$

$$\dot{P}_R = \frac{P_S - P_R}{C_R R_{SVR}} - \frac{P_R - P_{LV}}{R_M} \quad (5.7)$$

$$\dot{V}_{LV} = \frac{P_R - P_{LV}}{R_M} - Q_{LVAD} \quad (5.8)$$

$$\dot{Q}_{AO} = \dot{Q}_{LVAD} \quad (5.9)$$

Measurement equation :

$$\Delta P = P_{LV} - (L_C \dot{Q}_{LVAD} + R_C Q_{LVAD} + P_S) \quad (5.10)$$

Iso-volumic expansion/contraction ($D_A = 0$, $D_M = 0$)

State equations :

$$\dot{P}_S = \frac{Q_{LVAD}}{C_S} - \frac{P_S - P_R}{C_R R_{SVR}} \quad (5.11)$$

$$\dot{P}_R = \frac{P_S - P_R}{C_R R_{SVR}} \quad (5.12)$$

$$\dot{V}_{LV} = -Q_{LVAD} \quad (5.13)$$

$$\dot{Q}_{AO} = \dot{Q}_{LVAD} \quad (5.14)$$

Measurement equation :

$$\Delta P = P_{LV} - (L_C \dot{Q}_{LVAD} + R_C Q_{LVAD} + P_S) \quad (5.15)$$

Left ventricular pressure P_{LV} is a function of the left ventricular volume V_{LV} as well as the time-varying compliance C_{LV} . A normalized curve is scaled in amplitude and time to derive C_{LV} [96, 98].

5.3.3 Model Simulation vs hMCL CVS Model

The full CVS model as described in Section 3.2.2 and the reduced order systemic model detailed in Section 5.3 were simulated to assess how well the reduced order model could reproduce desired pressure and measurement signals of the full CVS model. Figure 5.3 shows the results of this simulation. From the figure it can be seen that there is a slight discrepancy as the mitral valve closes, causing a small spike in pressure as the ventricle transitions to ejection. The criteria of importance, however, is how well the differential pressure signals align as this is the measurement that the model based estimator will be using to update state and parameter estimates. It can be seen that the reduced order model differential pressure aligns well with that of the full CVS model, thus making it a suitable candidate for use in the model based estimator.

5.4 SVR Estimation Using EKF

5.4.1 Estimability and Convergence

The states of a dynamic system can be estimated using observers or filters, both of which need a model to dynamically propagate states, and measurements to update them. For linear dynamic systems, the Kalman Filter (KF) offers a way of doing this *optimally* [99]. A KF recursively propagates the states and estimation error covariance forward in time using known inputs. Available measurements are then used to update the state estimates and the

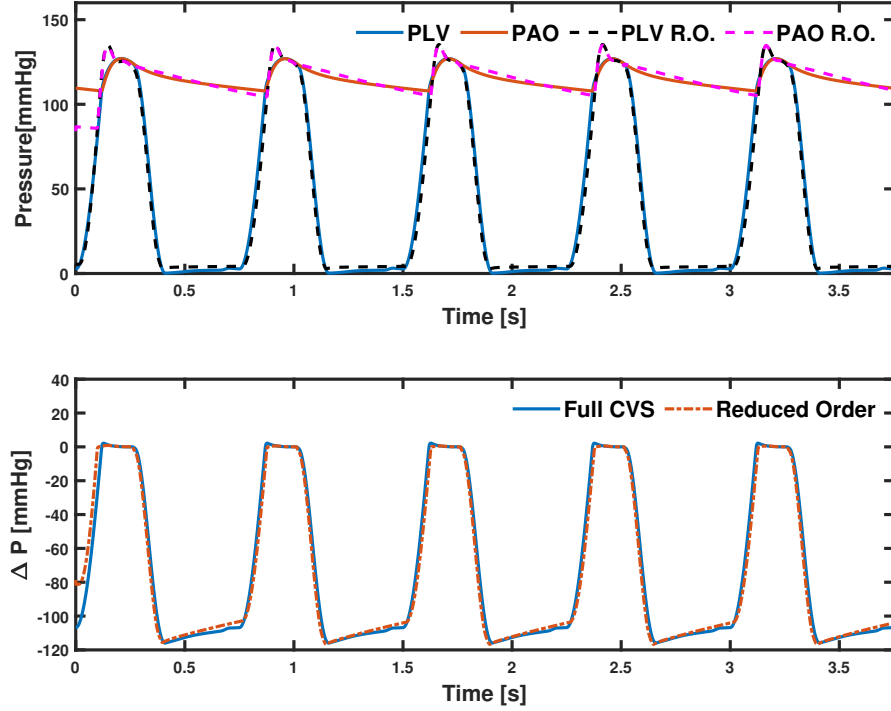


Figure 5.3: Reduced order systemic CVS model comparison versus full CVS model as defined in 3.2.2. (Top) left ventricular and aortic pressures are shown versus time, (Bottom) differential pressure measurements are shown versus time. Dashed lines represent reduced order systemic model outputs

error covariance. The *observability* criteria can be used to gauge the ability to estimate states using available measurements in the absence of process noise [35]. In the presence of process noise, however, *estimability* can provide a better indication of this ability. A system is deemed *estimable* if the measurement update step is able to reduce the magnitude of the error covariance [100], in turn providing more accurate state estimates. An Extended Kalman Filter extends the capability of KF to nonlinear systems by propagat-

ing estimator states according to the nonlinear model, while using a first-order approximation of the model evaluated at each time step for error covariance propagation. Table 5.1 summarizes the EKF algorithm when the nonlinear estimator model is propagated in continuous time, and measurements are taken in discrete time [35]. In addition to model states, system parameters (such as SVR) can be estimated by treating them as states, deriving a corresponding dynamic equation, and augmenting the state vector accordingly. The process of parameter estimation often makes a linear system nonlinear and forces the use of nonlinear observers or filters, such as EKF.

Table 5.1: Continuous - Discrete Extended Kalman Filter equations

| | |
|------------------------------|---|
| System Model | $\dot{\underline{x}}(t) = \underline{f}(\underline{x}(t), t) + \underline{w}(t); \underline{w}(t) \sim N(\underline{0}, Q(t))$ |
| Measurement Model | $\underline{z}_k = \underline{h}_k(\underline{x}(t_k)) + \underline{v}_k; k = 1, 2, \dots; \underline{v}_k \sim N(\underline{0}, R_k)$ |
| Initial Conditions | $\underline{x}(0) \sim N(\hat{\underline{x}}_0, P_0)$ |
| Other Assumptions | $E[\underline{w}(t)\underline{v}_k^T] = 0 \quad \forall \{k, t\}$ |
| State Estimate Propagation | $\dot{\hat{\underline{x}}}(t) = \underline{f}(\hat{\underline{x}}(t), t)$ |
| Error Covariance Propagation | $\dot{P}(t) = F(\hat{\underline{x}}(t), t)P(t) + P(t)F^T(\hat{\underline{x}}(t), t) + Q(t)$ |
| Innovation | $\underline{v}_k = \underline{z}_k - \underline{h}_k(\hat{\underline{x}}_k(-))$ |
| State Estimate Update | $\hat{\underline{x}}_k(+) = \hat{\underline{x}}_k(-) + K_k \underline{v}_k$ |
| Error Covariance Update | $P_k(+) = [I - K_k H_k(\hat{\underline{x}}_k(-))]P_k(-)$ |
| Gain Matrix | $K_k = P_k(-)H_k^T(\hat{\underline{x}}_k(-)) [H_k(\hat{\underline{x}}_k(-))P_k H_k^T(\hat{\underline{x}}_k(-)) + R_k]^{-1}$ |
| Definitions | $F(\hat{\underline{x}}(t), t) = \left. \frac{\partial \underline{f}(\underline{x}(t), t)}{\partial \underline{x}(t)} \right _{\underline{x}(t) = \hat{\underline{x}}(t)}$ $H_k(\hat{\underline{x}}(-)) = \left. \frac{\partial \underline{h}_k(\underline{x}(t_k))}{\partial \underline{x}(t_k)} \right _{\underline{x}(t_k) = \hat{\underline{x}}(-)}$ |

Current clinical methods for measuring SVR are based on time-averaged values of pressure and cardiac output [90–92]. Although the SVR estimation algorithm provides continuously-updated estimates using LVAD-based mea-

surements, time-averaged values can also be generated. An advantage of using an EKF algorithm is that error covariance can be used to guide any proposed averaging process. The error covariance output of the EKF algorithm, as seen in Table 5.1, dictates the point at which the time-averaging of the SVR estimates begin. The error covariance output is monitored for convergence into a steady-state, cyclically repeatable pattern with minimal magnitude changes between cycles. This convergence indicates that the EKF state estimates have also settled (due to minimal difference between measured and estimated differential pressure) and that SVR time-averaging may begin.

5.4.2 LVAD Flowrate and Differential Pressure

In order to implement real-time estimation of SVR, the LVAD flowrate, Q_{LVAD} , and differential pressure, ΔP , need to be available as input and measurement, respectively. Most modern LVADs approved for human implantation or under development use axial or centrifugal flow impeller pumps [101, 102]. Studies have reported on efforts to estimate pump flowrate and differential pressure based on the known and controlled impeller speed, ω_p , and motor current, i_m . However, despite having a good steady-state model relating pressure, flowrate, and speed, it is also necessary to know blood viscosity to infer differential pressure [103, 104]. This is an implicit complexity for all such Eulerian turbomachines [105]. On the other hand, pressure and flowrate can be determined for positive-displacement pumps, used by most pulsatile flow (PF) LVADs, without regard to fluid (blood) viscosity as demonstrated in [95].

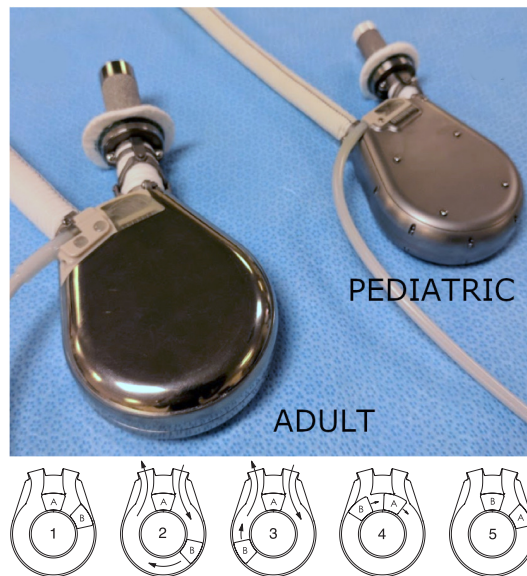


Figure 5.4: (top) Adult and pediatric TORVAD™ devices, (bottom) Illustration of pumping cycle for a TORVAD™

The TORVAD™ (Windmill Cardiovascular Systems, Inc., Austin, Texas) is a new class of implantable, positive-displacement, pulsatile LVAD shown in Figure 5.4 (top) [86,98]. This pump has a toroidal-shaped pumping chamber with inlet and outlet ports, with two pistons driven within the chamber lumen. As illustrated in the schematic of Figure 5.4 (bottom), pumping is achieved by driving one piston around the chamber while holding the other piston between the inlet and outlet ports. At the end of each stroke, pistons exchange functional roles to generate positive-displacement pulsatile flow without one-way valves, a distinct advantage over early generation pulsatile LVADs. The TORVAD™ pump controller monitors position and voltage on motors for each piston as well as ECG for heart rate. These onboard sensors can be used to

estimate unmeasurable pump states such as piston velocity, pump flowrate, and differential pressure across the pump using a real-time Kalman filter [89].

5.5 SVR Estimation Simulation Results

The estimation of SVR was first tested using model based simulations. Measurement data for these simulations were generated using the reference CVS model from Figure 3.3 at known VAD flow rates. Simulated differential pressure measurements ($\Delta P = P_{LV} - P_{AO}$) were taken from this reference model with the incorporation of additive Gaussian white noise, representative of high frequency noise found in sensors. To adequately test the convergence of the EKF estimates, various levels of VAD flow rates, sensor and process noise magnitudes, and initial conditions were applied in the simulation. From the simulation studies it was found that the EKF, which is applied to the model shown in Figure 5.2, provided accurate estimates (within 10%) of SVR over the expected range of operation and measurement accuracy, thus allowing for the next step of real-time estimation of SVR using hMCL based experimental measurements. Figure 5.5 depicts a sample simulation for evaluating EKF SVR estimation accuracy.

5.6 SVR Estimation Results using hMCL Data

Experimental studies were used to evaluate the effectiveness of an EKF estimation of SVR. Two different hMCLs with similar design were employed:

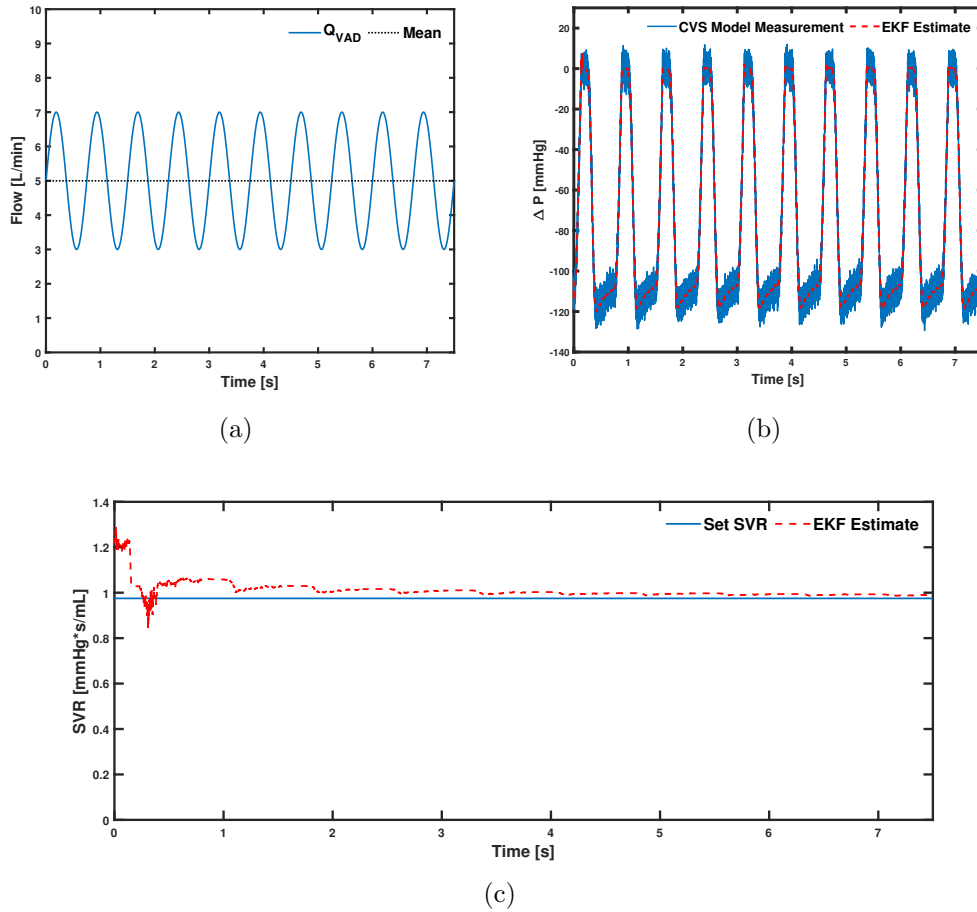


Figure 5.5: Simulated SVR estimation results for a sample experiment: (a) Model simulated continuous flow VAD input, (b) Reference CVS model generated differential pressure with additive noise and EKF estimate over time, (c) SVR EKF estimate using reduced order model over time versus set value used in reference model simulation

one to test a CF BIO-Pump[®](Medtronic, Minneapolis, MN, USA), the other for testing a PF TORVAD[™]. Each hMCL was comprised of a left ventricular (LV) pressure chamber, an aortic pressure chamber (AO), a recirculation

(back-flow) pump (BP), and cannulae coupling the pressure chambers to the inlet and outlet ports of each pump, as indicated in Figure 5.1. The BIO-Pump/hMCL system was controlled using a NI CompactRIO system, while the TORVADTM/hMCL system used a NI myRIO-1900 embedded device (both from National Instruments, Austin, TX, USA). Each of these controller platforms were used to implement the real-time simulation of the CVS reference model. NI LabVIEW software was used to program, communicate with, and control the NI hardware and hMCL experiments.

Both hMCLs used the CVS model described in Section 3.2.2 as the reference model. The estimator model for EKF estimation was taken as the reduced order, 4-element Windkessel model in Figure 5.2. The resistances of the entire systemic circulation in Figure 3.3 are summed into one resistance parameter to calculate equivalent SVR.

Table 5.2: Parameter values used for the state equations for when simulating a healthy patient and one with end-stage heart failure

| Parameter | Healthy | HF |
|---------------------------------|----------------|-----------|
| R_C (mmHg·s/mL) | 0.0398 | 0.0398 |
| L_C (mmHg·s ² /mL) | 0.0005 | 0.0005 |
| C_S (mmHg/mL) | 1.33 | 0.65 |
| C_R (mmHg/mL) | 4.4 | 4.4 |
| R_M (mmHg·s/mL) | 0.005 | 0.005 |
| R_A (mmHg·s/mL) | 0.0025 | 0.001 |

5.6.1 Test procedure

The EKF algorithm for SVR estimation was tested using experimental data gathered from the two mock loop experiments. The following procedure was used in each test.

1. Cardiovascular parameters corresponding to a patient with a healthy or failing heart are input to the CVS model operating on the MCL: Expected SVR is calculated as the sum of systemic resistances (arteries, arterial tree, veins) in the CVS reference model; i.e., $R_{SVR} = R_{SA} + R_{ST} + R_{SV}$ (see Figure 3.3)
2. Cardiovascular parameters corresponding to a healthy or heart failure patient as shown in Table 5.2 are used in the estimator model
3. Initial conditions for estimator states, $\underline{x}_{aug}(t = 0)$, are set at arbitrary values within the expected range of physiologically feasible state values; e.g., setting $R_{SVR}(t = 0) = 0.7$ would fall within the 0.6-0.9 mmHg·s/mL typical range for a healthy patient test
4. Hybrid MCL operation was coordinated with the pump under test (BIO-Pump[®] or TORVAD[™])
5. Differential pressure measurement data was used to update estimator model SVR estimate during hMCL operation, flowrate was used as a known (and measured) input to the estimation algorithm
6. SVR estimates were monitored, with averaged values compared to set

values

5.6.2 SVR estimation in CF pump testing

In the first test, the continuous flow BIO-Pump[®] was used to simulate a CF LVAD application. The CVS reference model was parameterized to simulate hemodynamics for a patient having a healthy heart, using parameter values as provided in [86]. For the estimator model, the cardiovascular parameters are summarized in Table 5.2.

Table 5.3: Results of the two SVR estimation experiments

| CVS Model | VAD | Q_{LVAD} | Set SVR | SVR Estimate | Error |
|---------------|---------------------|------------|-----------|---------------------------------|-------|
| | | L/min | mmHg·s/mL | Mean \pm St.Dev. mmHg·s/mL | % |
| Healthy | CF | 5.04 | 0.975 | 0.988 \pm 0.0043 | 1.3 |
| Heart Failure | TORVAD [™] | 2.26 | 1.057 | 1.050 \pm 0.0229 | 0.7 |

The graphs in Figure 5.6 plot measured and estimated data from CF testing with the BIO-pump[®]. Note that in this case the pump flowrate and differential pressure had to be measured using external sensors. Flowrate was measured on the outlet cannula using an ultrasonic flow probe (Model ME 11 PXL, Transonic Systems Inc., Ithaca, NY, USA), while differential pressure was determined using the LV and AO pressure sensors (Model PX409, Omega Engineering, Norwalk, CT) in the hMCL. The real-time model and EKF algorithm updated at a rate of 5 kHz. Figure 5.6(a) shows measured CF pump flowrate, which was used as an input to the EKF algorithm. The fluctuations in the CF BIO-pump[®] flowrate result because of the pressure difference induced

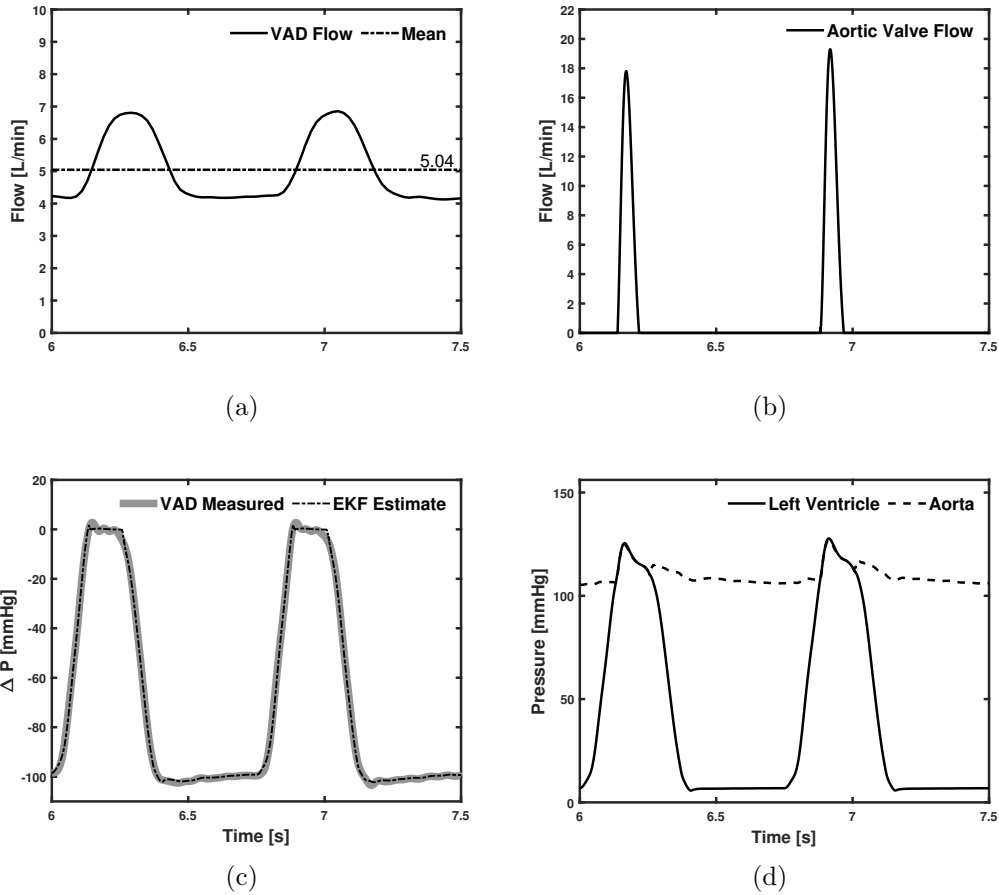


Figure 5.6: (a) Measured continuous flow BIO-Pump[®](VAD) input, (b) EKF estimated aortic valve flow, (c) measured versus EKF estimated differential pressure, and (d) EKF estimated hemodynamic pressures

across the pump connections. A lower pressure difference results in increased flowrate, as expected with typical pressure-flow characteristics for centrifugal pumps. The BIO-pump[®] controller was set to a rotor speed of 2,000 rpm, for a desired mean flowrate of approximately 5 L/min. Figure 5.6(c) compares the differential pressure measurements from the hMCL to the EKF estimates.

Note that the left ventricle pressure and aortic pressure were physically generated by the hMCL in real-time based on the reference model. The differential pressure was calculated as the difference of these measurements. The aortic valve flowrate as well as pressures of the left ventricle, aorta, and venous return estimated by the EKF during this experiment are shown in Figures 5.6(b) & (d), respectively. A mean value of the EKF estimated SVR was taken over the final 4.7 seconds of the 7.5 second experiment, once covariance of each state variable had converged to steady-state, showing cyclically repeatable values. The SVR estimate was 0.988 mmHg·s/mL, when the value set for SVR in the CVS reference model was set at 0.975 mmHg·s/mL, corresponding to a 1.3% error difference. A summary of this CF LVAD test is provided in Table 5.3.

5.6.3 SVR estimation in PF LVAD testing

Experiments were conducted on a second hMCL with a TORVADTM under test. In this case, the CVS reference model parameters were set to those more indicative of a patient experiencing heart failure [86]. The corresponding parameters for the EKF estimator model are found in Table 5.2. Input flowrate and differential pressure for the EKF algorithm were provided directly by the TORVADTM controller at a rate of 4800 Hz [89]. Two sample cardiac cycles of data from these experiments are shown in Figure 5.7. Figure 5.7(a) represents the pulsatile LVAD flow, used as input to the EKF while the TORVADTM was operating in a synchronous counterpulse mode [98], providing a mean flowrate of 2.26 L/min. Figure 5.7(c) compares the differential pressure measurements

output by the TORVADTM versus the EKF estimate output. The EKF estimates of aortic valve flow, as well as left ventricular, aortic, and venous return pressures are shown in Figures 5.7(b) & (d), respectively. Similarly to the previous test, a mean value of the EKF estimated SVR was taken over the final 3.2 seconds of the 5.7 second experiment, once covariance of each state variable had converged to steady-state, showing cyclically repeatable values. The experiment with the TORVADTM was used to demonstrate estimation of SVR for a patient experiencing heart failure. The mean SVR estimate was found to be 1.057 mmHg·s/mL, compared to the known (set) value of 1.05 mmHg·s/mL set in the hMCL CVS reference model, representing a 0.67% error difference. A summary of this PF TORVADTM test is provided in Table 5.3.

5.7 Discussion

An Extended Kalman Filter (EKF) was developed that uses the controlled LVAD flowrate and a measurement of LVAD differential pressure to estimate the systemic vascular resistance (SVR) of the cardiovascular system under assist by an implanted LVAD. The approach is similar to that of Yu et al. [34, 96], however in that work it was assumed that LVAD volume and arterial pressure would be available as measurements for a PF extracorporeal LVAD. The use of LVAD flowrate and differential pressure as described in this work is compatible with either a CF LVAD or PF LVAD and also makes it possible to adopt built-in LVAD sensing and thus application of SVR estimation to other

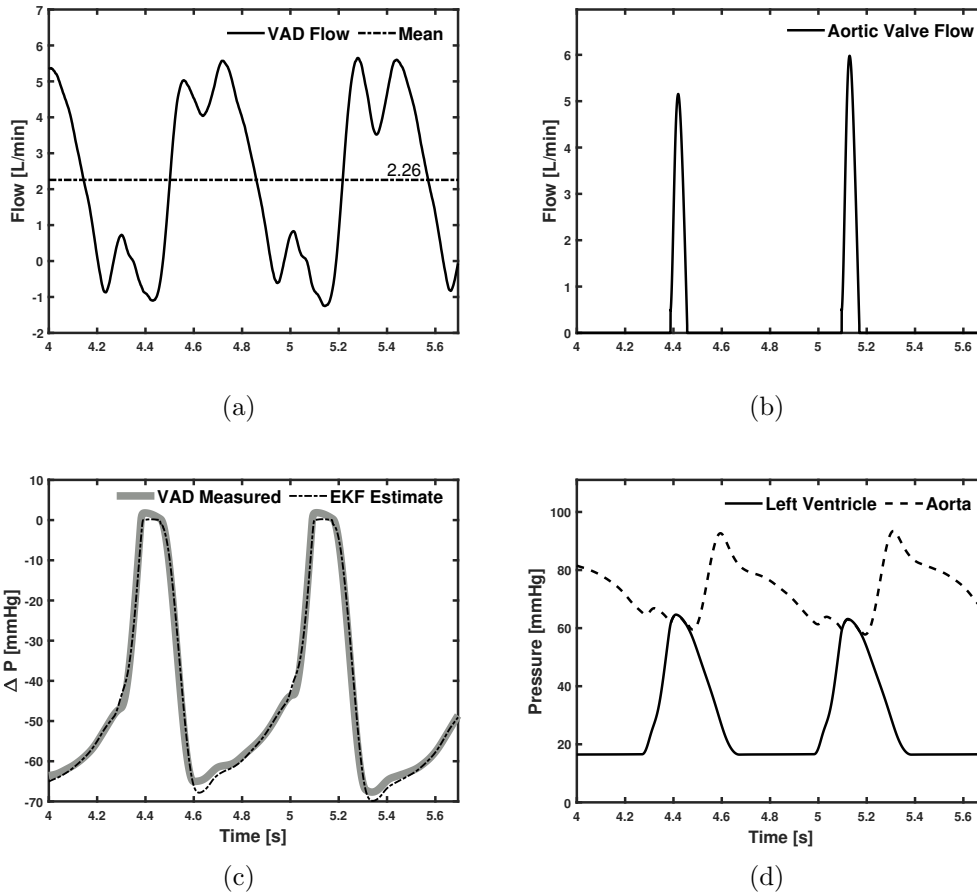


Figure 5.7: (a) Measured TORVADTM flow input, (b) EKF estimated aortic valve flow, (c) measured versus EKF estimated differential pressure, and (d) EKF estimated hemodynamic pressures

LVAD systems.

The EKF algorithm relies on a relatively simple model of the systemic circulation to estimate the model states and SVR. Experiments to evaluate the estimation algorithm were performed using a hybrid mock circulatory loop (hMCL) which allows values of SVR to be specified within a simulated refer-

ence model of the CVS hemodynamics. Tests were conducted with a CF LVAD (BIO-pump[®]) in one hMCL and a PF TORVAD[™] in a similar hMCL. The TORVAD[™] has built-in sensing and estimation [89], so no additional sensors and measurements are required. However, this is not currently the case for most CF LVADs, where measurement or estimation of differential pressure can be challenging without additional sensors (e.g., accounting for the effect of variability in blood viscosity, as stated previously [103, 104]).

Plots of the measured input CF and PF LVAD flowrates are shown in Figures 5.6(a) and 5.7(a), respectively. The hMCL controllers use these data in a synchronized, real-time simulation of the CVS reference model (Figure 3.3). The differential pressures are computed and then used to control the physical LV and AO pressure chambers (see Figure 5.1). Figures 5.6(c) and 5.7(c) show favorable comparison between the measured and EKF-estimated differential pressures applied across the CF and PF devices, respectively.

Figures 5.6(b), 5.6(d), 5.7(b), and 5.7(d) show hemodynamic variables estimated by the EKF algorithm in each case. These results convey the estimated CVS dynamics in the hMCL that cause the differential pressures across each LVAD. These dynamics provide insight into all the modeled hemodynamic variables (aortic valve flow, LV pressure, etc.) and key CVS model parameters. As such, changes in the CVS model parameters directly influence the LVAD, providing a basis to test how well the EKF algorithm, its underlying (simplified) model, and data on LVAD flowrate and differential pressure can estimate SVR. The errors in estimated values of SVR for each test case showed errors

of 1.3% and 0.7% for the CF and PF LVAD, respectively, providing support for pursuing this approach further.

An EKF algorithm is a dynamic system and will have a finite response time when inputs change. Figure 5.8 shows a representative response of how the EKF SVR estimate updates over time. To be clear, all the states of the estimator model (i.e., the states of the model in Figure 5.2) similarly update and converge over time. Upon initialization of the estimation algorithm, all states begin to update according to measurement inputs, thus causing the significant changes seen in SVR over the first second in Figure 5.8. Once model estimates begin converging, the innovations of the EKF begin to decrease in magnitude, allowing for the EKF estimates to settle into a steady-state, repeatable pattern.

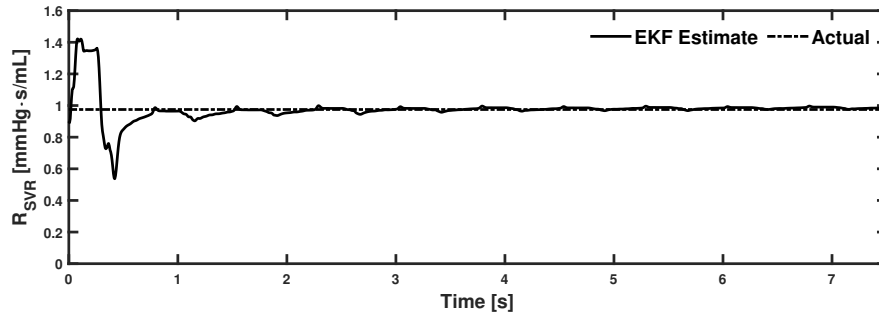


Figure 5.8: EKF estimate of parameter R_{SVR} over time compared to the true value set within the CVS model on the hMCL

The application of the EKF to data collected from both CF and PF LVADs opens up new avenues for personalized patient therapy and physiological monitoring. With the increasing communicative capabilities of implantable devices,

for example, it is already possible to save and analyze data in batch mode (i.e., exporting a collection of data saved over a certain time interval to a neighboring device or a separate online embedded processor). The EKF can be applied to each independent batch of data to estimate SVR, allowing for a time history of patient data to be saved and remotely monitored by a physician. The estimation data can also be useful in updating the control of the LVAD device, adjusting CVS support to detect and prevent the aforementioned complications such as hemorrhagic stroke.

The next level of personalized patient care in LVADs takes the form of real-time estimation and monitoring of physiological parameters, which is the driving factor in our decision to use a reduced order systemic circulation model for estimation. As stated previously, the size of the model and subsequent estimation equations greatly impacts the method of implementation, computing time, and memory capacity of the LVAD processor and controller. It is for these reasons the reduced order systemic circulation model used in this study will be further tested on the TORVADTM controller in conjunction with estimation algorithms already in place for LVAD flowrate and differential pressure. This will allow for a continuous estimation of SVR and the ability to detect and report SVR changes, facilitating precautionary LVAD control measures and physician/care-taker notification.

Chapter 6

hMCL Cardiac Event Generation

In this chapter the concepts of cardiac events, their relevancy in current VAD implanted patients, and methods for implementation in mock circulation loop are discussed in detail.

6.1 Cardiac Event Definition

Cardiac events refer to any incidents or events that adversely affect the heart or cardiovascular system. These events can be of varying severity (e.g., myocardial infarction or angina) and include arrhythmic events, such as atrial fibrillation. In this work, both arrhythmic as well as VAD induced cardiac events (e.g., valvular stenosis) are examined.

6.2 Objective

The next step in hMCL technology development is to include arrhythmic and VAD induced cardiac events to provide a controllable, repeatable environment for VADs to be tested in atypical hemodynamic conditions. This would not only be useful for the purposes of testing nominal VAD function during cardiac

dysfunction, but could also reduce the need for pharmacologically induced animal testing. Further, cardiac event generation in vitro would also facilitate the validation of onboard VAD patient monitoring applications as well as enhance the robustness of developing physiological control algorithms in next generation VADs.

6.3 State of the Art

To motivate the need for realizing arrhythmic cardiac events in vitro via mock circulation loops (MCLs), the literature review has been separated into two main categories: 1) MCLs with atypical heart function realization and 2) Physiological control and patient monitoring algorithms.

6.3.1 MCLs with Atypical Heart Function Realization

Typically, in order to assess implantable device performance in the presence of cardiac events, in vivo animal tests are required with arrhythmias induced via pharmacological means. In these tests, the animal under test is closely monitored in the attempt to keep pathological conditions constant. This, however, is not a simple task and is typically performed at the end of the in vivo test process in the event the animal goes into cardiac arrest. Thanks to advances in electrical and mechanical cardiovascular simulation, studies are now being done to incorporate these cardiac events into the more controllable, repeatable mock circulation loop environments.

Modern MCLs have the ability to recreate nominal hemodynamic operation (i.e., sinus rhythm) with great accuracy. Further, hybrid MCLs (hMCLs) allow for the adjustment of simulated patient health parameters to induce various pathological conditions in real-time (e.g., [106]). Few MCLs, however, have been documented with the ability to realize arrhythmic cardiac events. In 2000, Mouret et al. developed an MCL with separate atrial and ventricular chambers for the purposes of testing heart valve prostheses [107]. Both the atrium and ventricular chambers were molded based on human anatomy and contracted via a surrounding fluid filled chamber. Due to the use of independent chambers for the atrium and ventricle, they had the ability to induce both synchronous and asynchronous contraction of the left heart as well as adjust the magnitudes of the contractions. Though intended for mitral valve prosthesis testing rather than VAD validation, it documented the ability for an MCL to adjust atrial contraction timing and magnitude for the realization of atrial fibrillation.

Simulated models of heart electrophysiology have been developed and shown to recreate both sinus rhythm and various arrhythmic states [108]. However, for these models to be used for the purposes of VAD validation they must incorporate the electrical and mechanical/hydraulic components of the heart to simulate the CVS hemodynamics needed for realization in an hMCL, as is motivated in [77]. The work of Le et al. [109, 110] utilizes an approach which analyzes the measured electrical activity in patient ECG data to determine atrial and ventricular contraction timing. The contraction time information is

then used to inform a mechanical model of the heart, which is then used to simulate patient hemodynamics operating in sinus rhythm. Also using measured ECG patient data, the work of Bozkurt [111] detailed a computational CVS simulation with a continuous flow LVAD (CF-LVAD) which incorporated unimodal and bimodal forms of atrial fibrillation. Though the work of Le et al. and Bozkurt were implemented only in simulation, they can be easily be extended for use in an hMCL system.

6.3.2 Physiological Control and Patient Monitoring Algorithms

Currently, research is being done in next generation VADs and MCS devices to develop onboard algorithms for the purposes of patient health monitoring ([73, 112, 113]) and subsequent physiological control¹. These updates require advanced validation in the form of in vitro environments that can replicate both nominal and atypical patient health states (e.g., arrhythmias or changes in systemic vascular resistance) as well as VAD induced events (e.g., valvular stenosis or suction events). Thus, to evaluate these algorithms it is necessary to create an in vitro test environment that can repeatably recreate the desired failure modes or patient disease states for detection.

One metric of rising importance is the state of closure of the aortic valve during CF-VAD operation. Depending on the relative contractility of the LV and the relative support level of the CF-VAD, the aortic valve may not open

¹Physiological control refers to an adaptive control algorithm that adjusts VAD flow rate depending on detected changes in patient health or heart electrical activity.

fully or even at all during ventricular contraction; an issue that commonly leads to aortic insufficiency or valvular stenosis [114]. In response to this issue, researchers and VAD manufacturers have worked to develop VAD patient monitoring algorithms that actively work to detect or estimate the status of the aortic valve [115] as well as adjust the control of VAD flow based on the desired status of the valve [76, 116, 117]. The validation for such algorithms must be done before implementation, thus motivating the need for in vitro environments (such as hMCLs) that can recreate various levels of diseased valve states.

6.4 Methods of Cardiac Event Generation

Several methods can be used to implement arrhythmias and cardiac events in the hMCL, each of which with its own set of pros and cons. In each method, reference pressures for a specified time range are determined for the left ventricle (LV) and aorta (AO) using either a numerical simulation of the CVS running in real-time or reference arrays (via look-up tables) generated in prior simulations. Reference pressure data is then iterated at the desired 2 kHz hMCL control rate and then sent to the hMCL for generation at each pressure-generating interface (PGI). Lastly, acting as a measured disturbance, the VAD flow rate is set according to the desired mean value. For the cases where VAD flow is set to zero (0) LPM, the VAD input and output cannulas were clamped to prevent flow between the pressure chambers. Each method is described in detail in the following sub-sections.

6.4.1 Method 1 - CVS Model Parameter Modification

This method required the least amount of updates to the native hMCL system as all updates can be made in software to the existing CVS simulation running on the controller module FPGA. The hMCL is run on a computer with a Windows 10 operating system using NI LabVIEW 2018 software and a NI CompactRIO (cRIO) data acquisition device (CompactRIO-9034, National Instruments Corporation, Austin, TX). The NI cRIO is responsible for simulating the computational circulation model as defined in [86], acquiring sensor input, filtering measurements, and controlling the output of the mock loop all in real-time at the FPGA level. To transition from normal sinus rhythm (as is the baseline mode for hMCL operation) to a cardiac failure mode of aortic valve stenosis, the only update required is to increase the magnitude of the aortic valve resistance (a lumped parameter value that is already defined in the CVS model). The update to the resistance value will cause a decrease in computational aortic flow during the ejection phase of the cardiac cycle, resulting in decreased aortic pressure magnitude as shown in Figure 6.1. Similarly, parameter updates can be made regarding the simulated patient heart rate to increase it above 100 BPM (representative of tachycardia) as well as lower it below 50 BPM (representative of bradycardia).

6.4.2 Method 2 - Clinical Data Tracking

This method utilizes clinically diagnosed and measured left ventricular pressure (P_{LV}) data from a heart failure patient as documented in journals or

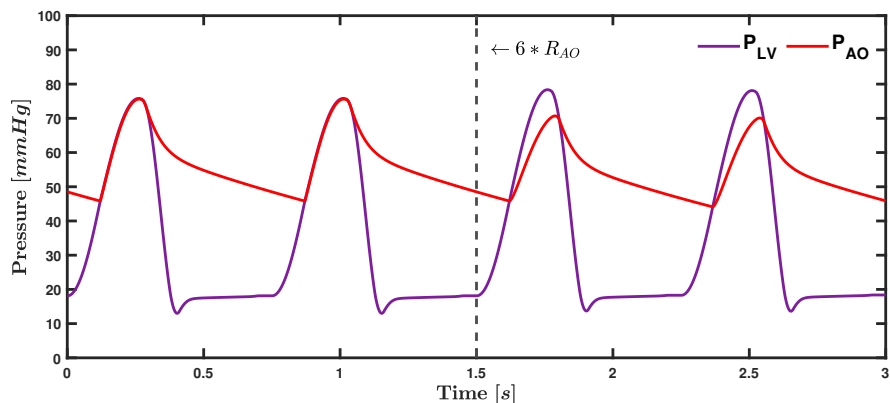


Figure 6.1: CVS model simulation of induced aortic stenosis where aortic valve resistance (R_{AO}) parameter has been increased by 6x with mean VAD flow set to 0 LPM.

reference texts such as [118, 119]. In the event both left ventricular and aortic pressure measurements are available, these signals could be interpolated as required and sent to the hMCL for controlled pressure tracking. However, these pressure trends would not allow for adjustments to VAD flow as the references would not change. In order to account for VAD induced changes to aortic pressure, a model of the systemic circulation can be used to allow for VAD flow rate adjustments and subsequent aortic pressure calculation. Using the systemic circulation portion of the CVS model from [86], the LV pressure data (P_{LV}), mean right atrium pressure (P_{RA}), and commanded VAD flow (Q_{VAD}) can be modeled as inputs and used to determine the subsequent aortic (P_{AO}) pressure trends. The LV and AO pressure trends are then used as reference arrays in the hMCL at the corresponding VAD flow rate. The systemic circulation model can be seen in Figure 6.2 and can be represented in nonlinear

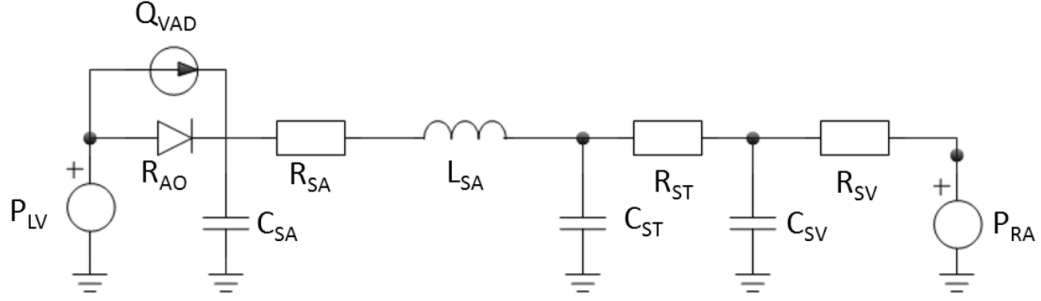


Figure 6.2: Electric analog model of systemic circulation with left ventricular pressure (P_{LV}), mean right atrium pressure (P_{RA}), and LVAD flow rate inputs. Aortic pressure (P_{AO}) is calculated at the intersection of LVAD and aortic valve flows where they connect with the systemic arterial compliance (C_{SA}).

state space form as,

$$\text{States: } \mathbf{x} = [P_{AO} \quad Q_{SA} \quad P_{ST} \quad P_{SV}]^T$$

$$\text{Inputs: } \mathbf{u} = [P_{LV} \quad Q_{VAD} \quad P_{RA}]^T$$

$$\text{Dynamics: } \dot{\mathbf{x}} = f(\mathbf{x}, \mathbf{u})$$

$$\text{Measurements: } \mathbf{y} = [P_{AO}]$$

where P_{AO} represents the aortic pressure of the systemic arterial system at the outlet of both the LVAD cannula and aortic valve flow connections, Q_{SA} is the flow through the systemic arterial system, P_{ST} is the systemic arterial tree pressure, and P_{SV} is the systemic vein pressure. The state equations for the systemic circulation model are presented below.

$$\dot{P}_{AO} = \frac{Q_{AO} + Q_{VAD} - Q_{SA}}{C_{SA}} \quad (6.1)$$

$$\dot{Q}_{SA} = \frac{P_{AO} - P_{ST} - R_{SA}Q_{SA}}{L_{SA}} \quad (6.2)$$

$$\dot{P}_{ST} = \frac{1}{C_{SA}} \left(Q_{SA} - \frac{P_{ST} - P_{SV}}{R_{ST}} \right) \quad (6.3)$$

$$\dot{P}_{SV} = \frac{1}{C_{SV}} \left(\frac{P_{ST} - P_{SV}}{R_{ST}} - \frac{P_{SV} - P_{RA}}{R_{SV}} \right) \quad (6.4)$$

where C_{SA} , R_{SA} , and L_{SA} are the systemic arterial system compliance, resistance, and inductance, respectively. Similarly, C_{ST} and R_{ST} are the systemic arterial tree lumped compliance and resistance, respectively. Lastly, C_{SV} and R_{SV} are the lumped compliance and resistance for the systemic veins, respectively. The aortic valve flow, Q_{AO} , is modeled as nonzero only during the ejection phase of the cardiac cycle. The flow rate is calculated by taking the square root of the pressure difference across the valve divided by the lumped resistance value, R_{AO} .

$$Q_{AO} = \begin{cases} \frac{\sqrt{P_{LV} - P_{AO}}}{R_{AO}} & \text{if } P_{LV} > P_{AO} \\ 0, & \text{if } P_{AO} \geq P_{LV} \end{cases} \quad (6.5)$$

Through the use of this model, it is possible to attain aortic pressure trends that can be varied according to desired LVAD flow rates and then recreated in vitro using the hMCL.

6.4.3 Method 3 - CVS Model with Processed ECG Input

Cardiac arrhythmias are a result of electrical signal failures in various parts of the heart. Thus, to induce these arrhythmic states in the simulated heart, it is required to adapt a CVS model that incorporates both the electrical and mechanical properties of the myocardium. Using the work of [109] and documented cardiac patient data from the PhysioNet MGH/MF Waveform Database [120], a model of the CVS which utilizes measured ECG data as an input has been updated to simulate both nominal and arrhythmic patient hemodynamics.

This method is the most extensive in terms of implementation. It requires the processing of clinically measured (and diagnosed) patient ECG data to determine the time and magnitudes of left atrium and left ventricular contraction. This information is then used to scale the normalized elastance functions inherent in the simulated CVS model, subsequently modulating reference pressure data for the hMCL to track.

The methods used for ECG processing are described in detail in [109] and extended further in [110]. Originally used to recreate sinus rhythm in a MCL, this method has been extended for the use of ECG data with clinically diagnosed arrhythmia (Note: diagnoses were made by licensed physicians and documented in the MGH/MF Waveform Database; no diagnoses were made by our team). Processing the ECG data allowed for the determination of the respiratory signal and the fiducial points of the cardiac cycle. These points,

which refer to the onset of the P-wave, the components of the QRS complex, and the offset of the T-wave are used to compute the atrial and ventricular activation functions that dictate contraction timing and magnitude in the CVS model simulation. A flowchart of the steps performed in Method 3 (similar to that of Figure 1 in [109]) is provided in Figure 6.3.

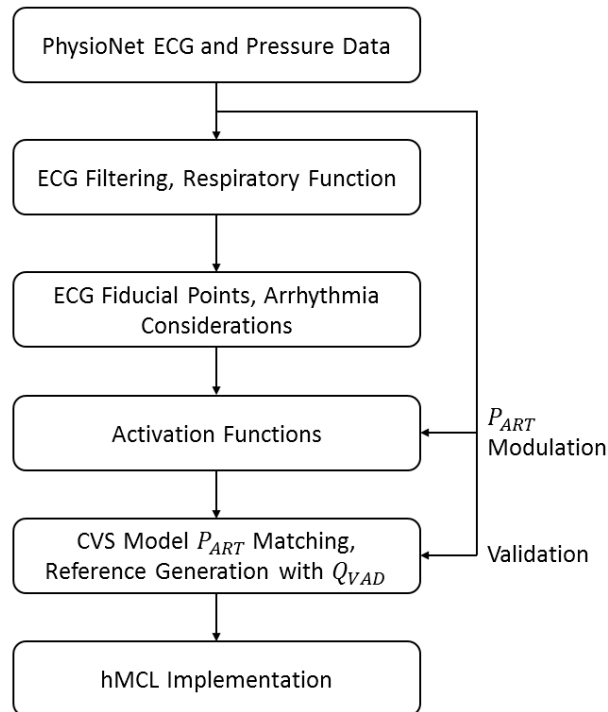


Figure 6.3: Flowchart describing each step of Method 3 for ECG processing and subsequent CVS model and hMCL implementation.

A summary of determining the ECG based activation functions using MATLAB 2020b software (The MathWorks, Inc., Natick, Massachusetts) is provided below.

1. Patient data is collected from the MGH/MF Waveform Database, which includes three (3) leads of ECG data, systemic arterial pressure, pulmonary arterial pressure, and central venous pressure. Patients are grouped based on clinician arrhythmia diagnoses according to the database Patient Guide.
2. The respiratory signal was determined using Method II as defined in [121]. First, patient ECG data is pre-processed using a 20th order, high pass, linear phase FIR filter with a Kaiser window ($\beta = 4$) and the cutoff frequency set at 0.05 Hz. This allows for baseline wander in the ECG data to be removed without filtering any information required for fiducial point determination. The R peaks in the ECG signal are then detected to form an averaged RR interval pulse series which can then be modulated based on relative mean R peak magnitude over a 20ms time span. This modulated series is then processed through a low pass Butterworth filter with a cutoff frequency of 0.4 Hz and time shifted based on actual measured RR interval spacing. The result is the estimated respiratory signal, $Resp(t)$, to be used to calculate the atrial and ventricular activation functions.
3. The fiducial points of the ECG were determined following the phase space method as depicted in [122]. Raw ECG data was again pre-processed, this time using a band-pass filter with frequency a range of 0.5 and 60 Hz, which minimizes any measurement artifacts, respiration, baseline drift, and other high frequency noise. The prefiltered data was then sent

through a wavelet transform, which allowed for R peaks to be determined using a peak finding algorithm for local maxima detection. Lastly, the prefiltered ECG was transformed into phase space as defined in [122] to determine the fiducial points of P-wave, QRS complex, and T-wave. Special considerations were made for the cases of atrial and ventricular fibrillation, as they do not present all fiducial points in an ECG. These special considerations are discussed further in Section 6.5. An example of the phase space representation of Sinus Rhythm for documented Patient #11 can be seen in Figure 6.4 with specific wavelet transform peaks used to determine fiducial points.

4. Once the fiducial points were determined for each ECG dataset, the activation functions were calculated using the same trigonometric relationships and previously found respiratory function as described in Equations 6.6-6.9 from [109]. These equations detail the relationship between the pressure and volume of each heart chamber as they contract which can be modeled computationally as a time-varying elastance. The measured timing of the ECG fiducial points inform the elastance functions of the atrium ($AtrFunc(t)$) and ventricle ($VenFunc(t)$) in the CVS model, which are then utilized to determine the dynamic pressures and flows between heart chambers and systemic/pulmonary circulations. Using the arterial pressure (P_{ART}) measurements provided in the PhysioNet database for each patient, the elastance functions are modulated based on their corresponding P_{ART} peak, normalized from 0-1, and are then

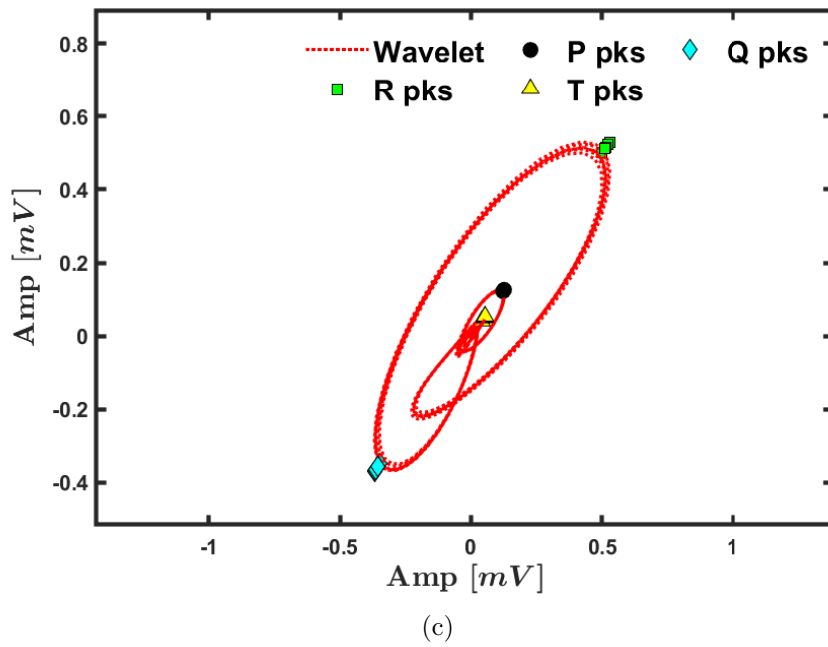
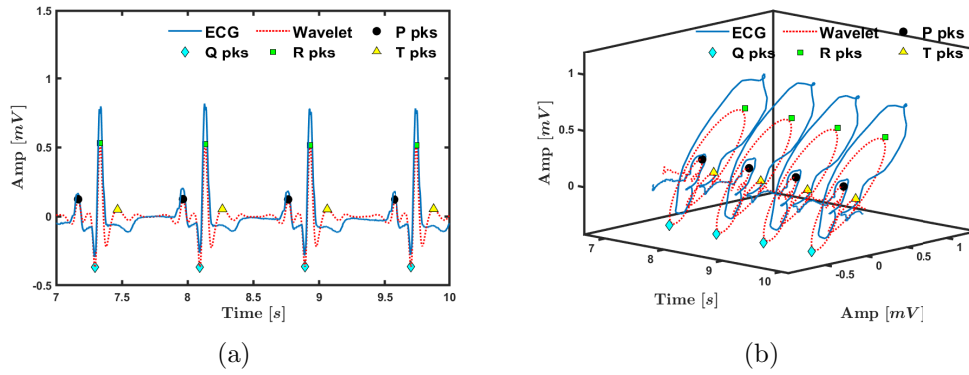


Figure 6.4: (a) Filtered ECG and wavelet transform with fiducial points, (b) ECG and wavelet representation in 3D phase space, (c) Zoomed wavelet transform in 2D phase space.

used as a replacement for the elastance functions in the CVS Model from [86]. The output from this process can be seen in Figure 6.5(b).

$$DiaAct(t) = \begin{cases} 0, & \text{if } 0 \leq t < T_1 \\ \sin(\frac{\pi(t-T_1)}{T_2-T_1}), & \text{if } T_1 \leq t \leq T_2 \\ 0, & T_4 \leq t \end{cases} \quad (6.6)$$

$$SysAct(t) = \begin{cases} 0, & \text{if } 0 \leq t < T_3 \\ \sin(\frac{\pi(t-T_3)}{T_4-T_3}), & \text{if } T_3 \leq t \leq T_4 \\ 0, & T_4 \leq t \end{cases} \quad (6.7)$$

$$VenFunc(t) = SysAct(t) + \alpha Resp(t) \quad (6.8)$$

$$AtrFunc(t) = DiaAct(t) + \alpha Resp(t) \quad (6.9)$$

In these equations, T_1 represents the onset of the P-wave, T_2 is the Q peak, T_3 is the R peak, T_4 is the offset of the T-wave, and $Resp(t)$ is the respiration function with weighted coefficient α .

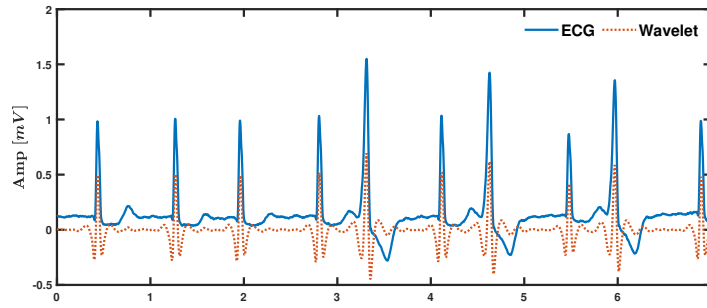
5. Following the implementation of the atrial and ventricular activation functions in the CVS model, the initial conditions and the lumped parameters of the model systemic circulation were tuned (within physiologically feasible ranges) such that the simulated aortic pressure and measured arterial pressure were able to match within 5-9% for the 0 LPM of mean VAD flow case (since none of the patients were documented with VAD support). Once tuned parameters were found, the same parameter values and activation functions were used to simulate the arrhythmic conditions with 3.5 LPM of mean VAD flow support.

Figure 6.5(c) provides an example of pressure output matching for the case of atrial fibrillation at 0 LPM of mean VAD flow. For the purposes of implementation in the hMCL, tuned CVS model output was scaled within the operating bounds of 0-120 mmHg when necessary.

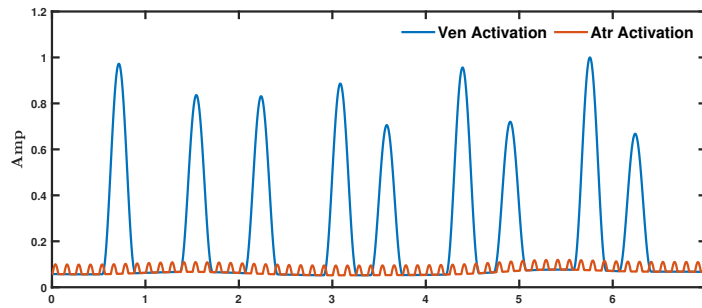
6.5 Cardiac Event List

Provided here is a list of simulated cardiac events as well as how the arrhythmic events present in the measured ECG. All ECG diagnoses were made by licensed clinicians at Massachusetts General Hospital and documented in the patient guide in the referenced database.

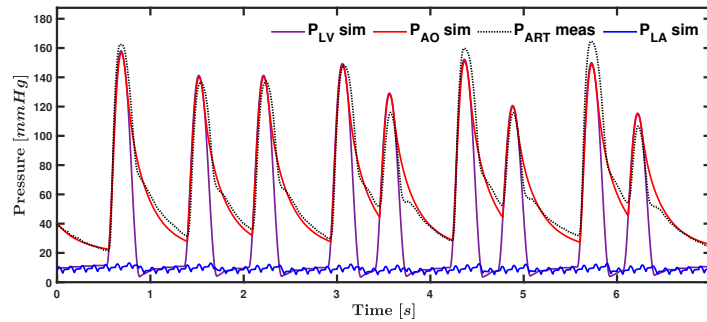
By definition, arrhythmias present as abnormal rhythms in the ECG, therefore the fiducial point determination method from [122] required modifications between each processed arrhythmia. For sinus bradycardia and tachycardia, which relate to the frequency at which the heart beats, the phase space method did not require modification as all fiducial points of the ECG were present. However, as stated previously, special considerations were made to account for atrial and ventricular fibrillation. The following list details the methods used to generate specific events as well as any adaptations performed if using Method 3.



(a)



(b)



(c)

Figure 6.5: (a) FIR filtered ECG signal and wavelet transform for AFib patient #23 from PhysioNet database, (b) Modulated and normalized atrial and ventricular activation functions with respiratory variation, (c) Parameter-tuned CVS model pressure reference output at 0 LPM mean VAD flow rate.

6.5.1 Aortic Valve Stenosis (AoSten)

Method 1 was used to generate aortic valve stenosis by updating the lumped valve resistance value in the real-time CVS model both with and without VAD flow support.

6.5.2 Sinus Bradycardia (S.Brady) and Tachycardia (S.Tach)

Irregular pacing of the heart in the form of sinus bradycardia and tachycardia (or IST) were generated using both Method 1 & 3. For Method 1, the heart rate of the real-time CVS model was updated to induce either irregularly slow (bradycardia) or fast (tachycardia) heart pacing. For generation using Method 3, no updates were required for fiducial point determination as all points are present in the ECG. Therefore, bradycardia and tachycardia were able to be implemented in the hMCL at both 0 LPM and 3.5 LPM of mean VAD flow support without any special considerations.

6.5.3 Atrial Fibrillation (AFib)

The generation of atrial fibrillation was done using both Methods 2 & 3. For Method 2, a figure of clinically measured data from [118] was imported into MATLAB and traced using the built in ‘imread’, ‘imshow’, and ‘ginput’ functions, which allow for pixel data to be saved and transformed per each click of the computer mouse. The traced waveform is then scaled according to appropriate time and magnitude units for use in the systemic circulation model.

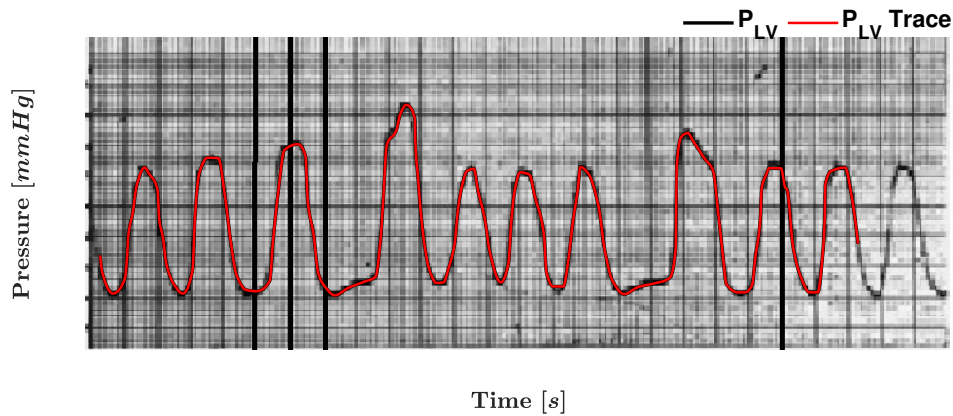


Figure 6.6: Image from Dodge 1957 ([118]) of measured left ventricular pressure during atrial fibrillation with traced waveform used for analysis.

For Method 3, it was necessary to account for the fact that atrial fibrillation presents with no P-wave in the ECG, instead fibrillation waves (referred to as F-waves) of irregular magnitude and frequency are present [123]. By looking at the frequencies present in the filtered atrial fibrillation ECG signal of patient #23, the F-waves frequencies were most prevalent in the 6-10 Hz ranges. Subsequently, the atrial contraction timing calculation from Method 3 (which requires P-wave and Q peak times) was instead replaced with a simulated fibrillation wave at a mean frequency of 8 Hz. The magnitude of the fibrillation wave was the normalized value of the max F-wave peak versus the max R wave peak (approximately 9%). Lastly, the simulated F-wave was then added to the respiratory function ($Resp(t)$) to account for respiratory variations.

6.5.4 Ventricular Fibrillation (VFib)

Ventricular fibrillation was generated using Method 3, though some considerations were necessary for analysis and simulation. Similar to atrial fibrillation, the P-wave of the ECG is absent and instead replaced with F-waves. These F-waves, however, are much larger in magnitude and typically also replace the QRS and T-waves, causing difficulty in ECG fiducial point determination [123]. In the event of *coarse* F-waves, which are defined based on relative magnitude [124], it is possible to determine the distinct peaks of ventricular contraction. Using the wavelet transform, the R peaks were found for these coarse F-waves and confirmed using the arterial pressure peaks as a reference (in terms of both quantity and magnitude). Rather than using the time difference between R peak and T-wave offset, ventricular contraction timing was determined heuristically by calculating the average arterial pressure frequency and adding half the period to the R peak times. Atrial contraction timing was simulated at the same rate as ventricular contraction with a time offset of half the period of oscillation.

Chapter 7

Cardiac Event Generation Results

In this chapter, preliminary test results of cardiac event generation in the hMCL are discussed in detail along with considerations for future improvement.

7.1 Preliminary hMCL Realization Results

7.1.1 Performance Criteria for Evaluation

The metrics used to assess the ability of the hMCL to recreate the desired cardiac events include calculations of RMS and mean percent error for dynamic pressure reference tracking as well as mean magnitude-squared coherence (MSC) value between the FFT of both reference and measured pressure content up to 30 Hz. First, RMS and mean percent error calculations provide insight into the accuracy of the hMCL to track the desired reference pressure signals. For pressure tracking error calculations, the 30 Hz low-pass filtered pressure measurements were used for comparison with the 20ms input-delayed pressure reference inputs. Secondly, the MSC algorithm provides a method to compare the similarity in frequency content of two signals [125], which is used to ensure the hMCL is realizing the desired frequency content of arrhythmic events. The MSC provides an output value in the range of 0 to 1 for each

discrete frequency assessed, where a value of 1 represents matching frequency content and a 0 value represents dissimilar frequency content. For each repeating cycle of pressure reference data, a Fast Fourier Transform (FFT) was taken of both the reference and measured data for both the AO and LV. Following the FFT, the magnitude of the MSC for the entire frequency spectrum was determined using the function ‘mscohere’ in MATLAB to compare the reference and measured FFT signals for both the AO and LV with a 1000 point hamming window. The resulting output was averaged from 0-30 Hz (the bandwidth of the hMCL) to provide the mean MSC value. The MSC calculation process can be seen in Figure 7.3 and quantitative results for all test cases can be seen in Table 7.1.

7.1.2 Method 1 - CVS Model Parameter Modification

This method utilized the inherent lumped parameters of the CVS model to recreate aortic valve stenosis and induced bradycardia/tachycardia by adjusting the parameters of aortic valve resistance and simulated patient heart rate, respectively. Figure 7.1 depicts the hMCL realization of aortic valve stenosis at 0 LPM of VAD flow with pressure references shown in dashed, black lines and measurements of P_{AO} and P_{LV} are shown in red and magenta, respectively. The distinctive pressure differential between LV and AO pressure during ejection is apparent in each cardiac cycle and can be adjusted based on aortic valve resistance magnitude.

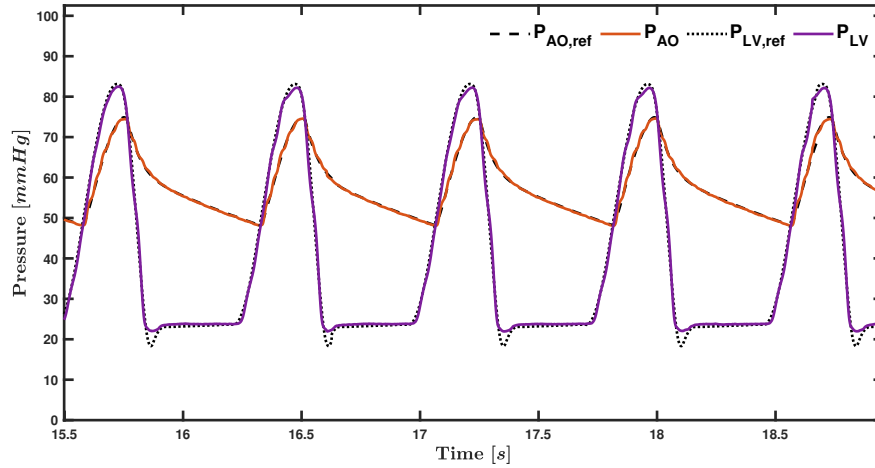
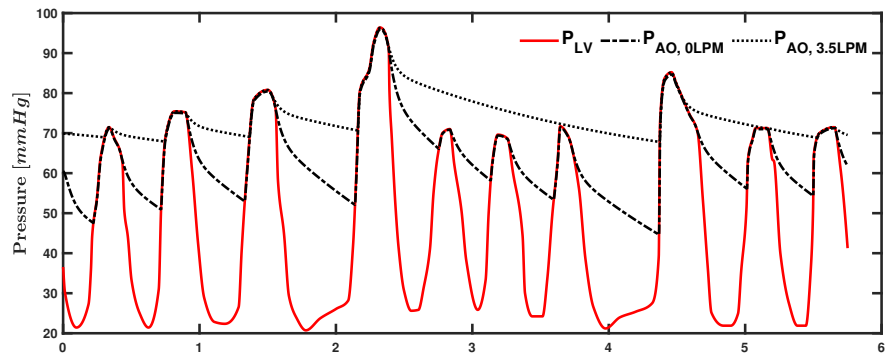


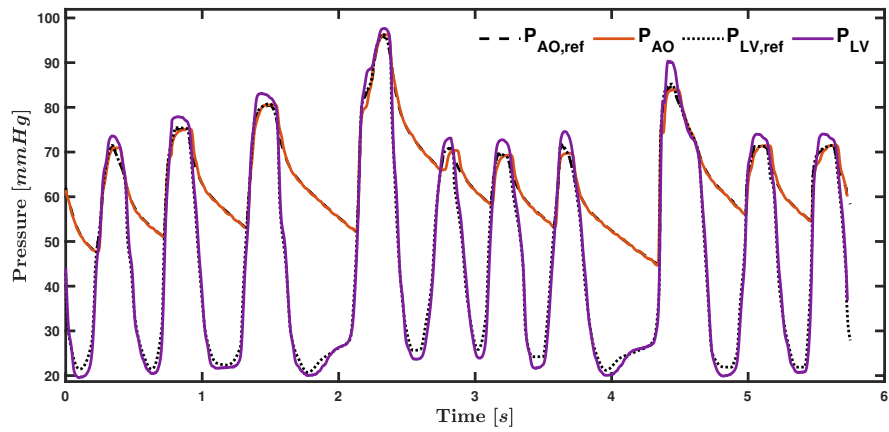
Figure 7.1: Hybrid MCL pressure tracking results for CVS model simulated aortic stenosis where valve resistance (R_{AO}) has been increased by 6x and mean VAD flow is set to 0 LPM.

7.1.3 Method 2 - Clinical Data Tracking

The systemic circulation model in Method 2 was propagated in two test cases using the left ventricular pressure (P_{LV}) data documented in [118] for a patient experiencing atrial fibrillation. The first test case was for a mean VAD flow rate of 0 LPM and the second had mean VAD flow rate set equal to 3.5 LPM. The results of Method 2 can be seen in Figure 7.2(a) where traced P_{LV} is shown in red and subsequent aortic pressure outputs (P_{AO}) of each simulation are shown in black, dashed lines. The trends of P_{LV} , P_{AO} , and the value of mean VAD flow rate were then utilized as reference inputs to the hMCL for the realization of atrial fibrillation. The corresponding results of the hMCL implementation for the 0 LPM mean VAD flow case can be seen in Figure 7.2(b).



(a)



(b)

Figure 7.2: (a) Systemic circulation model output of aortic pressure for 0 LPM and 3.5 LPM mean VAD flow cases, (b) hMCL pressure tracking results for 0 LPM mean VAD flow rate case.

7.1.4 Method 3 - CVS Model with Processed ECG Input

Using the ECG processing procedure as described in Method 3, cardiac arrhythmias of atrial fibrillation, sinus bradycardia and tachycardia, as well as ventricular fibrillation were recreated in the hMCL. Results of each test case

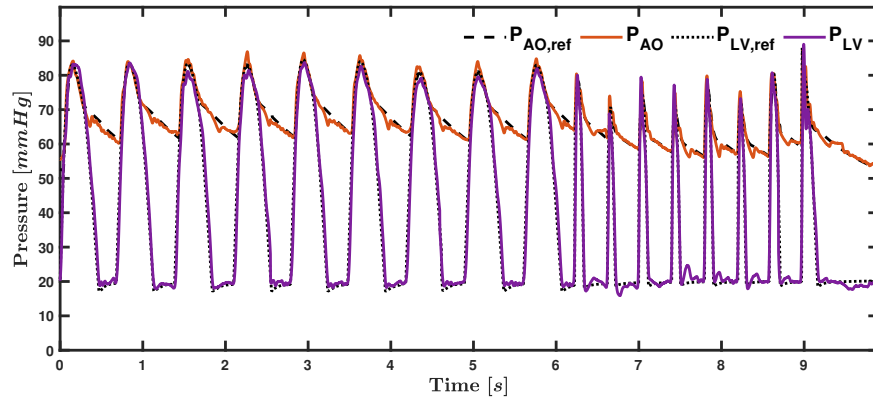
with mean VAD flow rates of 0 LPM and 3.5 LPM are presented in Table 7.1 along with the corresponding patient number as documented in the PhysioNet MGH/MF Waveform database. Figure 6.5 depicts the stages of processing measured patient ECG data to determine the hMCL pressure references for active pressure tracking. Example hMCL pressure realization from this process can be seen in Figure 7.3.

Table 7.1: Results from all 3 methods of cardiac event generation.

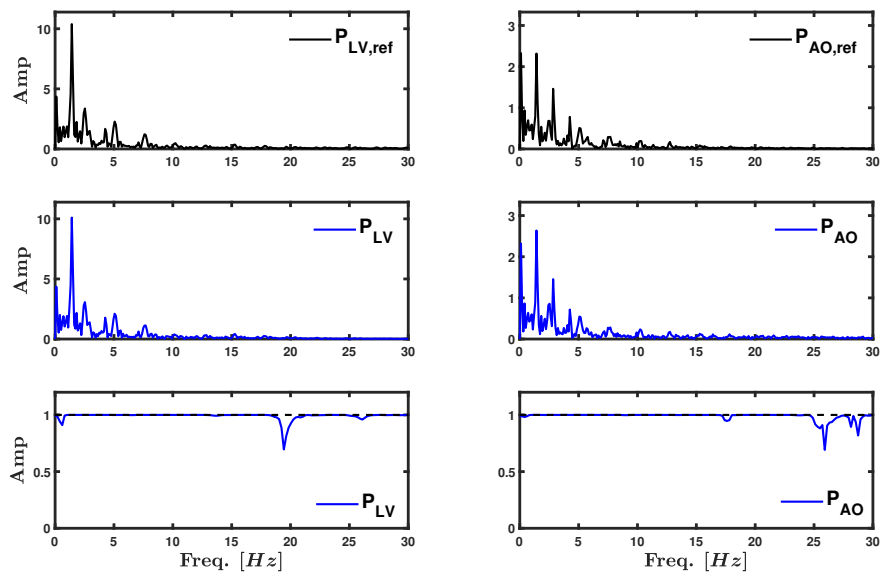
| Method | Test Case | Q_{VAD} [LPM] | Mean % Error AO, LV | $RMSE$ [mmHg] AO, LV | Mean MSC [0 - 1] AO, LV |
|--------|---------------------|--------------------|---------------------------|----------------------------|---------------------------------|
| 1 | AoSten: $6xR_{AO}$ | 0 | 0.39, 0.62 | 0.33, 1.16 | 0.96223, 0.99425 |
| | AoSten: $6xR_{AO}$ | 3.5 | 1.00, 2.56 | 1.19, 2.30 | 0.94509, 0.99730 |
| | AoSten: $8xR_{AO}$ | 3.5 | 0.97, 2.45 | 1.11, 1.49 | 0.96731, 0.99920 |
| | S.Brady: 50 BPM | 3.5 | 1.09, 3.85 | 1.18, 1.17 | 0.89672, 0.99770 |
| | S.Tach: 150 BPM | 3.5 | 1.66, 3.79 | 1.82, 2.52 | 0.99134, 0.99955 |
| 2 | AFib: Dodge 1957 | 0 | 0.99, 1.17 | 1.24, 2.36 | 0.97884, 0.98373 |
| | AFib: Dodge 1957 | 3.5 | 0.96, 1.82 | 1.07, 2.20 | 0.99814, 0.99180 |
| 3 | AFib: Patient 23 | 0 | 0.52, 0.76 | 0.54, 1.77 | 0.99965, 0.99983 |
| | AFib: Patient 23 | 3.5 | 1.52, 3.47 | 1.44, 2.08 | 0.98841, 0.99516 |
| | S.Brady: Patient 35 | 0 | 0.57, 0.78 | 0.74, 1.64 | 0.99919, 0.99082 |
| | S.Brady: Patient 35 | 3.5 | 1.49, 3.67 | 1.55, 2.71 | 0.99604, 0.99319 |
| | VFib: Patient 41 | 0 | 0.57, 0.64 | 0.84, 2.85 | 0.99860, 0.93733 |
| | VFib: Patient 41 | 3.5 | 1.21, 1.88 | 1.14, 2.44 | 0.98379, 0.96648 |
| | S.Tach: Patient 46 | 0 | 0.69, 0.90 | 1.00, 2.54 | 0.99915, 0.98942 |
| | S.Tach: Patient 46 | 3.5 | 1.75, 3.70 | 1.70, 3.21 | 0.97898, 0.97258 |

7.2 Discussion

Presented in this work are three potential methods for incorporating arrhythmic cardiac events and VAD induced aortic stenosis in hybrid mock circulation loop technology for the purposes of enhanced in vitro VAD validation. The



(a)



(b)

Figure 7.3: (a) Hybrid MCL pressure tracking results for tachycardic patient #46 with 3.5 LPM mean VAD flow support, (b) FFT frequency content results for the repeating 10s reference pressure input sequence (top) and measured hMCL pressures (middle), as well as subsequent MSC values (bottom) for all frequency content up to 30 Hz.

hMCL realization results for each method are presented in Table 7.1 and are discussed further in each following subsection along with limitations and future considerations.

7.2.1 Method 1 - CVS Model Parameter Modification

From Table 7.1 it can be seen that aortic stenosis with varying levels of valve resistance, as well as sinus bradycardia and tachycardia can be realized with low error or disparity in frequency content using Method 1. Figure 7.1 also shows the close dynamic tracking performance of the hMCL. In the case of bradycardia with 3.5 LPM of mean VAD flow, the mean MSC value for aortic pressure tracking was the lowest of all three tests. This seemed to be due to hardware limitations of the aortic voice coil actuator in the hMCL as it had to track to the limits of allowable pressure generation (± 50 mmHg).

One benefit of using this method is that both VAD flow rate and CVS model parameter adjustments can be made in real-time to vary the dynamic pressure references. A limitation of this method is that the ability to generate arrhythmias depends primarily on CVS model complexity and the adjustments that can be made therein. With the ability to adjust simulated patient heart rate, sinus rhythm pacing can be modified, however fibrillation and other atypical heart pacing events are difficult or impossible to emulate in the model presented here.

7.2.2 Method 2 - Clinical Data Tracking

Method 2 documented a method of utilizing clinically measured P_{LV} data as well as a model of the systemic circulation to generate aortic pressure reference trends based on simulated VAD flow. Figure 7.2 and Table 7.1 show low tracking error or disparity in frequency content generation for the tracking of measured atrial fibrillation data. This method is most applicable when clinical measurement data is available and various VAD flow rates are desired for examination. The systemic circulation model allows for extensions in simulated VAD flow profiles as well as the incorporation of a VAD dynamic model or pressure-flow (P-Q) look up table. The hMCL then tracks the pressure references and the VAD under test is set up such that the flow rate matches the simulated profile.

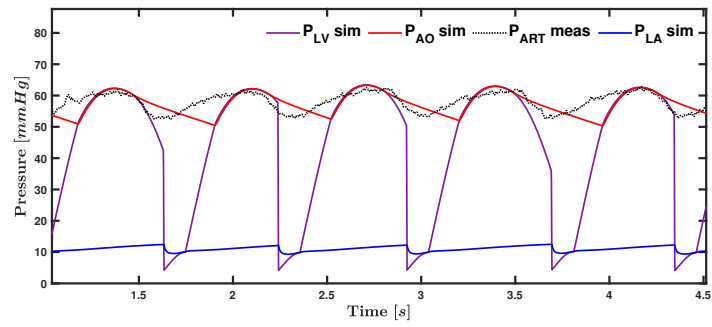
One limitation in Method 2 is that left ventricular pressure is not updated based on the flow being commanded by the VAD. As we know from the Frank-Starling Mechanism of the heart, heart contractility (and subsequent P_{LV}) increases as venous return increases during ventricular filling. Through this principle, as mean VAD flow increases, the volume of blood in the ventricle would be reduced during filling, thus decreasing P_{LV} magnitude during contraction. One method that could be used to account for this is to scale the reference P_{LV} based on desired mean VAD flow rate (e.g., scale the P_{LV} by a factor of 0.9x for a mean VAD flow rate of 3.5 LPM). This scaling factor could be approximated experimentally for various flow rates through the use of the CVS model in Method 1, in which the Frank-Starling Mechanism is

implemented.

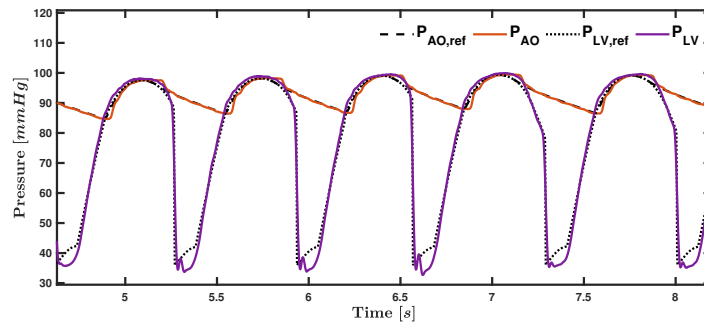
7.2.3 Method 3 - CVS Model with Processed ECG Input

As stated previously, Method 3 required the most analysis and processing for the purposes of arrhythmic cardiac event generation. This method required the analysis of measured and clinically diagnosed patient ECG data to inform the activation functions (or normalized elastances) of the atria and ventricles in the CVS model from Method 1. The results in Table 7.1 show minimal error and close frequency content correlation between the reference and measured signals for several patients experiencing different arrhythmic events. For each event tested, the percent error increased for the case with 3.5 LPM of mean VAD flow, however the AO and LV percent errors remained under 2% and 4%, respectively. By achieving low percent error, any discrepancies in frequency content were mitigated, resulting in acceptable mean MSC values near the maximum value of 1.

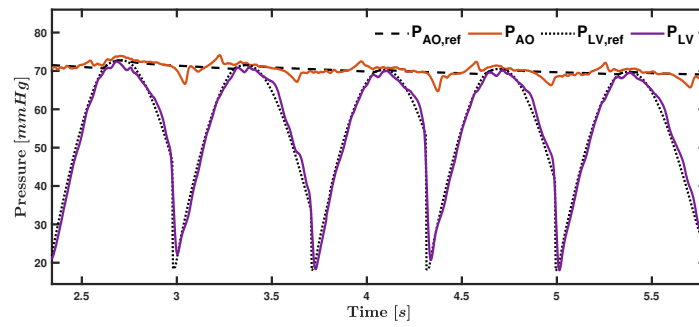
Though tracking error was minimal and frequency content was comparable to that of the ECG and arterial pressure measurements, the need for special considerations per each fibrillation event proved to be a limitation in this method. Specifically, the incorporation of ventricular fibrillation (VFib) required the most amount of hand adjusting via heuristic tuning of activation timing parameters. This tuning difficulty can be seen primarily in 7.4(a) as the simulated aortic and measured arterial pressures have greater disparity in overall pressure trend than that of the other arrhythmic cases (even though



(a)



(b)



(c)

Figure 7.4: Ventricular fibrillation in patient #41 - (a) CVS parameter tuning results and subsequent hMCL pressure tracking results for (b) 0 LPM mean VAD flow and (c) 3.5 LPM mean VAD flow cases.

mean absolute error was only $\approx 5\%$). Subsequent hMCL pressure realization for VFib can be seen in Figures 7.4(b) and 7.4(c) for both the 0 LPM and 3.5 LPM mean VAD flow cases.

Further, model limitations in diastolic aortic pressure trends (i.e., the rate of aortic pressure decay during diastole) made CVS parameter tuning difficult. These difficulties would arise for each independent patient profile, thus analyzing multiple patients worth of data would prove to be a tedious and difficult task. For future VFib implementation, the use of clinically measured data and use of Method 2 would be recommended. Atrial fibrillation (AFib) required some additional analysis of the ECG in terms of assessing frequency content for atrial activation function simulation, however this was much less intensive than VFib and could be automated in code for the analysis of various patient datasets. Further, the tuning of CVS initial conditions and systemic circulation parameter values could also be automated using optimization techniques such as least squares estimation for error minimization.

Chapter 8

Conclusion and Future Work

8.1 Conclusion

Hardware-in-the-loop (HIL) methods have been employed to test systems in the aerospace, automotive, and electrical power systems domain. Their capability of quickly and safely testing new designs and algorithms makes them increasingly suitable for implantable MCS devices, such as VADs. The development and use of HIL systems called hybrid mock circulation loops (hMCLs) for VAD testing has become the standard for in vitro validation procedures. Subsequently, as VAD technology advances towards more optimal performance and patient specific monitoring, so too must the design and dynamic capabilities of hMCLs. This work details the design and qualification of a prototype hMCL along with methods in which hMCL technology can improve in function for the specific purpose of enhancing VAD (or other MCS device) hardware and software validation procedures before being approved for human implantation. Current hMCL designs vary in literature and are often made based on manufacturer specific needs. Though hMCL technology has been around for several decades, there is little consensus on best design practices or methods for evaluation. This work takes some steps in this direction by suggesting a framework

of performance qualification through model-based design and experimental testing. Preliminary experiments demonstrate the capability of the prototype hMCL to realize various levels of simulated patient heart failure, reject VAD flow disturbances without incurring additional tracking errors, as well as show sensitivity to real-time changes in physiological parameters. Results from the experiments conducted can be used to guide design revisions aimed to maximize performance regarding these desired capabilities.

In recent years, VAD technology has improved in the area of physiological algorithms using both onboard measurements and clinically available data for the purposes of patient specific monitoring and adaptive pump control. Improved monitoring and diagnostics are essential in order to avoid physiological states that can lead to complications known to be responsible for serious and life-threatening conditions. By assessing hMCL sensitivity to changes in physiological parameters, it is possible to determine if the hMCL is capable of validating these developing VAD algorithms. One such example investigated in this work is estimation of systemic vascular resistance (SVR) using the onboard measurements from the pulsatile flow TORVADTM. The approach described shows that no additional sensing is required to provide additional ease of mind by providing a basis for automated diagnostics and therapy. This is highly desirable given that LVAD patients have made a significant investment through the implantation procedure. These algorithms will be deployed on the TORVADTM controller and future work is planned to test and evaluate the real-time estimation of SVR in both acute and chronic animal experiments.

This includes building a better understanding for how the SVR estimation algorithm responds subject to expected beat-to-beat variability, as well as other changes in patient hemodynamics. These issues can also be further studied with more advanced CVS models in the hMCL.

As VAD technology advances towards onboard patient monitoring and reactive physiological control, it is imperative that these algorithms undergo rigorous testing before implementation. Though hMCL technology has advanced to realize a wide range of simulated patient hemodynamic pressures, one area that has limited documentation is generation of atypical heart conditions, such as arrhythmias and valvular stenosis. These conditions, specifically, affect a large percentage of VAD implanted patients, thus motivating the need for hMCL ability to generate these events for analysis during VAD validation. In this work, methods which utilize both cardiovascular system (CVS) models and clinically documented arrhythmic patient data are presented for the purposes of realizing arrhythmic cardiac events and VAD induced valvular stenosis. For each method examined, it can be seen that the hMCL can track the generated pressure reference data with minimal error as well as recreate the desired frequency content of the presented arrhythmias. These results provide a means for implementation in future hMCLs for the purposes of enhanced VAD validation regarding arrhythmia or valvular stenosis monitoring/detection and subsequent physiological control applications.

8.2 Future Work

SVR Estimation

Chapter 5 details the feasibility of estimating systemic vascular resistance using only onboard VAD measurements in an hMCL. Further work in this area is necessary in terms of assessing estimation algorithm robustness and accuracy given a wide range of physiologically feasible initial conditions and cardiovascular model parameters. This could be done via a Monte Carlo simulation to aid in determining estimator accuracy bounds, settling time, and overall stability. Further, since heart failure patient health changes over time, it is important for the estimator to re-initialize periodically to ensure it is sensitive to physiological changes over long periods. This re-initialization process could include offline batch file or clinical measurement based system identification of cardiovascular model parameters for better absolute SVR estimate value accuracy. Lastly, as computational speeds and memory increases onboard VADs, more complex systemic CVS models as well as estimation algorithms (e.g., particle filters or machine learning) can be evaluated for use.

Cardiac Event Generation

A major component of generating arrhythmias in an hMCL is the actuator bandwidth required to recreate these high frequency oscillatory signals. The use of an additional voice coil actuator for the purposes of low magnitude, high frequency pressure generation is being investigated for new methods in hMCL arrhythmia realization. This method could be used in conjunction with the

methods presented here, or separately based on desired operational modes.

A prototype cardiac event generator (CEG) is shown in Figure 8.1. This prototype is comprised of a linear voice coil actuator with internal bearings (MotiCont GVCM-Series, MotiCont, Van Nuys, CA), a press-fit 3D printed piston, and a 3D printed frame that houses an 11/16 inch outer diameter tygon tubing. The frame was designed with an open housing such that it can be superimposed on existing hMCL tubing without the need to adjust any hMCL components. Further, the frame compresses the housed tubing such that the combination of the voice coil and the housing act in a similar fashion to that of a proportional flow valve. Depending on commanded voice coil duty cycle, the effective area of the tubing can be modulated to control the pressure differential across the CEG, thus inducing pressure changes in the hMCL.

By using a lightweight, press-fit 3D printed piston ($\approx 6\text{g}$), the mass of the voice coil piston assembly is minimized in order to maximize the allowable frequency range of the CEG. As Ropella et al. details in [126], mean magnitude-squared coherence (MSC) values in the range of 0-60 Hz for both fibrillatory and nonfibrillatory rhythms presents a potential means for future arrhythmia detection. Therefore, the CEG was designed with an allowable 0-60 Hz frequency range. Preliminary experimental results can be seen in Figure 8.2 where the pressure differential across the VAD, ($\Delta P = P_{LV} - P_{AO}$), is shown for both in nominal HF conditions and 60 Hz additive CEG conditions. Since the LV and AO PGIs controllers use the 30 Hz low-pass filtered measurements to calculate control output, as stated in Chapter 3, the 60 Hz superimposed CEG signal does not

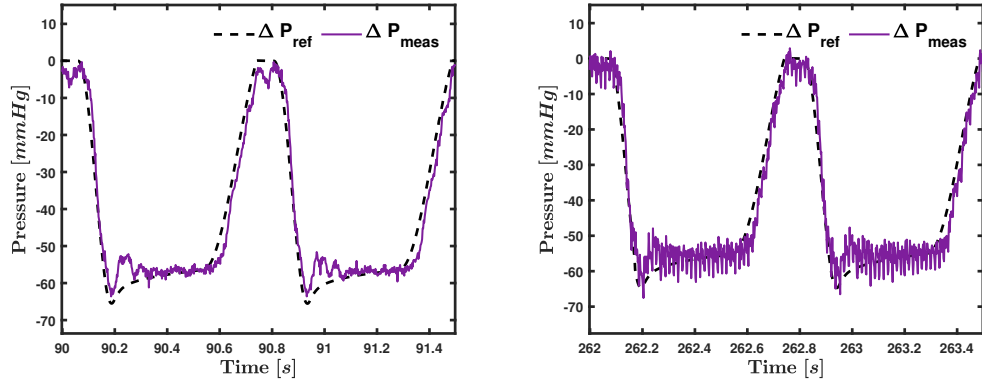


Figure 8.1: Prototype Cardiac Event Generator (CEG) for high frequency arrhythmia generation and suction event implementation.

affect PGI controller output or stability.

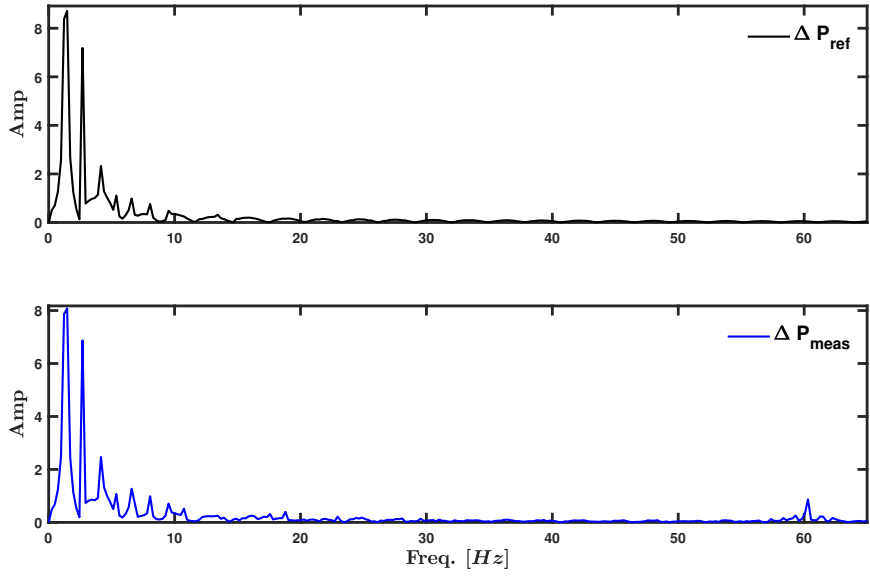
For this experiment, the CEG was housed on the hMCL between the recirculation pump and LV PGI, the mean VAD flow was set to 3.5 LPM, and the CEG commanded duty cycle was a 60 Hz sine wave with 50% duty magnitude and 50% duty offset. The frequency spectrum from Figure 8.2(c) shows a distinct peak at the 60 Hz operating point confirming the potential of using this CEG method for high frequency content generation. Lastly, due to its ability to be superimposed onto existing hMCL tubing, the CEG has the potential to be used to simulate varying levels of severity of VAD suction events at the outlet

of the LV PGI. This method of implementation and overall CEG design is still under evaluation.



(a)

(b)



(c)

Figure 8.2: CEG preliminary experiment for differential pressure across the VAD (a) before CEG operation, (b) during 60 Hz CEG operation, and (c) subsequent FFT frequency spectrum for 60 Hz CEG operation.

Appendices

Appendix A

List of Publications

A.1 Publications

Ethan S. Rapp, Suraj R. Pawar, Erik R. Larson, Jeffrey R. Gohean, and Raul G. Longoria. Estimation of systemic vascular resistance using built-in sensing from an implanted left ventricular assist device. *ASME Journal of Engineering and Science in Medical Diagnostics and Therapy, Special Issue on Novel and Emergent Personalized Cardiovascular Medicine*, 2019.

Ethan S. Rapp, Suraj R. Pawar, Erik R. Larson, Jeffrey R. Gohean, and Raul G. Longoria. Evaluating a Hardware-in-the-Loop System Intended for Testing Ventricular Assist Device Control and Sensing Algorithms. *American Control Conference*, 2020.

A.2 Conference Poster Presentations

Rapp, E. Orji, D., Gohean, J.R., Larson, E., Kurusz, M., Smalling, R.W., & Longoria, R.G. (2016). Design and Development of a Hybrid Mock Circulation Loop for Hardware-in-the-Loop Validation of VADs. *ASAIO 63rd Annual Conference*, Chicago, IL.

A.3 Master's Thesis

Rapp, E. (2016). Brushless DC Motor Modeling and Optimal Control: A Cardiovascular Application. Master's Thesis, The University of Texas at Austin, Austin, TX. <http://hdl.handle.net/2152/41207>

A.4 Papers Submitted

Suraj R. Pawar, **Ethan S. Rapp**, Jeffrey R. Gohean, and Raul G. Longoria. Parameter Identification of Cardiovascular System Model used for Left Ventricular Assist Device Algorithms. *ASME Journal of Engineering and Science in Medical Diagnostics and Therapy*, Submitted March 2021.

Ethan S. Rapp, Suraj R. Pawar, and Raul G. Longoria. Generation of Arrhythmic Cardiac Events and Valvular Stenosis in a Mock Circulatory Environment. *IEEE Transactions on Biomedical Engineering*, To Be Submitted August 2021.

Appendix B

Electromechanical hMCL System Dynamic Equations

The dynamic equations for the hMCL system in Figure 3.5 are defined here using bond graph modeling principles. There are a total of 13 independent, energy storing elements that make up the lumped parameter bond graph model as summarized in Section 3.4. For clarity, the linear state space representation of the hMCL system is again provided here for reference.

$$\text{States: } \mathbf{x}(1 : 4) = [i_{ao} \quad x_{1,ao} \quad v_{ao} \quad x_{2,ao}]^T$$

$$\mathbf{x}(5 : 8) = [v_{pao} \quad x_{dao} \quad V_{ao} \quad V_{lv}]^T$$

$$\mathbf{x}(9 : 13) = [x_{dlv} \quad v_{plv} \quad x_{1,lv} \quad v_{lvt} \quad i_{lv}]^T$$

$$\text{Inputs: } \mathbf{u} = [u_{ao} \quad u_{lv} \quad Q_{rc}]^T$$

$$\text{Disturbances: } \mathbf{\Gamma} = [Q_{vad} \quad g]^T$$

$$\text{Dynamics: } \dot{\mathbf{x}} = A\mathbf{x} + B\mathbf{u} + E\mathbf{\Gamma}$$

$$\text{Measurements: } \mathbf{y} = [P_{ao} \quad P_{lv} \quad h_{LVIT}]^T = C\mathbf{x} + D\mathbf{u} + F\mathbf{\Gamma}$$

The detailed state equations can be written as,

$$\dot{i}_{ao} = \frac{1}{L_{cao}} (u_{ao} - R_{cao}i_{ao} - r_{ao}v_{ao}) \quad (\text{B.1})$$

$$\dot{x}_{1,ao} = -v_{ao} \quad (\text{B.2})$$

$$\dot{v}_{ao} = \frac{1}{m_{ao}} (kx_{1,ao} + r_{ao}i_{ao} + m_{ao}g - kx_{2,ao}) \quad (\text{B.3})$$

$$\dot{x}_{2,ao} = v_{ao} - v_{pao} \quad (\text{B.4})$$

$$\dot{v}_{pao} = \frac{1}{m_{pao}} \left(kx_{2,ao} + m_{pao}g - R_{pao}v_{pao} - \frac{x_{dao}}{C_{dao}} \right) \quad (\text{B.5})$$

$$\dot{x}_{dao} = v_{pao} - \frac{1}{A_p} (Q_{vad} - Q_{rc} + \lambda) \quad (\text{B.6})$$

$$\dot{V}_{ao} = Q_{vad} - Q_{rc} + \lambda \quad (\text{B.7})$$

$$\dot{V}_{lv} = Q_{rc} - Q_{vad} - \lambda \quad (\text{B.8})$$

$$\dot{x}_{dlv} = v_{plv} - \frac{1}{A_p} (Q_{rc} - Q_{vad} - \lambda) \quad (\text{B.9})$$

$$\dot{v}_{plv} = \frac{1}{m_{plv}} \left(kx_{1,lv} + m_{plv}g - R_{plv}v_{plv} - \frac{x_{dlv}}{C_{dlv}} \right) \quad (\text{B.10})$$

$$\dot{x}_{1,lv} = v_{lvt} - v_{plv} \quad (\text{B.11})$$

$$\dot{v}_{lvt} = \frac{1}{m_{lvt}} (r_{lv}i_{lv} + m_{lvt}g - kx_{1,lv}) \quad (\text{B.12})$$

$$\dot{i}_{lv} = \frac{1}{L_{clv}} (u_{lv} - R_{clv}i_{lv} - r_{lv}v_{lvt}) \quad (\text{B.13})$$

where λ represents the algebraic loop elements due to ideal flow source leakage resistances and R_{eq} is the equivalent leakage resistance.

$$\lambda = R_{eq} \left(\frac{V_{lv}}{C_{lv}} + \frac{x_{dao}}{A_p C_{dao}} - \frac{V_{ao}}{C_{ao}} - \frac{x_{dlv}}{A_p C_{dlv}} \right) \quad (\text{B.14})$$

$$R_{eq} = \frac{R_{rc} + R_{vad}}{R_{rc} R_{vad}} \quad (\text{B.15})$$

Output equations for the system can be defined as,

$$P_{ao} = \frac{V_{ao}}{C_{ao}} + \frac{x_{dao}}{A_p C_{dao}} \quad (\text{B.16})$$

$$P_{lv} = \frac{V_{lv}}{C_{lv}} + \frac{x_{dlv}}{A_p C_{dlv}} \quad (\text{B.17})$$

$$h_{LVIT} = x_{1,lv} \quad (\text{B.18})$$

Using MATLAB's built in 'jacobian' function, which can be used to take the gradient of the dynamic equations with respect to the states (i.e., solve for the linear, state space A matrix), as well as the 'eig' function, which determines the eigenvalues of the linear system, the following eigenvalues for the open-loop system were found:

Table B.1: Calculated open-loop eigenvalues found for the hMCL simulation.

| Eigenvalues |
|-----------------------------|
| 0 |
| 0 |
| 0 |
| -1.608e-1 |
| -4.882e1 ± 1.014e2 <i>i</i> |
| -8.265e1 ± 3.499e2 <i>i</i> |
| -1.153e3 |
| -2.273e3 |
| -1.851e3 ± 7.386e3 <i>i</i> |
| -2.272e3 ± 2.390e4 <i>i</i> |

Note that all open-loop eigenvalues are zero or have negative real parts, thus confirming the stability of the simulated model.

Table B.2 provides the lumped parameter values used for the simulation and for eigenvalue calculation.

Table B.2: Parameter values used for hMCL simulation in MATLAB. Note: piston mass, diaphragm compliance, and tank capacitance for the AO and LV PGIs are the same in magnitude.

| Parameter | Value | Units |
|--------------------|----------------|---------------------|
| ρ | 998 | kg/m ³ |
| g | 9.81 | m/s ² |
| A_p | 4.56e-3 | m ² |
| R_{cao}, R_{clv} | 3.9, 3 | Ohm |
| L_{cao}, L_{clv} | 1.6e-3, 2.4e-3 | H |
| r_{ao}, r_{lv} | 9.6, 14.5 | N/A |
| k | 9036.55 | N/m |
| m_{ao}, m_{lv} | 0.15, 0.774 | kg |
| m_{pao}, m_{plv} | 0.1 | kg |
| R_{pao}, R_{plv} | 250, 350 | N·s/m |
| C_{dao}, C_{dlv} | 1.75e-7 | m/N |
| C_{ao}, C_{lv} | 4.66e-7 | m ³ /Pa |
| R_{rc} | 1.597e9 | Pa·s/m ³ |
| R_{vad} | 8.541e7 | Pa·s/m ³ |

Appendix C

Physiological Effects of VAD Support

The aortic valve flows versus time corresponding to the various mean VAD flow rate tests were also plotted to show the inverse correlation between mechanical circulatory support and output aortic flow. As shown in Figure C.1, a decrease in mean VAD flow subsequently increases the flow rate out of the aortic valve.

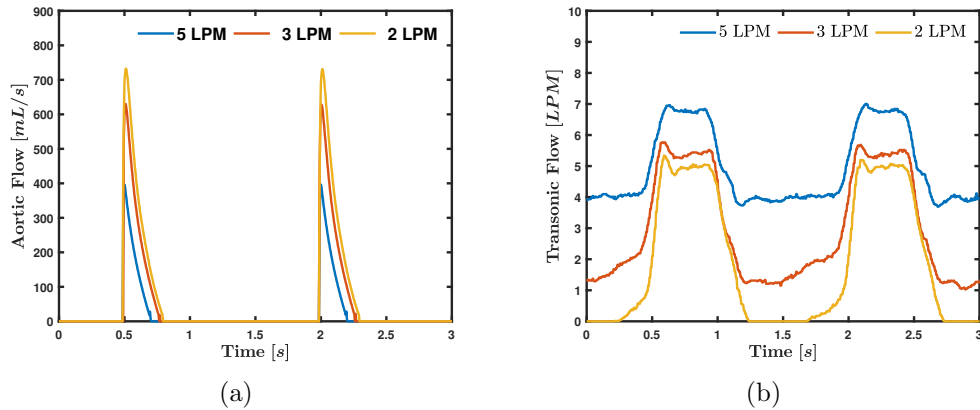


Figure C.1: (a) CVS model propagated aortic valve flow versus time for 5, 3, and 2 LPM VAD flow rate cases shown in (b).

Bibliography

- [1] Benjamin, E. J., Muntner, P., Alonso, A., Bittencourt, M. S., Callaway, C. W., Carson, A. P., Chamberlain, A. M., Chang, A. R., Cheng, S., Das, S. R., Delling, F. N., Djousse, L., Elkind, M. S. V., Ferguson, J. F., Fornage, M., Jordan, L. C., Khan, S. S., Kissela, B. M., Knutson, K. L., Kwan, T. W., Lackland, D. T., Lewis, T. T., Lichtman, J. H., Longenecker, C. T., Loop, M. S., Lutsey, P. L., Martin, S. S., Matsushita, K., Moran, A. E., Mussolino, M. E., O’Flaherty, M., Pandey, A., Perak, A. M., Rosamond, W. D., Roth, G. A., Sampson, U. K. A., Satou, G. M., Schroeder, E. B., Shah, S. H., Spartano, N. L., Stokes, A., Tirschwell, D. L., Tsao, C. W., Turakhia, M. P., VanWagner, L. B., Wilkins, J. T., Wong, S. S., and Virani, S. S., 2019. “Heart disease and stroke statistics - 2019 update: A report from the american heart association”. *Circulation*, **139**(1), pp. e70–e86.
- [2] Givertz, M. M., 2011. “Ventricular assist devices”. *Circulation*, **124**(12), pp. e305–e311.
- [3] Colvin, M., Smith, J. M., Hadley, N., Skeans, M. A., Uccellini, K., Lehman, R., Robinson, A. M., Israni, A. K., Snyder, J. J., and Kasiske, B. L., 2019. “OPTN/SRTR 2017 annual data report: Heart”. *American Journal of Transplantation*, **19**(S2), pp. 1–81.

- [4] D.Pagani, F., Miller, L. W., Russell, S. D., Aaronson, K. D., John, R., Boyle, A. J., Conte, J. V., Bogaev, R. C., MacGillivray, T. E., Naka, Y., Mancini, D., Massey, H. T., Chen, L., Klodell, C. T., Aranda, J. M., Moazami, N., Ewald, G. A., Farrar, D. J., and Frazier, O. H., 2009. “Extended mechanical circulatory support with a continuous-flow rotary left ventricular assist device”. *Journal of the American College of Cardiology*, **54**(4), pp. 312–321.
- [5] John, R., Kamdar, F., Liao, K., Colvin-Adams, M., Boyle, A., and Joyce, L., 2008. “Improved survival and decreasing incidence of adverse events with the HeartMate II left ventricular assist device as bridge-to-transplant therapy”. In Forth-fourth Annual Meeting of The Society of Thoracic Surgeons, Vol. 86, The Society of Thoracic Surgeons, pp. 1227–1235.
- [6] Briasoulis, A., Inampudi, C., Akintoye, E., Adegbala, O., Alvarez, P., and Bhama, J., 2018. “Trends in utilization, mortality, major complications, and cost after left ventricular assist device implantation in the united states (2009 to 2014)”. *American Journal of Cardiology*, **121**(10), pp. 1214–1218.
- [7] Lahpor, J., Khaghani, A., Hetzer, R., Pavie, A., Friedrich, I., Sander, K., and Strüber, M., 2009. “European results with a continuous-flow ventricular assist device for advanced heart-failure patients”. *European Journal of Cardio-thoracic Surgery*, **37**, pp. 357–361.

- [8] Birks, E. J., George, R. S., Firouzi, A., Wright, G., Bahrami, T., Yacoub, M. H., and Khaghani, A., 2012. “Long-term outcomes of patients bridged to recovery versus patients bridged to transplantation”. *The Journal of Thoracic and Cardiovascular Surgery*, **14**(1), pp. 190–196.
- [9] Prinzing, A., Herold, U., Berkefeld, A., Krane, M., Lange, R., and Voss, B., 2016. “Left ventricular assist devices – current state and perspectives”. *Journal of Thoracic Disease*, **8**, pp. E660–E666.
- [10] Jakovljevic, D. G., McDiarmid, A., Hallsworth, K., Seferovic, P. M., Ninkovic, V. M., Parry, G., Schueler, S., Trenell, M. I., and MacGowan, G. A., 2014. “Effect of left ventricular assist device implantation and heart transplantation on habitual physical activity and quality of life”. *The American Journal of Cardiology*, **114**(1), pp. 88–93.
- [11] Kiernan, M. S., Sundareswaran, K. S., Pham, D. T., Kapur, N. K., Pereira, N. L., Strueber, M., Farrar, D. J., Denofrio, D., and Rogers, J. G., 2016. “Preoperative determinants of quality of life and functional capacity response to left ventricular assist device therapy”. *Journal of Cardiac Failure*, **22**(10), pp. 797–805.
- [12] Jakovljevic, D. G., Yacoub, M. H., Schueler, S., MacGowan, G. A., Velicki, L., Seferovic, P. M., Hothi, S., Tzeng, B.-H., Brodie, D. A., Birks, E., and Tan, L.-B., 2017. “Left ventricular assist device as a bridge to recovery for patients with advanced heart failure”. *Journal of the American College of Cardiology*, **69**(15), pp. 1924–1933.

- [13] Rogers, J. G., Pagani, F. D., Tatooles, A. J., Bhat, G., Slaughter, M. S., Birks, E. J., Boyce, S. W., Najjar, S. S., Jeevanandam, V., Anderson, A. S., Gregoric, I. D., Mallidi, H., Leadley, K., Aaronson, K. D., Frazier, O., and Milano, C. A., 2017. “Intrapericardial left ventricular assist device for advanced heart failure”. *New England Journal of Medicine*, **376**(5), pp. 451–460.
- [14] Mehra, M. R., Goldstein, D. J., Uriel, N., Cleveland, J. C., Yuzefpolskaya, M., Salerno, C., Walsh, M. N., Milano, C. A., Patel, C. B., Ewald, G. A., Itoh, A., Dean, D., Krishnamoorthy, A., Cotts, W. G., Tatooles, A. J., Jorde, U. P., Bruckner, B. A., Estep, J. D., Jeevanandam, V., Sayer, G., Horstmanshof, D., Long, J. W., Gulati, S., Skipper, E. R., OConnell, J. B., Heatley, G., Sood, P., and Naka, Y., 2018. “Two-year outcomes with a magnetically levitated cardiac pump in heart failure”. *New England Journal of Medicine*, **378**(15), pp. 1386–1395.
- [15] Kormos, R. L., McCall, M., Althouse, A., Lagazzi, L., Schaub, R., Kormos, M. A., Zaldonis, J. A., Sciortino, C., Lockard, K., Kuntz, N., Dunn, E., and Teuteberg, J. J., 2017. “Left ventricular assist device malfunctions”. *Circulation*, **136**, pp. 1714–1725.
- [16] Gohean, J. R., Larson, E. R., Hsi, B. H., Kurusz, M., Smalling, R. W., and Longoria, R. G., 2017. “Scaling the low-shear pulsatile torvad for pediatric heart failure”. *ASAIO Journal*, **63**(2), pp. 198–206.
- [17] Bartoli, C. R., Hennessy-Strahs, S., Gohean, J., Villeda, M., Larson,

- E., Longoria, R., Kurusz, M., Acker, M., and Smalling, R., 2018. “A novel toroidal-flow left ventricular assist device minimizes blood trauma: Implications of improved ventricular assist device hemocompatibility”. *The Annals of Thoracic Surgery (In Press)*.
- [18] Zayat, R., Moza, A., Grottke, O., Grzanna, T., Fechter, T., Motomura, T., Schmidt-Mewes, C., Breuer, T., Autschbach, R., Rossaint, R., et al., 2019. “In vitro comparison of the hemocompatibility of two centrifugal left ventricular assist devices”. *The Journal of thoracic and cardiovascular surgery*, **157**(2), pp. 591–599.
- [19] Yoshizawa, M., Sato, T., Tanaka, A., Abe, K., Takeda, H., Yambe, T., Nitta, S., and Nosé, Y., 2002. “Sensorless estimation of pressure head and flow of a continuous flow artificial heart based on input power and rotational speed”. *ASAIO Journal*, **48**, pp. 43–448.
- [20] Ayre, P. J., Lovell, N. H., and Woodard, J. C., 2003. “Non-invasive flow estimation in an implantable rotary blood pump: a study considering non-pulsatile and pulsatile flows”. *Physiological Measurement*, **24**, pp. 179–181.
- [21] AlOmari, A. H., Savkin, A. V., Karantonis, D. M., Lim, E., and Lovell, N. H., 2009. “Non-invasive estimation of pulsatile flow and differential pressure in an implantable rotary blood pump for heart failure patients”. *Physiological Measurement*, **30**, pp. 371–386.
- [22] Reyes, C., Voskoboynikov, N., Chorpenning, K., LaRose, J. A., Brown,

- M. C., Nunez, N. J., Burkhoff, D., and Tamez, D., 2016. “Accuracy of the HVAD pump flow estimation algorithm”. *ASAIO Journal*, **62**, pp. 15–19.
- [23] Shida, S., Masuzawa, T., and Osa, M., 2019. “Flow rate estimation of a centrifugal blood pump using the passively stabilized eccentric position of a magnetically levitated impeller”. *The International Journal of Artificial Organs*, **42**(6), pp. 291–298.
- [24] Pauls, J. P., Stevens, M. C., Bartnikowski, N., Fraser, J. F., Gregory, S. D., and Tansley, G., 2016. “Evaluation of physiological control systems for rotary left ventricular assist devices: An in-vitro study”. *Annals of Biomedical Engineering*, **44**(8), Aug, pp. 2377–2387.
- [25] Tchantchaleishvili, V., Luc, J. G. Y., Cohan, C. M., Phan, K., Hbbert, L., Day, S. W., and Massey, H. T., 2017. “Clinical implications of physiologic flow adjustment in continuous-flow left ventricular assist devices”. *ASAIO Journal*, **63**(3), pp. 240–250.
- [26] Ochsner, G., Wilhelm, M. J., Amacher, R., Petrou, A., Cesarovic, N., Staufert, S., Röhrnbauer, B., Maisano, F., Hierold, C., Meboldt, M., and Daners, M. S., 2017. “*In vivo* evaluation of physiologic control algorithms for left ventricular assist devices based on left ventricular volume or pressure”. *ASAIO Journal*, **63**, pp. 568–577.
- [27] Petrou, A., Kanakis, M., Boës, S., Pergantis, P., Meboldt, M., and Daners, M. S., 2018. “Viscosity prediction in a physiologically controlled

- ventricular assist device”. *IEEE Transactions on Biomedical Engineering*, **65**(10), pp. 2355–2364.
- [28] Topkara, V. K., Kondareddy, S., Malik, F., Wang, I.-W., Mann, D. L., Ewald, G. A., and Moazami, N., 2010. “Infectious complications in patients with left ventricular assist device: Etiology and outcomes in the continuous-flow era”. *The Annals of Thoracic Surgery*, **90**(4), pp. 1270–1277.
- [29] Compostella, L., Russo, N., Setzu, T., Tursi, V., Bottio, T., Tarzia, V., Compostella, C., Covolo, E., Livi, U., Gerosa, G., Sani, G., and Bellotto, F., 2013. “Cardiac autonomic dysfunction in the early phase after left ventricular assist device implant: Implications for surgery and follow-up?”. *The International Journal of Artificial Organs*, **36**(6), pp. 410–418.
- [30] Kadado, A. J., Akar, J. G., and Hummel, J. P., 2018. “Arrhythmias after left ventricular assist device implantation: Incidence and management”. *Trends in Cardiovascular Medicine*, **28**(1), pp. 41–50.
- [31] Gopinathannair, R., Cornwell, W. K., Dukes, J. W., Ellis, C. R., Hickey, K. T., Joglar, J. A., Pagani, F. D., Roukoz, H., Slaughter, M. S., and Patton, K. K., 2019. “Device therapy and arrhythmia management in left ventricular assist device recipients: A scientific statement from the american heart association”. *Circulation*, **139**(20), pp. e967–e989.
- [32] Gopinathannair, R., Cornwell, W. K., Dukes, J. W., Ellis, C. R., Hickey,

- K. T., Joglar, J. A., Pagani, F. D., Roukoz, H., Slaughter, M. S., and Patton, K. K., 2019. “Device therapy and arrhythmia management in left ventricular assist device recipients: A scientific statement from the american heart association”. *Circulation*, **139**(20), pp. e967–e989.
- [33] Sims, D. B., Rosner, G., Uriel, N., González-Costello, J., Ehlert, F. A., and Jorde, U. P., 2012. “Twelve hours of sustained ventricular fibrillation supported by a continuous-flow left ventricular assist device”. *Pacing and Clinical Electrophysiology*, **35**(5), pp. e144–e148.
- [34] Yu, Y.-C., 1998. “Minimally invasive estimation of cardiovascular parameters”. PhD thesis, University of Pittsburgh.
- [35] Gelb, A., 1974. *Applied Optimal Estimation*. The MIT Press.
- [36] Kolff, W. J., 1959. “Mock circulation to test pumps designed for permanent replacement of damaged hearts”. *Cleveland Clinic Quarterly*, **26**, pp. 223–226.
- [37] Ochsner, G., Amacher, R., Amstutz, A., Plass, A., Schmid Daners, M., Tevæarai, H., Vandenberghe, S., Wilhelm, M. J., and Guzzella, L. A., 2013. “Novel interface for hybrid mock circulations to evaluate ventricular assist devices”. *IEEE Transactions On Biomedical Engineering*, **60**(2), pp. 507–516.
- [38] Haruyuki, M., Helmut, R., and Jurgen, R., 1978. “Development of a hydraulic analog of the human circulatory system for testing artificial

- hearts". *KEO Engineering Reports*, **31**.
- [39] Oh, T., 1974. "Dynamic response of the mock circulation". *Langenbecks Arch Chiv*, **335**, pp. 75–82.
- [40] Klain, M., 1970. "Comparative testing of artificial hearts and heart valves in a mock circulation". *Adv Biomed Eng Med Phys*, **3**, p. 131.
- [41] Mrava, G., 1970. "Mock circulation for artificial hearts". *Adv Biomed Eng Med Phys*, **3**, p. 115.
- [42] Wallner, F., 1974. "Development of a circulation mock-up". *Langenbecks Arch Chiv*, **335**, p. 61.
- [43] Wolf Jr, L., and Clinch, J. M., 1972. "Mock circulatory system for intra-aortic balloon testing". *IEEE Trans Biomed Eng*, **19**, p. 38.
- [44] O'Bannon, W., Lloyd III, J. M., and DeBakey, M. E., 1979. "In vitro testing of artificial heart power unit and ventricles in closed mock circulatory loop". In First US-USSR Symposium on Mechanically Assisted Circulation.
- [45] Westerhof, N., Elzinga, G., and Sipkema, P., 1971. "An artificial arterial system for pumping hearts". *J Appl Physiol*, **31**, p. 776.
- [46] Reul, H., Tesch, B., Schoenmackers, J., and Effert, S., 1974. "A hydromechanic model of left ventricle, aorta and its branches, simulation of geometry, haemodynamics, and elasticity". *Basic Res Cardiol*, **69**, p. 257.

- [47] High, K. M., Brighton, J. A., Brickman, A. D., and Pierce, W. S., 1977. “Analysis of an artificial ventricle and mock circulatory system”. *Trans ASME J Biomech Eng*, **99**(K), p. 184.
- [48] Donovan Jr., F. M., 1975. “Design of a hydraulic analog of the circulatory system for evaluating artificial hearts”. *Biomaterials Medical Devices Artificial Organs*, **3**(4), pp. 439–449.
- [49] Rosenberg, G., Phillips, W., Landis, D., and Pierce, W., 1981. “Design and evaluation of the pennsylvania state university mock circulatory system”. *ASAIO Journal*, **4**(2), 1, pp. 41–49.
- [50] Ferrari, G., Mimmo, R., Tosti, G., Gorczinska, K., and Grodzicki, K., 1987. “A new hydraulic simulator of the circulatory system. some experimental results reproducing a physiological and a pathological state”. *Biocybernetics and Biomedical Engineering*, **7**, pp. 87–103.
- [51] Ferrari, G., Lazzari, C. D., Mimmo, R., Ambrosi, D., and Tosti, G., 1994. “Mock circulatory system for in vitro reproduction of the left ventricle, the arterial tree and their interaction with a left ventricular assist device”. *Journal of Medical Engineering & Technology*, **18**(3), pp. 87–95.
- [52] Williams, J., Antaki, J., Boston, J., Williams, S., Woodard, J., Miller, P., and Kormos, R., 1994. “Load sensitive mock circulatory system for left ventricular assist device controller evaluation and development”. In Proceedings of 16th Annual International Conference of the IEEE

Engineering in Medicine and Biology Society, pp. 89–90.

- [53] Baloa, L. A., Boston, J. R., and Antaki, J. F., 2001. “Elastance-based control of a mock circulatory system”. *Annals of Biomedical Engineering*, **29**(3), pp. 244–251.
- [54] Loh, M., and Yu, Y.-C., 2004. “Feedback control design for an elastance-based mock circulatory system”. In Proceedings of the 2004 American Control Conference, IEEE, pp. 1639–1644.
- [55] Ferrari, G., Lazzari, C. D., Mimmo, R., Tosti, G., Ambrosi, D., and Gorczynska, K., 1998. “A computer controlled mock circulatory system for mono- and biventricular assist device testing”. *The International Journal of Artificial Organs*, **24**(7), pp. 456–462.
- [56] Pantalos, G. M., Koenig, S. C., Gillars, K. J., Giridharan, G. A., and Ewert, D. L., 2004. “Characterization of an adult mock circulation for testing cardiac support devices”. *ASAIO Journal*, **50**, pp. 37–46.
- [57] Liu, Y., Allaire, P., Wood, H., and Olsen, D., 2005. “Design and initial testing of a mock human circulatory loop for left ventricular assist device performance testing”. *Artif Organs*, **29**(4), pp. 341–345.
- [58] Liu, Y., Allaire, P., Wu, Y., Wood, H., and Olsen, D., 2006. “Construction of an artificial heart pump performance test system”. *Cardiovasc Eng*, **6**, pp. 153–160.
- [59] Timms, D., Hayne, M., McNeil, K., and Galbraith, A., 2005. “A com-

- plete mock circulation loop for the evaluation of left, right, and biventricular assist devices”. *Artificial Organs*, **29**(7), pp. 564–572.
- [60] Timms, D., Hayne, M., Tan, A., and Pearcy, M., 2005. “Evaluation of left ventricular assist device performance and hydraulic force in a complete mock circulation loop”. *Artificial Organs*, **29**(7), pp. 573–580.
- [61] Gregory, S. D., Stevens, M., Timms, D., and Pearcy, M., 2011. “Replication of the frank-Starling response in a mock circulation loop”. In 33rd Annual International Conference of the IEEE EMBS, IEEE, pp. 6825–6828.
- [62] Sharp, M. K., Richards, C. M., Gillars, K. J., Giridharan, G., and Pantalos, G. M., 2008. “The influence of mock circulation input impedance on valve acceleration during *in vitro* cardiac device testing”. *ASAIO Journal*, **54**, pp. 341–346.
- [63] Ferrari, G., Kozarski, M., Lazzari, C. D., Clemente, F., Merolli, M., Tosti, G., Guaragno, M., Mimmo, R., Ambrosi, D., and Glapinski, J., 2001. “A hybrid (numerical-physical) model of the left ventricle”. *The International Journal of Artificial Organs*, **24**(7), pp. 456–462.
- [64] Ferrari, G., De Lazzari, C., Kozarski, M., Clemente, F., Grczyska, K., Mimmo, R., Monnanni, E., Tosti, G., and Guaragno, M., 2002. “A hybrid mock circulatory system: Testing a prototype under physiologic and pathological conditions”. *ASAIO journal (American Society for Artificial Internal Organs : 1992)*, **48**, 09, pp. 487–94.

- [65] Pillon, M., Duffour, H., and Jufer, M., 1992. “In vitro experiments: Circulatory assist device interaction with a virtual cardiovascular system”. In 1992 14th Annual International Conference of the IEEE Engineering in Medicine and Biology Society, Vol. 2, pp. 740–741.
- [66] Kozarski, M., Ferrari, G., Clemente, F., Gorczynska, K., De Lazzari, C., Darowski, M., Mimmo, R., Tosti, G., and Guaragno, M., 2003. “A hybrid mock circulatory system: development and testing of an electrohydraulic impedance simulator”. *Int J Artif Organs*, **26**(1), pp. 53–63.
- [67] Hanson, B. M., Levesley, M. C., Watterson, K., and Walker, P. G., 2005. “Simulation of the human cardiovascular system for real-time physical interaction with an assist device”. In Proceedings of the 2005 IEEE Engineering in Medicine and Biology 27th Annual Conference, IEEE, pp. 409–412.
- [68] Hanson, B. M., Levesley, M. C., Watterson, K., and Walker, P., 2007. “Hardware-in-the-loop-simulation of the cardiovascular system, with assist device testing application”. *Med Eng Phys*, **29**(3), pp. 367–74.
- [69] Timms, D. L., Gregory, S. D., Greatrex, N. A., Percy, M. J., Fraser, J. F., and Steinseifer, U., 2010. “A compact mock circulation loop for the in vitro testing of cardiovascular devices”. *Artificial Organs*, **35**(4), pp. 384–391.
- [70] Karabegovic, A., Hinteregger, M., Janeczek, C., Reichenfelser, W., Soragnese, V., Mohl, W., and Gföhler, M., 2014. “A systemic mock circula-

tion for in-vitro testing of a pneumatically operated left ventricular assist device”. In Proceedings of the 19th World Congress The International Federation of Automatic Control, IFAC, pp. 8409–8414.

- [71] Fresiello, L., Zieliski, K., Jacobs, S., Di Molfetta, A., Pako, K. J., Bernini, F., Martin, M., Claus, P., Ferrari, G., Trivella, M. G., Greczyska, K., Darowski, M., Meyns, B., and Kozarski, M., 2014. “Reproduction of continuous flow left ventricular assist device experimental data by means of a hybrid cardiovascular model with baroreflex control”. *Artificial Organs*, **38**(6), pp. 456–468.
- [72] Misgeld, B. J. E., Rüschen, D., Schwandtner, S., Heinke, S., Walter, M., and Leonhardt, S., 2015. “Robust decentralised control of a hydrodynamic human circulatory system simulator”. *Biomedical Signal Processing and Control*, **20**, pp. 35–44.
- [73] Rapp, E. S., Pawar, S. R., Larson, E. R., Gohean, J. R., and Longoria, R. G., 2019. “Estimation of systemic vascular resistance using built-in sensing from an implanted left ventricular assist device”. *ASME Journal of Engineering and Science in Medical Diagnostics and Therapy, Special Issue on Novel and Emergent Personalized Cardiovascular Medicine*, **2**(4).
- [74] Ochsner, G., Amacher, R., and Schmid Daners, M., 2013. “Emulation of ventricular suction in a hybrid mock circulation”. In European Control Conference (ECC), EUCA, pp. 3108–3112.

- [75] Boës, S., Ochsner, G., Amacher, R., Petrou, A., Meboldt, M., and Daners, M. S., 2017. “Control of the fluid viscosity in a mock circulation”. *Artificial Organs*, **42**(1), pp. 68–77.
- [76] Petrou, A., Pergantis, P., Ochsner, G., Amacher, R., Krabatsch, T., Falk, V., Meboldt, M., and Daners, M. S., 2017. “Response of a physiological controller for ventricular assist devices during acute patho-physiological events: an *in vitro* study”. *Biomed Tech (Berl)*, **62**(6), pp. 623–633.
- [77] Korn, L., Rüschen, D., Zander, N., Leonhardt, S., and Walter, M., 2017. “Real-time eeg simulation for hybrid mock circulatory loops”. *Artificial Organs*, **42**(2), pp. 131–140.
- [78] Franzetti, G., Daz-Zuccarini, V., and Balabani, S., 2019. “Design of an *in vitro* mock circulatory loop to reproduce patient-specific vascular conditions: Toward precision medicine”. *ASME Journal of Engineering and Science in Medical Diagnostics and Therapy*, **2**, pp. 041004: 1–11.
- [79] Darowski, M., Kozarski, M., Ferrari, G., Górczyska, K., Szczepanowski, A., Pako, K., Fresiello, L., and Molfetta, A. D., 2013. “A new hybrid (hydro-numerical) model of the circulatory system”. *Bulletin of the Polish Academy of Sciences*, **61**(4), pp. 993–1003.
- [80] Jahren, S. E., Ochsner, G., Shu, F., Amacher, R., Antaki, J. F., and Vandenberghe, S., 2014. “Analysis of pressure head-flow loops of pulsatile rotodynamic blood pumps”. *Artificial Organs*, **38**(4), pp. 316–326.

- [81] Ren, W., Steurer, M., and Baldwin, T. L., 2008. “Improve the stability and the accuracy of power hardware-in-the-loop simulation by selecting appropriate interface algorithms”. *IEEE Transactions on Industry Applications*, **44**(4), July, pp. 1286–1294.
- [82] Bighamian, R., Parvinian, B., Scully, C. G., Kramer, G., and Hahn, J.-O., 2018. “Control-oriented physiological modeling of hemodynamic responses to blood volume perturbation”. *Control Engineering Practice*, **73**, pp. 149 – 160.
- [83] Parvinian, B., Scully, C., Wiyor, H., A, A. K., and Weininger, S., 2018. “Regulatory considerations for physiological closed-loop controlled medical devices used for automated critical care: Food and drug administration workshop discussion topics”. *Anesthesia Analgesia*, **126**, pp. 1916–1925.
- [84] Mirinejad, H., Parvinian, B., Ricks, M., Zhang, Y., Weininger, S., Hahn, J., and Scully, C., 2019. “Evaluation of fluid resuscitation control algorithms via a hardware-in-the-loop test bed”. *IEEE Transactions on Biomedical Engineering*, **Early access**.
- [85] ISO 14708-5:2019(E), 2019. Implants for surgery - Active implantable medical devices - Part 5: Circulatory support devices. Standard, International Organization for Standardization, Geneva, CH, Mar.
- [86] Gohean, J. R., George, M. J., Pate, T. D., Kurusz, M., Longoria, R. G., and Smalling, R. W., 2013. “Verification of a computational cardiovas-

cular system model comparing the hemodynamics of a continuous flow to a synchronous valveless pulsatile flow left ventricular assist device”. *ASAIO Journal*, **59**(2), pp. 107–116.

- [87] Karnopp, D., Margolis, D., and Rosenberg, R., 2000. *System Dynamics: Modeling and Simulation of Mechatronic Systems (3rd edition)*. Wiley-Interscience, New York.
- [88] Skogestad, S., and Postlethwaite, I., 2007. *Multivariable feedback control: analysis and design*, Vol. 2. Wiley New York.
- [89] Gohean, J. R., 2019. “Heirarchical control of a two-piston toroidal pump”. PhD thesis, University of Texas at Austin, Walker Department of Mechanical Engineering. <http://dx.doi.org/10.26153/tsw/2137>.
- [90] Ganz, W., Donoso, R., Marcus, H. S., Forrester, J. S., and Swan, H. J., 1971. “A new technique for measurement of cardiac output by thermodilution in man”. *American Journal of Cardiology*, **27**(4), pp. 392–396.
- [91] Stefadouros, M. A., Dougherty, M. J., Grossman, W., and Craige, E., 1973. “Determination of systemic vascular resistance by a noninvasive technic”. *Circulation*, **47**, pp. 101–107.
- [92] O’Dwyer, J., King, J., Wood, C., Taylor, B., and Smith, G., 1994. “Continuous measurement of systemic vascular resistance”. *Anaesthesia*, **49**, pp. 587–590.
- [93] Lee, Q. Y., Redmond, S. J., Chan, G. S., Middleton, P. M., Steel, E.,

- Malouf, P., Critoph, C., Flynn, G., O’Lone, E., and Lovell, N. H., 2013. “Estimation of cardiac output and systemic vascular resistance using a multivariate regression model with features selected from the finger photoplethysmogram and routine cardiovascular measurements”. *BioMedical Engineering OnLine*, **12**(1), Mar, p. 19.
- [94] Wang, L., Ansari, S., Najarian, K., Ward, K. R., and Oldham, K. R., 2017. “Estimation of peripheral artery radius using non-invasive sensors and kalman filtering of local dynamics”. In 2017 American Control Conference (ACC), pp. 807–812.
- [95] Tasch, U., Koontz, J. W., Ignatoski, M. A., and Geselowitz, D. B., 1990. “An adaptive aortic pressure observer for the penn state electric ventricular assist device”. *IEEE Transactions on Biomedical Engineering*, **37**(4), April, pp. 374–383.
- [96] Yu, Y.-C., Boston, J. R., Simaan, M. A., and Antaki, J. F., 2001. “Minimally invasive estimation of systemic vascular parameters”. *Annals of Biomedical Engineering*, **29**(7), Jul, pp. 595–606.
- [97] Maybeck, P. S., 1979. *Stochastic Models, Estimation, and Control*. New York: Academic Press.
- [98] Gohean, J. R., George, M. J., Chang, K.-W., Larson, E. R., Pate, T. D., Kurusz, M., Longoria, R. G., and Smalling, R. W., 2014. “Preservation of native aortic valve flow and full hemodynamic support with the torvad using a computational model of the cardiovascular system.”. *ASAIO*

- Journal (American Society for Artificial Internal Organs: 1992)*, **59**, pp. 259–265.
- [99] Kalman, R. E., 1960. “A new approach to linear filtering and prediction problems”. *Journal of basic Engineering*, **82**(1), pp. 35–45.
- [100] Baram, Y., and Kailath, T., 1988. “Estimability and Regulability of Linear Systems”. *IEEE Transactions on Automatic Control*, **33**(12), pp. 1116–1121.
- [101] Farrar, D. J., Bourque, K., Dague, C. P., Cotter, C. J., and Poirier, V. L., 2007. “Design features, developmental status, and experimental results with the heartmate iii centrifugal left ventricular assist system with a magnetically levitated rotor”. *ASAIO journal*, **53**(3), pp. 310–315.
- [102] LaRose, J. A., Tamez, D., Ashenuga, M., and Reyes, C., 2010. “Design concepts and principle of operation of the heartware ventricular assist system”. *ASAIO Journal*, **56**(4), pp. 285–289.
- [103] Kitamura, T., Matsushima, Y., Tokuyama, T., Kono, S., Nishimura, K., Komeda, M., Yanai, M., Kijima, T., and Nojiri, C., 2000. “Physical model-based indirect measurements of blood pressure and flow using a centrifugal pump”. *Artificial Organs*, **24**(8), pp. 589–593.
- [104] LaRose, J. A., and Singh, U., 2013. Sensorless flow estimation for implanted ventricle assist device. US Patent 8,506,470 B2.
- [105] Paynter, H. M., and Longoria, R., 1997. “Two-port canonical bond

- graph models of lossy power transduction”. In IEEE International Conference on Systems, Man, and Cybernetics, pp. 1533–1537.
- [106] Rapp, E. S., Pawar, S. R., Gohean, J. R., Larson, E., and Longoria, R. G., 2020. “Evaluating a hardware-in-the-loop system intended for testing ventricular-assist device control and sensing algorithms”. In 2020 American Control Conference (ACC), pp. 1341–1346.
- [107] Mouret, F., Garitey, V., Gandelheid, T., Fusseri, J., and Rieu, R., 2000. “A new dual activation simulator of the left heart that reproduces physiological and pathological conditions”. *Medical & biological engineering & computing*, **38**, 10, pp. 558–61.
- [108] Niederer, S. A., Lumens, J., and Trayanova, N. A., 2019. “Computational models in cardiology”. *Nat Rev Cardiol.*, **16**(2), pp. 100–111.
- [109] Le, T. Q., Bukkapatnam, S. T., Sangasoongsong, A., and Komanduri, R., 2010. “Towards virtual instruments for cardiovascular healthcare: Real-time modeling of cardiovascular dynamics using ecg signals”. In 2010 IEEE International Conference on Automation Science and Engineering, pp. 903–910.
- [110] Le, T. Q., Bukkapatnam, S. T. S., and Komanduri, R., 2013. “Real-time lumped parameter modeling of cardiovascular dynamics using electrocardiogram signals: Toward virtual cardiovascular instruments”. *IEEE Transactions on Biomedical Engineering*, **60**(8), pp. 2350–2360.

- [111] Bozkurt, S., 2020. “Computational simulation of cardiac function and blood flow in the circulatory system under continuous flow left ventricular assist device support during atrial fibrillation”. *Applied Sciences*, **10**(3).
- [112] Christensen, D. M., VanderPluym, C., Conway, J., Lorts, A., Buchholz, H., Schlöglhofer, T., Viericke, J., Stepanenko, A., Kauffman, F., and Sorenson, G., 2017. “Outpatient management: The role of the vad coordinator and remote monitoring”. In *Mechanical Circulatory Support in End-Stage Heart Failure: A Practical Manual*, A. Montalto, A. Loforte, F. Musumeci, T. Krabatsch, and M. S. Slaughter, eds. Springer International Publishing, Cham., pp. 445–465.
- [113] Reiss, N., Schmidt, T., Boeckelmann, M., Schulte-Eistrup, S., Hoffmann, J.-D., Feldmann, C., and Schmitto, J. D., 2018. “Telemonitoring of left-ventricular assist device patientscurrent status and future challenges”. *Journal of Thoracic Disease*, **10**(15).
- [114] Wang, T. S., Hernandez, A. F., Felker, G. M., Milano, C. A., Rogers, J. G., and Patel, C. B., 2014. “Valvular heart disease in patients supported with left ventricular assist devices”. *Circulation: Heart Failure*, **7**(1), pp. 215–222.
- [115] Granegger, M., Masetti, M., Laohasurayodhin, R., Schloeghofer, T., Zimpfer, D., Schima, H., and Moscato, F., 2016. “Continuous monitoring of aortic valve opening in rotary blood pump patients”. *IEEE*

Transactions on Biomedical Engineering, **63**(6), pp. 1201–1207.

- [116] Pugovkin, A., Markov, A., Selishchev, S., Korn, L., Walter, M., Leonhardt, S., Bockeria, L., Bockeria, O., and Telyshev, D., 2019. “Advances in hemodynamic analysis in cardiovascular diseases investigation of energetic characteristics of adult and pediatric sputnik left ventricular assist devices during mock circulation support”. *Cardiology Research and Practice*, **2019**.
- [117] Petukhov, D., Korn, L., Walter, M., and Telyshev, D., 2019. “A novel control method for rotary blood pumps as left ventricular assist device utilizing aortic valve state detection”. *BioMed Research International*, **2019**.
- [118] Dodge, H. T., Kirkham Jr., F. T., and King, C. V., 1957. “Ventricular dynamics in atrial fibrillation”. *Circulation*, **15**(3), pp. 335–347.
- [119] Bolanos, R., Selzman, K. A., Jantac, L., and Stouffer, G. A., 2017. “Hemodynamics of arrhythmias and pacemakers”. In *Cardiovascular Hemodynamics for the Clinician*. John Wiley & Sons, Ltd, ch. 27, pp. 321–340.
- [120] Welch, J. P., Ford, P. J., Teplick, R. S., and Rubsamen, R. M., 1991. “The massachusetts general hospital-marquette foundation hemodynamic and electrocardiographic database – comprehensive collection of critical care waveforms”. *J Clinical Monitoring*, **7**(1), pp. 96–97.

- [121] OBrien, C., and Heneghan, C., 2007. “A comparison of algorithms for estimation of a respiratory signal from the surface electrocardiogram”. *Computers in Biology and Medicine*, **37**(3), pp. 305–314.
- [122] Bukkapatnam, S., Komanduri, R., Yang, H., Rao, P., Lih, W.-C., Malshé, M., Raff, L. M., Benjamin, B., and Rockley, M., 2008. “Classification of atrial fibrillation episodes from sparse electrocardiogram data”. *Journal of Electrocardiology*, **41**(4), pp. 292–299.
- [123] O’Keefe, J. H., Hammill, S. C., Freed, M. S., and Pogwizd, S. M., 2008. *The Complete Guide to ECGs (3rd edition)*. Jones and Bartlett Publishers.
- [124] Goldberger, A. L., Goldberger, Z. D., and Shvilkin, A., 2012. *Goldberger’s Clinical Electrocardiograph: A Simplified Approach (8th edition)*. Saunders, an imprint of Elsevier, Inc.
- [125] Malekpour, S., Gubner, J. A., and Sethares, W. A., 2018. “Measures of generalized magnitude-squared coherence: Differences and similarities”. *Journal of the Franklin Institute*, **355**(5), pp. 2932–2950.
- [126] Ropella, K. M., Sahakian, A. V., Baerman, J. M., and Swiryn, S., 1989. “The coherence spectrum - a quantitative discriminator of fibrillatory and nonfibrillatory cardiac rhythms”. *Circulation*, **80**(1), pp. 112–119.